

Inaugural Dissertation

zur
Erlangung der Doktorwürde
der
Gesamtfakultät für
Mathematik, Ingenieur- und Naturwissenschaften
der
Ruprecht-Karls-Universität
Heidelberg

vorgelegt von
Mike Boger, M.Sc.
aus Nürtingen

Tag der mündlichen Prüfung
10.11.2022

**Comparative morphological, metabolic
and transcriptome analyses in *elmo1*^{-/-}, *elmo2*^{-/-} and *elmo3*^{-/-}
zebrafish mutants**

Gutachter:

Prof. Dr. Markus Hecker

Prof. Dr. Jens Kroll

Die vorliegende Arbeit wurde zwischen Januar 2019 und August 2022 in der Abteilung für Vaskuläre Biologie und Tumorangio-genese des „*European Center of Angioscience*“ der Medizinischen Fakultät Mannheim der Universität Heidelberg angefertigt.

Teile dieser Arbeit wurden am 8. Juli 2022 unter folgendem Titel in der Zeitschrift *Frontiers in Cell and Developmental Biology* veröffentlicht

Comparative morphological, metabolic and transcriptome analyses in *elmo1*^{-/-}, *elmo2*^{-/-} and *elmo3*^{-/-} zebrafish mutants identified a functional non-redundancy of the Elmo proteins

Mike Boger, Katrin Bennewitz, David Philipp Wohlfart, Ingrid Hausser, Carsten Sticht, Gernot Poschet, Jens Kroll

Ich erkläre hiermit, dass es sich bei der eingereichten Dissertation um meine eigenständig erbrachte Leistung handelt. Ich habe nur die angegebenen Quellen und Hilfsmittel benutzt und mich keiner unzulässigen Hilfe Dritter bedient. Wörtlich oder sinngemäß aus anderen Werken übernommene Inhalte habe ich als solche kenntlich gemacht. Ich habe weder die Arbeit noch Teile dieser Arbeit an einer Hochschule des In- oder Auslandes als Bestandteil einer Prüfungs- oder Qualifikationsleistung vorgelegt. Ich erkläre hiermit die Richtigkeit der vorstehenden Erklärung und bin mir der Folgen einer unrichtigen oder unvollständigen eidesstattlichen Versicherung bewusst. Ich versichere an Eides statt, dass ich nach bestem Wissen die reine Wahrheit erklärt und nichts verschwiegen habe.

Mannheim, den _____

Mike Boger

Danksagung

Zuallererst danke ich Prof. Jens Kroll für die Möglichkeit bei ihm meine Doktorarbeit durchführen zu können, für seine intensive Betreuung und die langjährige Unterstützung des Projekts und meiner Arbeit.

Ich danke Prof. Markus Hecker für die Bereitschaft als Erstgutachter zu fungieren und für seine Betreuung, seine Unterstützung und seinen Rat.

Des Weiteren danke ich Prof. Hans-Peter Hammes für seine Unterstützung und seinen nie endenden Enthusiasmus.

Ebenfalls danke ich den vielen Kollaborateur*innen, die mit ihren Fähigkeiten und ihrem Fachwissen diese Arbeit um einiges bereichert haben. Danke neben allen anderen an Dr. Ingrid Haußer, Dr. Carsten Sticht, Dr. Carolina De La Torre und Dr. Gernot Poschet.

Natürlich geht ein großer Dank an das Team im Labor und meine ganzen Leidensgenoss*innen in Mannheim und Heidelberg. Neben Elisabeth Lodd, Chiara Middel, Lena Metzger, Rafael Saup, Linda Kessler und Isabel Porth danke ich allen die das Labor belebt haben. Besonderer Dank geht an David Wohlfart, Christoph Tabler, Bowen Lou, Katrin Bennewitz und Haozhe Qi für ihre Unterstützung und dafür, dass sie mit ihrem Fachwissen, unzähligen Diskussionen und mit viel Humor den Doktorandenalltag leichter gemacht haben.

Danke auch an meine Freunde, für viel gute Laune und ihr Verständnis mich jahrelang der Wissenschaft zu widmen

Großer Dank geht an meine Familie, besonders an meine Eltern, meinen Bruder und meine Großeltern, die mich immer unterstützt und an mich geglaubt haben und damit dafür gesorgt haben, dass ich so viel erreiche.

Mein größter Dank geht an meine Freundin Silvana. Für ihr Wissen und ihr Verständnis für Wissenschaft und die komplexen Vorgänge der Biologie. Danke für all die Diskussionen über das vermeintlich schlauste Vorgehen bei allen möglichen Experimenten. Am meisten bin ich aber dankbar für die unendliche Unterstützung, die Motivation und für das unermüdliche Vertrauen in mein Können.

Table of contents

Abstract	VI
Zusammenfassung	VII
1 Introduction	1
1.1 The small GTPase RAC1	1
1.2 ELMO proteins	2
1.3 ELMOs and RAC1 in vascular development	4
1.4 ELMOs and RAC1 in kidney function and disease	5
1.5 ELMOs and RAC1 in insulin mediated glucose uptake and diabetes mellitus... ..	7
1.7 Zebrafish as a model organism in general and diabetes research	9
1.8 Aim of the thesis	10
2 Results	11
2.1 Zebrafish Elmo1, Elmo2 and Elmo3 show structural differences in the amino acid sequence	11
2.2 Generation of <i>elmo1</i> ^{-/-} , <i>elmo2</i> ^{-/-} and <i>elmo3</i> ^{-/-} zebrafish lines	13
2.3 Validation of <i>elmo1</i> ^{-/-} , <i>elmo2</i> ^{-/-} and <i>elmo3</i> ^{-/-} zebrafish lines on DNA, RNA and protein level	15
2.4 The loss of Elmo3 led to a decreased survival rate	16
2.5 Analyses of the <i>elmo</i> expression patterns in wild type and <i>elmo1</i> ^{-/-} , <i>elmo2</i> ^{-/-} and <i>elmo3</i> ^{-/-} zebrafish	18
2.6 Differential changes in vascular structures in <i>elmo1</i> ^{-/-} , <i>elmo2</i> ^{-/-} and <i>elmo3</i> ^{-/-} zebrafish	21
2.7 Morphological analysis of adult <i>elmo1</i> ^{-/-} , <i>elmo2</i> ^{-/-} and <i>elmo3</i> ^{-/-} zebrafish kidneys revealed different changes in glomerular structures	25
2.8 Elmo1 regulates adult blood glucose in zebrafish	28
2.9 Transcriptome analyses of <i>elmo1</i> ^{-/-} , <i>elmo2</i> ^{-/-} and <i>elmo3</i> ^{-/-} zebrafish larvae revealed that the Elmo proteins transcriptionally modulate vascular and neuronal development	32
2.10 Metabolome analyses of <i>elmo1</i> ^{-/-} , <i>elmo2</i> ^{-/-} and <i>elmo3</i> ^{-/-} zebrafish larvae revealed an increase of amino acids due to the loss of Elmo1 and an increase of fatty acids due the loss of Elmo2	37
2.11 <i>elmo1</i> ^{-/-} , <i>elmo2</i> ^{-/-} double knockout zebrafish exhibit no stronger alterations than single knockout lines	44
3 Discussion	47
3.1 Vascular changes in <i>elmo1</i> ^{-/-} , <i>elmo2</i> ^{-/-} and <i>elmo3</i> ^{-/-} zebrafish indicate shared and varying regulatory functions within the Elmo protein family	47
3.2 Elmo1, Elmo2 and Elmo3 regulate the ECM and affect the glomerular morphogenesis	49

3.3	Elmo1 as a novel blood glucose regulator.....	51
3.4	Elmo1 is a potential risk factor for the development of diabetes and DN	53
3.5	The larval transcriptome is unequally regulated in <i>elmo1</i> ^{-/-} , <i>elmo2</i> ^{-/-} and <i>elmo3</i> ^{-/-} zebrafish.....	55
3.6	Elmo proteins fulfill common, but mainly individual functions	55
3.7	Conclusion.....	56
4	Material and Methods.....	58
4.1	Material.....	58
4.1.1	Equipment.....	58
4.1.2	Software.....	59
4.1.3	Consumables	60
4.1.4	Chemicals	61
4.1.5	Solutions	61
4.1.6	Further materials.....	64
4.1.7	Antibodies	65
4.1.8	Enzymes and buffers	65
4.1.9	Plasmids	66
4.1.10	Oligonucleotides	66
4.1.11	Bacterial strains	69
4.1.12	Zebrafish transgenic lines.....	69
4.1.13	Gene and transcript sequences.....	69
4.2	Methods.....	69
4.2.1	Zebrafish husbandry	69
4.2.2	Mutant generation	70
4.2.2.1	Target site design	70
4.2.2.2	Oligonucleotide annealing.....	70
4.2.2.3	CRISPR plasmid generation	70
4.2.2.4	Transformation of <i>Escherichia coli</i>	71
4.2.2.5	Plasmid mini preparation.....	71
4.2.2.6	Identification of successful ligated CRISPR constructs.....	71
4.2.2.7	Plasmid midi preparation.....	72
4.2.2.8	<i>In vitro</i> transcription of CRISPR gRNA and Cas9 mRNA.....	72
4.2.2.9	CRISPR/Cas9 injection.....	72
4.2.2.10	Germline transmission and further breeding	72
4.2.2.11	Generation of a double gene knockout mutant zebrafish line	73
4.2.3	Preparation of adult zebrafish organs and blood glucose measurement.....	73

4.2.4	Western Blot analysis	73
4.2.4.1	Protein lysate generation	73
4.2.4.2	Determination of protein concentration	74
4.2.4.3	SDS-PAGE and Western Blot	74
4.2.4.4	Immunohistochemistry	74
4.2.5	Microscopy and analysis of vascular structures	74
4.2.5.1	Analysis of the larval trunk	74
4.2.5.2	Analysis of the larval hyaloid	75
4.2.5.3	Analysis of the larval hyaloid vessel permeability	75
4.2.5.4	Analysis of the adult retina	75
4.2.5.5	Analysis of the adult brain	75
4.2.6	Microscopy and analysis of the kidney morphology	76
4.2.6.1	Paraffin embedding and PAS staining	76
4.2.6.2	Fixation and electron microscopy analysis	76
4.2.7	Collection of zebrafish larval samples	77
4.2.8	Whole body glucose measurement in larvae	77
4.2.9	Isolation of genomic DNA	77
4.2.10	RNA purification	77
4.2.10.1	Larvae samples	77
4.2.10.2	Organ samples	78
4.2.11	Polymerase chain reaction (PCR)	78
4.2.12	Reverse-transcription PCR (RT-PCR)	78
4.2.13	Reverse-transcription quantitative PCR (RT-qPCR)	79
4.2.14	RNA-sequencing and transcriptome analysis	79
4.2.15	Metabolome analyses	80
4.2.16	Genotyping	80
4.2.17	Protein sequence alignment	80
4.2.18	Statistics	80
	Appendix	82
	Abbreviations	93
	References	98

List of Figures

Figure 1. Zebrafish Elmo1, Elmo2 and Elmo3 showed 43 % identity in amino acid sequence.....	12
Figure 2. Generation of <i>elmo1</i> , <i>elmo2</i> and <i>elmo3</i> knockout zebrafish lines with the CRISPR/Cas9 system.	14
Figure 3. Validation of the loss of the Elmo1 protein in the <i>elmo1</i> ^{-/-} zebrafish lines..	15
Figure 4. Validation of <i>elmo1</i> , <i>elmo2</i> and <i>elmo3</i> mutations in zebrafish lines at RNA level.	16
Figure 5. The general morphology was not changed between wild type and homozygous <i>elmo1</i> , <i>elmo2</i> and <i>elmo3</i> mutant zebrafish in larval and adult stage...	17
Figure 6. The loss of Elmo3 led to a reduced survivability of <i>elmo3</i> ^{-/-} zebrafish.	17
Figure 7. Differential expression of <i>elmo1</i> , <i>elmo2</i> and <i>elmo3</i> in development and in adult eyes and kidneys of wildtype zebrafish.....	19
Figure 8. Indicated compensation of <i>elmo1</i> in <i>elmo2</i> ^{-/-} zebrafish larvae due to increased <i>elmo1</i> RNA levels.....	20
Figure 9. The loss of Elmo1 led to decreased sprouts in the larval trunk vasculature in zebrafish at 96 hpf.	22
Figure 10. The loss of Elmo1 and Elmo3 respectively led to an increased diameter of hyaloid blood vessels in zebrafish larvae.....	23
Figure 11. Different regulation of the retinal vasculature through Elmo1, Elmo2 and Elmo3 in adult zebrafish.	24
Figure 12. Different regulation of the glomerular structure through Elmo1, Elmo2 and Elmo3 in the kidney of adult zebrafish.	26
Figure 13. The loss of Elmo3 led to a thickened glomerular basement membrane in adult zebrafish kidneys.	28
Figure 14. The loss of Elmo1 led to altered blood glucose levels in adult zebrafish.	29
Figure 15. Unaltered expression of <i>preproinsulin</i> and <i>insulin receptor</i> genes in larval <i>elmo1</i> ^{-/-} , <i>elmo2</i> ^{-/-} , and <i>elmo3</i> ^{-/-} zebrafish.	30
Figure 16. The loss of Elmo1 led to altered expression of individual glucose level regulating genes in adult postprandial zebrafish livers.	32
Figure 17. Regulation of the transcriptome in larval zebrafish after loss of Elmo1, Elmo2 or Elmo3 only showed limited similarities.	36

Figure 18. The loss of Elmo1 led to an increase of amino acids in zebrafish larvae.	38
Figure 19. The loss of Elmo2 led to an increase of fatty acids in zebrafish larvae....	40
Figure 20. The loss of Elmo1 and Elmo3 respectively led to decreased ADP and ATP levels in zebrafish larvae.	41
Figure 21. No alterations in glutathione ratios in <i>elmo1^{-/-}</i> , <i>elmo2^{-/-}</i> and <i>elmo3^{-/-}</i> zebrafish larvae.	42
Figure 22. Comparison of <i>elmo1^{-/-}</i> , <i>elmo2^{-/-}</i> and <i>elmo3^{-/-}</i> phenotype in zebrafish indicates different functions of Elmo1, Elmo2 and Elmo3.	43
Figure 23. The loss of Elmo1 and Elmo2 led to a downregulation of the retinal vasculature in adult zebrafish.	44
Figure 24. Unaltered glomerular basement membrane thickness in kidneys of adult <i>elmo1^{-/-}</i> , <i>elmo2^{-/-}</i> zebrafish.	45
Figure 25. The loss of Elmo1 and Elmo2 led to decreased fasting blood glucose levels in adult zebrafish.	46

List of Tables

Table 1. The loss of Elmo3 led to more changes in the regulation of the transcriptome of zebrafish larvae than the loss of Elmo1 or Elmo2.	32
---	----

Abstract

The engulfment and cell motility (ELMO) proteins are cytoplasmic adaptor proteins which are evolutionary conserved in several organisms. In higher vertebrates the ELMO protein family consists of the three paralogs ELMO1, ELMO2 and ELMO3. All three ELMO proteins regulate the activity of the Rac family small GTPase 1 (RAC1). As RAC1 regulators, individual ELMO proteins facilitate basic and major cell functions such as cytoskeleton organization, cell migration, phagocytosis, the engulfment of apoptotic cells and myoblast fusion. Several studies have shown that the ELMO proteins are involved in a variety of cellular and developmental processes and linked to multiple diseases, such as cancer, diabetes mellitus, inflammatory bowel disease and developmental disorders. However, the individual functions of ELMO1, ELMO2 and ELMO3 are hardly understood and since barely any studies cover comparative data about all three ELMO proteins, it is mostly unknown whether the Elmo proteins have similar functions and act redundantly or not. To address this question, *elmo1*^{-/-}, *elmo2*^{-/-} and *elmo3*^{-/-} knockout zebrafish were generated using the CRISPR/Cas9 technique and with these mutants a comprehensive comparison of the phenotypic changes in organ morphology, transcriptome and metabolome was performed. The main results were decreased fasting and increased postprandial blood glucose levels in adult *elmo1*^{-/-}, as well as a decreased vascular formation in the adult retina of *elmo1*^{-/-}, but an increased vascular formation in the adult retina of *elmo3*^{-/-} zebrafish. The comparison provided few similarities between the knockout lines, as increased Bowman space areas in adult *elmo1*^{-/-} and *elmo2*^{-/-} kidneys, an increased hyaloid vessel diameter in *elmo1*^{-/-} and *elmo3*^{-/-} and a transcriptional downregulation of the vascular development in *elmo1*^{-/-}, *elmo2*^{-/-}, and *elmo3*^{-/-} zebrafish larvae. Despite that, *elmo1*^{-/-}, *elmo2*^{-/-}, and *elmo3*^{-/-} zebrafish exhibited several distinct changes in the vascular and glomerular structure, as well as in the metabolome and the transcriptome. Especially, *elmo3*^{-/-} zebrafish showed extensive differences due to a strong transcriptional dysregulation in larvae and an impaired survivability. Together, the data demonstrate that the three zebrafish Elmo proteins regulate not only similar but many divergent biological processes and mechanisms and show a low functional redundancy.

Zusammenfassung

Die *engulfment and cell motility* (ELMO) Proteine sind in vielen Organismen konservierte zytoplasmatische Adapterproteine. In höheren Vertebraten besteht die ELMO Proteinfamilie aus den drei Paralogen ELMO1, ELMO2 und ELMO3. Alle drei ELMO Proteine regulieren die Aktivität von *Rac family small GTPase 1* (RAC1). Durch ihre Funktion als RAC1 Regulatoren, vermitteln die individuellen ELMO Proteine grundlegende und wichtige Zellfunktionen, wie die Zytoskelett Organisation, die Zellmigration, die Phagozytose, die Verschlingung von apoptotischen Zellen und die Myoblastenfusion. Studien haben gezeigt, dass die ELMO Proteine an einer Vielzahl unterschiedlicher Prozesse in der Zelle und in der Entwicklung beteiligt sind und dass sie in verschiedenen Krankheiten, wie Krebs, Diabetes mellitus, chronisch-entzündliche Darmerkrankungen und Entwicklungsstörungen eine Rolle spielen. Jedoch sind die einzelnen Funktionen von ELMO1, ELMO2 und ELMO3 wenig verstanden und durch den Mangel an Studien mit vergleichbaren funktionellen Daten zu allen drei Proteinen ist größtenteils unbekannt, ob die Funktionen der ELMO Proteine gleich sind oder nicht. Um diese Fragestellung zu untersuchen, wurden mit Hilfe des CRISPR/Cas9 Systems *elmo1*^{-/-}, *elmo2*^{-/-} and *elmo3*^{-/-} Zebrafisch Mutanten erstellt und deren Phänotypen umfassend morphologisch, metabolisch und transkriptionell untersucht und miteinander verglichen. Die bedeutendsten Ergebnisse waren verringerte nüchterne und erhöhte postprandiale Blutglucosewerte in adulten *elmo1*^{-/-} Fischen, sowie eine Reduktion der Vaskulatur in der adulten Retina von *elmo1*^{-/-}, aber eine Erhöhung der Vaskulatur in der adulten Retina von *elmo3*^{-/-} Fischen. Der Vergleich ergab mehrere Überschneidungen in den phänotypischen Veränderungen, wie eine Vergrößerung des Bowman Kapselraums in adulten *elmo1*^{-/-} and *elmo2*^{-/-} Nieren, einen vergrößerten Gefäßdurchmesser bei Hyaloiden in *elmo1*^{-/-} and *elmo3*^{-/-} und eine transkriptionelle Herunterregulation der vaskulären Entwicklung in *elmo1*^{-/-}, *elmo2*^{-/-}, and *elmo3*^{-/-} Larven. Trotz dessen zeigten *elmo1*^{-/-}, *elmo2*^{-/-}, and *elmo3*^{-/-} Zebrafische zahlreiche unterschiedliche Veränderungen in der vaskulären und glomerulären Struktur, sowie im Metabolom und im Transkriptom. Besonders *elmo3*^{-/-} Fische wiesen deutliche Unterschiede durch eine enorme transkriptionelle Fehlregulation in Larven und eine reduzierte Überlebensrate auf. Zusammenfassend demonstrieren die Ergebnisse, dass die einzelnen Elmo Proteine nicht nur gleiche, sondern viele unterschiedliche Prozesse regulieren und dass somit eine geringe Redundanz in ihren Funktionen besteht.

1 Introduction

Parts of this chapter have been published in the following publication in *Frontiers in Cell and Developmental Biology* in 2022 and have been originally written by myself.

Comparative morphological, metabolic and transcriptome analyses in *elmo1*^{-/-}, *elmo2*^{-/-} and *elmo3*^{-/-} zebrafish mutants identified a functional non-redundancy of the Elmo proteins

Mike Boger, Katrin Bennewitz, David Philipp Wohlfart, Ingrid Hausser, Carsten Sticht, Gernot Poschet, Jens Kroll

1.1 The small GTPase RAC1

The subfamily of Ras homologue (Rho) GTPases belongs to the protein superfamily of Ras-related small GTPases. GTPases are molecular switches which alternate between an active state binding a guanosine triphosphate (GTP) and an inactive state binding a guanosine diphosphate (GDP) [1]. Their activation is accomplished by binding guanine nucleotide exchange factors (GEFs) which replace the bound GDP to GTP, whereas their inactivation is facilitated by GTPase-activating proteins (GAPs) which accelerate the hydrolysis of GTP to GDP [2–5]. Several GEFs and GAPs spatiotemporally regulate the activity of RAC1 and depending on the tissue and the executed function it differs which ones are responsible. To maintain an inactive form, Rho guanine dissociation inhibitors (GDIs) bind to GTPases. The best characterized Rho GTPases are Rac family small GTPase 1 (RAC1), cell division cycle 42 (CDC42) and Ras homolog family member A (RhoA). RAC1 is a pleiotropic regulator and a major factor in the organization and reorganization of the actin cytoskeleton [6–10]. Fulfilling this role, RAC1 affects fundamental processes such as cell motility, cell migration, cell division, cellular structure definition, vesicle transport, endocytosis and chemotaxis [11–14]. RAC1 further regulates cell proliferation, cell adhesion, cell survival and cell cycle progression [7, 15–17]. Through the involvement in this magnitude of substantial functions, dysregulation of RAC1 plays a role in the development and progression of various diseases. For instance, RAC1 regulates multiple processes relevant in cancer development [18–20], is involved in developmental and neuronal disorders and diabetes mellitus [21, 22]. Furthermore, RAC1 affects the redox status and therefore contributes to the development of diseases, such as cardiovascular disease, by

mediation of the production of reactive oxygen species (ROS) by NADPH oxidases (NOX) [23–28].

1.2 ELMO proteins

The engulfment and cell motility (ELMO) proteins are cytoplasmic adaptor proteins which are evolutionary conserved in several organisms [29]. Their ortholog Cell death abnormality protein 12 (CED-12) is present in *C. elegans* and *D. melanogaster*. Higher vertebrates such as zebrafish, mice and humans possess the full ELMO protein family consisting of the three paralogs ELMO1, ELMO2 and ELMO3 [30–32]. All three ELMO proteins regulate the activity of RAC1 [33–36]. When recruited, ELMO1 or ELMO2 bind to dedicator of cytokinesis (DOCK) proteins and the ELMO/DOCK heterodimers function as GEFs for RAC1, promoting its activity [37–39]. The ELMO/DOCK complex binds nucleotide-free RAC1 with the Docker domain of DOCK proteins and facilitates GTP loading [37, 40]. Direct interaction of ELMO3 with DOCK or RAC1 has not been proven yet. The ELMO proteins have three known domains (Figure 1, Supplementary Figure 1): The C-terminal pleckstrin homology (PH) domain regulates the interaction with DOCK proteins for RAC1 activity [34, 39, 41, 42]. The N-terminal armadillo-like helical domain is of unknown function and the ELMO protein-characteristic ELMO domain is not well described. It was proposed to bind and regulate the activity of members of another subfamily of small GTPases, the adenosine diphosphate-ribosylation factors (Arf) but this has just been shown in ELMOD proteins, the other protein family containing ELMO domains [42, 43]. As upstream regulators of ELMO/DOCK/RAC signaling, Ras homolog family member G (RhoG), brain-specific angiogenesis inhibitor 1 (BAI1), AXL receptor tyrosine kinase (AXL) and Netrin-1 were identified [44–47]. To bind RhoG and BAI1, ELMO proteins have an N-terminal sequence which has been shown for ELMO1 and ELMO2 so far.

As RAC1 regulators, ELMO proteins facilitate basic and major cell functions such as cytoskeleton organization, cell migration, phagocytosis, the engulfment of apoptotic cells and myoblast fusion [31, 36–38, 44, 48–53]. Furthermore, ELMO proteins are involved in a variety of cellular and developmental processes which bring them into focus of disease-oriented research. ELMO1 and ELMO2 are involved in nervous system development and disorders [33, 36, 54–58] as both promote axon guidance [59] and *elmo1*^{-/-} zebrafish exhibited reduced apoptotic neuronal deaths and a reduced regulation of axon myelination and neuronal numbers [60]. Also mutations of ELMO3

were recently suggested to be the cause of developmental delay in humans [36]. Moreover, ELMO proteins were linked to multiple other diseases, such as cancer, diabetes mellitus, inflammatory bowel disease and arthritis [47, 61–64]. Respective studies provided insights into the variety of the ELMO proteins' functions as they are promotive factors for cell growth, proliferation and metastasis in multiple human carcinomas [65–67]. Overexpression of ELMO3 is commonly suggested as a negative prognostic marker in different cancer types [68–70]. Additionally, ELMO3 was recently described as a regulator of RAC1 activity promoting cell migration [36] and thereby shown to act similar to ELMO1 and ELMO2. Further functions of ELMO3 regarding developmental processes are still poorly understood.

In mouse models, ELMO1 was identified as a microbial sensor in epithelial and phagocytic cells that activates inflammatory signals and is a required factor for bacterial internalization and monocyte recruitment in inflammatory bowel disease [64]. *Elmo1*^{-/-} mouse models of osteoporosis and arthritis showed reduced bone erosion and identified ELMO1 as a positive regulator of osteoclast function and bone loss [63]. In addition *Elmo1* was described as a promotor of angiogenesis and early vascular development in zebrafish [46, 71]. Remarkably, worldwide genetic studies in humans reported a susceptibility of diabetic patients with gene variants of *ELMO1*, *ELMO2* or *ELMO3* to the development of kidney damage [62, 72–78] and studies in mouse models reported ELMO1 as responsible for the aggravation of nephropathy in diabetic mice [61, 62]. ELMO2 was shown to regulate the insulin dependent expression and membrane translocation of GLUT4 in human skeletal muscle cells and adipocytes, indicating a potential involvement in glucose homeostasis [79].

Together, these studies have identified various functions of the individual ELMO proteins, but also left many open questions. Mainly, the exact role of the ELMO proteins within these functions and their underlying mechanisms are not fully understood. Furthermore, it is often unknown, whether the conducted function is mediated over RAC1 activation or not. Sun *et al.* reported that ELMO2 regulates the GLUT4 translocation in human adipocytes but RAC1 does not, revealing that ELMO proteins can fulfill functions independently of RAC1 [79]. This finding emphasizes the difficulty about the understanding of the ELMO proteins' functions because not only a reported function of RAC1 is not automatically mediated by ELMO proteins, but also a reported function of one of the ELMO proteins is not automatically mediated over RAC1. Another difficulty is that a described function of one ELMO protein does not automatically apply

to the other two ELMO proteins and must be investigated separately to identify whether a function is shared or not.

1.3 ELMOs and RAC1 in vascular development

In higher organisms as vertebrates, the circulatory system is the network of heart and blood vessels which transports blood to ensure the oxygen and nutrient supply of cells, tissues and organs [80]. The main types of blood vessels are arteries, arterioles, veins, venules and capillaries [81, 82]. In most arteries and the smaller arterioles oxygenated blood gets transported away from the heart to the oxygen dependent tissues and in most veins and the smaller venules deoxygenated blood gets transported back from the tissues to the heart [83]. Capillaries, the smallest type of blood vessels, are mainly organized as networks and connect arterioles and venules in tissues and organs. Blood vessels are formed through vasculogenesis and angiogenesis [84]. Vasculogenesis is the formation of new blood vessels through the differentiation of angioblasts, endothelial precursor cells derived from the embryonic mesoderm, into endothelial cells [85, 86]. It mainly occurs during embryogenesis when the cardiovascular system is built [87]. Angiogenesis is the formation of new blood vessels from pre-existing vessels and is responsible for the growth of most blood vessels during development and disease [88–92]. It is divided into two mechanisms. Sprouting angiogenesis is defined through endothelial cells proliferating out of a weakened blood vessel wall into the surrounding matrix and forming a solid sprout [84, 86]. Such sprouts can grow and connect with other sprouts to develop a full vessel with lumen connecting the two initial vessels. Intussusceptive angiogenesis is the splitting of an existing blood vessel through the building of transvascular pillars into the vessel lumen resulting in the separation of the primary vessel into two vessels [93–95]. Size and inner diameter of blood vessels can also be flexibly modulated through vasoconstriction and vasodilation [96]. Vasoconstriction is the narrowing and vasodilation the expansion of the blood vessels through contraction or relaxation of the vascular smooth muscle cells within the blood vessel walls [97]. Both results in changes of the blood pressure and blood flow.

RAC1 is an important regulator of endothelial cell function, angiogenesis and vascular development [98, 99]. Endothelial cells lacking RAC1 revealed reduced tubulogenesis, migration and permeability in response to vascular endothelial growth factor (VEGF) [100, 101]. Mice with endothelial cell specific excision of Rac1 showed embryonic

lethality and massive developmental disorders, thereby exhibiting an impaired development of major vessels and lack of small vessels [102]. RAC1 is also involved in vascular tone and pressure, as Shirai *et al.* suggested a RAC1-dependent regulation of nitric oxide in vascular smooth muscle cells and both vasodilator and vasoconstrictor effects of RAC1 have been reported [103–105].

Zebrafish studies described Elmo1 also as promotive regulator of vascular development. It is highly expressed in embryonic vascular structures and regulates Rac1 activity in endothelial cells [46]. Vascular formation was shown to be reduced through Elmo1 silencing and it was suggested that Elmo1 mediates angiogenesis induction by Rac1 activation. Furthermore, Elmo1 supports the formation of blood vessels through reduction of endothelial cell apoptosis [71].

1.4 ELMOs and RAC1 in kidney function and disease

The kidney is one of the major organs in vertebrates, such as humans, mice and zebrafish, and functions as a blood filtration system [106]. The main functions of the kidney are the maintenance of various electrolyte concentrations, water content, fluid osmolarity and acid-base balance, as well as the removal of metabolite byproducts and toxins [107, 108]. In humans and mice, the kidney parenchyma is divided into the outer renal cortex and the inner renal medulla, in which the functional units of the kidney, the nephrons, are located [106, 109–112]. A nephron consists of a renal corpuscle and a renal tubule [107]. The renal corpuscle is located at the beginning of the nephron and is built up of a glomerulus, which is a network of capillary slings, and the beginning of the proximal tubule, which lies around the glomerulus and forms the Bowman space [113]. The glomerular capillaries are covered with podocyte foot processes. Between the podocytes and the capillaries, there is an extracellular matrix layer, the glomerular basement membrane (GBM) [114, 115]. Together with the fenestrated capillary endothelium and the filtration slits, which lay between the podocyte foot processes at the GBM, it represents the filtration unit [116, 117]. Through this filter the capillary blood from the glomerulus gets filtrated and water and other small substances, such as glucose, minerals, amino acids and urea pass the filtration barrier and end up as primary urine in the Bowman space [107, 118]. The primary urine then passes through the different parts of the tubule, such as proximal tubule, Henle's loop and distal tubule, where useful substances as ions and metabolites, together with water, get reabsorbed and led back to the blood [106, 111]. Several tubules lead to one collecting duct, which

also takes part in reabsorption [108]. In the tubule compartments and the collecting duct, the primary urine gets concentrated to the secondary urine, which then exits the kidney through the renal pelvis [112].

During the development of humans and mice, three kidney generations are formed. In embryos, the pronephros is built and develops to the second embryonic kidney generation, the mesonephros [110, 119–121]. The mesonephros then develops to the metanephros, the third and final kidney generation. The zebrafish kidney is somehow different as after the embryonic pronephros, the kidney development stops at the mesonephros, which represents the final kidney form in adult zebrafish [122–124]. The zebrafish mesonephros exhibits mainly structural differences in the kidney parenchyma but it does, especially functionally, not significantly differ from the metanephros of other vertebrates, as they all use nephrons with highly similar molecular and segmental organization as filtration unit [123, 125–127].

Regarding kidney development and disease, RAC1 has mainly been described in podocyte related research. It contributes to podocyte cytoskeleton reorganization through its role in actin cytoskeleton dynamics [128–130]. Studies which investigated the development of renal diseases described RAC1 activity as either beneficial or deleterious. Increased activity in mouse podocytes led to proteinuria and podocyte foot process effacement [131, 132] and reduced activity in podocytes in mice led to an impaired glomerular repair and to more severe changes in kidneys developing glomerulosclerosis [133]. On the other hand, inhibition of RAC1 in mice protected them from podocyte injury and glomerulosclerosis [134, 135].

All three ELMO proteins have also been associated with nephropathy but predominantly in the context of diabetes. The role of the ELMO proteins in kidney and kidney disease development are mainly unknown but multiple studies report a susceptibility of diabetes patients to develop nephropathy when one of the ELMO proteins is mutated [62, 72–78]. Furthermore, the presence of ELMO1 was shown to be adverse during the development of nephropathy, aggravating pathological changes as thickening of the GBM [61]. Shimazaki *et al.* suggested that ELMO1 participates in the development of glomerular injury through a dysregulation of the extracellular matrix (ECM) [136].

1.5 ELMOs and RAC1 in insulin mediated glucose uptake and diabetes mellitus

Diabetes is a metabolic disease caused by an impaired insulin secretion or impaired insulin sensitivity which leads to an increase of the blood glucose level [137]. Insulin is a hormone produced by the beta cells located in the pancreatic islets. It gets secreted into the blood and together with its antagonist hormone glucagon, it represents the primary regulatory system of the blood glucose level [138]. Insulin binds to insulin receptor proteins located at the cell surface of target cells, such as skeletal muscle cells initiating a signaling cascade in which glucose transporter 4 (GLUT4) containing vesicles are translocated and fuse with the cell membrane [139, 140]. This results in an increased glucose influx from the blood into the cell. In diabetes mellitus, this sensible insulin-regulated glucose uptake is impaired resulting in hyperglycemia. The two predominant types of diabetes are type one diabetes (T1D) and type two diabetes (T2D) [141]. T1D is caused by the destruction of the insulin producing beta cells in the pancreas through the immune system, leading to hypoinsulinemia [142, 143]. T2D is caused by a disturbed insulin sensitivity of cells, mainly skeletal muscle cells, adipocytes and liver cells, leading to decreased uptake of glucose from the blood [137]. This insulin resistance triggers a feedback loop which causes an overproduction of insulin in the beta cells attempting to compensate the impaired glucose uptake. The overstraining of the beta cells leads to a period of hyperinsulinemia and ultimately to their death and a consequent hypoinsulinemia, which results in a permanent hyperglycemia.

Hyperglycemia can, besides other factors, cause diabetic complications like neuropathy, retinopathy and nephropathy [144]. It promotes glycation of proteins, protein cross-linking and the generation of advanced glycated end products (AGES) and ROS [145, 146]. As a result of these processes, prolonging hyperglycemia leads to damage in tissues such as the vasculature, causing microvascular complications [147, 148]. One of these microvascular changes is the thickening of the capillary basement membrane, especially in glomerular arterioles, retina, myocardium, skin and muscles. This leads to microangiopathy, altered blood vessel functions, apoptosis, leakage through damaged vessels and eventually to the death of small blood vessels [146, 149]. This results in impaired organ perfusion and thus in insufficient oxygen supply. Especially organs depending on an extensive microvascular oxygen supply, namely retina, kidney and the nervous system get damaged [146]. In a diabetic state, hyperglycemia causes glycation of neurons and oxidative stress in the peripheral

nervous system. This and the reduction of the oxygen supply results in neuron damage and neurodegeneration [150]. In the retina, increased blood glucose levels lead to apoptosis of pericytes and endothelial cells, reduced blood vessel stability and hemorrhage through vessel leakage. A following insufficient oxygen supply promotes angiogenesis and thus the proliferation of blood vessels and increased bleeding, both leading to a decrease of eyesight [148, 149]. In the glomeruli in the kidney, diabetes can cause a thickening of the glomerular basement membrane, mesangial expansion and damage to the podocyte foot processes [151, 152]. Subsequently, hypertonia and hyperfiltration develop, leading to the death of podocytes and endothelial cells and to the collapse of the glomerular filtration barrier [149]. A prolonged exposure to these conditions can lead to an impairment and eventually to a total loss of the organ function with dramatic consequences for health.

Through its function as regulator of fundamental cell mechanisms, RAC1 affects several processes involved in the development of diabetes and diabetic complications. The RAC1 dependent actin cytoskeleton reorganization of the pancreas and the pancreatic islets is crucial for the glucose induced transport of insulin vesicles and the subsequent insulin secretion [1, 153]. In skeletal muscle cells the insulin dependent RAC1 activation correlates with membrane translocation of GLUT4 and glucose uptake [79, 154]. Additionally, a reduced RAC1 activity in skeletal muscle cells is associated with insulin resistance. Improved RAC1 activation due to diabetic hyperglycemia mediates the activation of NOX leading to ROS production and the subsequent development of diabetic retinopathy [27, 155] and nephropathy [26, 156].

The ELMO proteins themselves were also linked to diabetes relevant mechanisms, especially to the development and progression of diabetic nephropathy (DN). Worldwide genetic studies in humans reported a susceptibility to develop diabetic nephropathy of diabetic patients with *ELMO* gene variants, predominantly single nucleotide polymorphisms (SNPs). This was mostly found in patients with variants of *ELMO1* [62, 72–76, 78], but also in patients with variants of *ELMO2* [77] and *ELMO3* [78]. These findings suggest a contribution of dysfunction of the *ELMO* gene family in the development of diabetic nephropathy. Studies analyzing the role of the ELMO1 protein in renal disease pathogenesis described the development of nephropathy in mice with T1D, dependent on ELMO1 [61, 62]. It was aggravated by the presence and ameliorated by the absence of ELMO1. Moreover, one study reported an involvement of ELMO2 in glucose metabolism, as insulin regulates the localization and membrane

translocation of ELMO2, and ELMO2 regulates the insulin dependent RAC1 activation and membrane translocation of GLUT4 in human muscle cells and adipocytes [79].

1.7 Zebrafish as a model organism in general and diabetes research

Danio rerio (zebrafish) belongs to the family of *Cyprinidae* and is a freshwater fish native in South Asia [157]. Due to several characteristics which make it easy and beneficial to work with, it is broadly used in laboratories as a vertebrate model organism for scientific research [158]. It needs little maintenance and husbandry care, has a short generation time of approximately three months and due to its high fertility and the external fertilization of eggs, adult animals can be mated and offspring collected once per week. With the possibility to get up to 300 eggs per mating, the zebrafish is optimal for high throughput screenings, where many animals or multiple conditions are needed. Drug testing with zebrafish larvae is also a common approach as the incubation through the surrounding medium ensures an even distribution and dosage of the tested compound. Zebrafish embryos and larvae are optimal for developmental and functional studies *in vivo* as embryos and early larvae are transparent [159]. In combination with reporter lines causing the expression of fluorescent proteins in specific cells and organs, it provides ideal possibilities for *in vivo* analyses and imaging. Further, zebrafish develop rapidly, reaching an organism with a general body plan within 24 hours and preliminary organs within 48 hours [160]. In addition, zebrafish have organs such as heart, liver, kidney, skeletal muscle and eye, as well as a closed circulatory system, a neuronal and a hormone system [123, 125, 161]. Therefore and due to its genome sharing an identity of 70 % with the human genome [162], it is a suitable model for disease-oriented research. This genome and the respective transcriptome can be manipulated by different approaches, as RNA-morpholinos are common tools to generate a transient gene expression knockdown [163] and permanent mutations can be created by TALENs (transcription activator-like effector nucleases) [164] or the CRISPR/Cas9 (clustered regularly interspaced short palindromic repeats/CRISPR-associated protein-9 nuclease) system [165, 166]. For diabetes research the zebrafish is attractive because of the presence of all major organ systems commonly affected by diabetic microvascular complications, insulin sensitive tissues [167] and a pancreas, an insulin signaling pathway and a glucose metabolism comparable to humans [168–170]. Furthermore, it was shown that zebrafish can develop hyperglycemia and subsequent alterations in the kidney, the retina and the neuron system [171–176].

1.8 Aim of the thesis

The individual ELMO proteins have been shown to regulate a variety of cell functions but these regulations are hardly understood. Since existing studies generally describe the function of only one specific ELMO family member and barely any studies cover comparative data about all three, it is mostly unknown whether ELMO1, ELMO2 and ELMO3 share described functions of one ELMO variant or not. Furthermore, most ELMO studies used variable research topics and inconsistent experimental parameters, which makes a comparison of the findings difficult. To address the question, if ELMO proteins function redundantly and to explore and identify new functions of the ELMO proteins, I generated *elmo1*, *elmo2* and *elmo3* single knockout zebrafish lines, which lack either the Elmo1, Elmo2 or Elmo3 protein. The aim of this thesis was to determine and then compare the phenotypical changes of the three lines. Besides basal characterization, morphological analyses of the larval and adult vasculature and of the adult renal and glomerular structure should be performed. Furthermore, the larval transcriptome and aspects of the metabolome and the glucose metabolism should be investigated

2 Results

Parts of this chapter have been published in the following publication in *Frontiers in Cell and Developmental Biology* in 2022 and have been originally written by myself.

Comparative morphological, metabolic and transcriptome analyses in *elmo1*^{-/-}, *elmo2*^{-/-} and *elmo3*^{-/-} zebrafish mutants identified a functional non-redundancy of the Elmo proteins

Mike Boger, Katrin Bennewitz, David Philipp Wohlfart, Ingrid Hausser, Carsten Sticht, Gernot Poschet, Jens Kroll

2.1 Zebrafish Elmo1, Elmo2 and Elmo3 show structural differences in the amino acid sequence

The first step of the comparative analysis of the Elmo proteins was to analyze them on a structural basis, therefore comparing the amino acid sequences of zebrafish Elmo1, Elmo2 and Elmo3 including their functional domains. Elmo proteins contain an armadillo-like helical domain of unknown function, an ELMO domain which function is also largely unknown and a pleckstrin homology domain regulating the interaction with Dock proteins to promote Rac1 [34, 39, 41–43]. A subsequent alignment of the amino acid sequences of Elmo1, Elmo2 and Elmo3 showed a shared identity of 43 % within all three proteins (Figure 1). Similarly to zebrafish, human ELMO1, ELMO2 and ELMO3 exhibited an identity of 45 % in amino acid sequence (Supplementary Figure 1). It is currently elusive whether known functions of the human ELMO proteins can be transferred to zebrafish Elmo proteins, however based on the structural similarity, a functional similarity is possible. Zebrafish Elmo1 and Elmo2 displayed an identity of 63 %, Elmo1 and Elmo3 58 % and Elmo2 and Elmo3 50 % in the amino acid sequence. The armadillo-like helical domain was 41 % identical, the ELMO domain is 40 % identical and the pleckstrin homology domain shares 58 % identity between Elmo1, Elmo2 and Elmo3 [34, 39, 41–43]. Despite the described similarities, the amino acid sequences exhibited remarkable differences, therefore, zebrafish Elmo1, Elmo2 and Elmo3 are not highly conserved and a functional difference between the different Elmo proteins can be expected.

2.2 Generation of *elmo1*^{-/-}, *elmo2*^{-/-} and *elmo3*^{-/-} zebrafish lines

elmo1, *elmo2* and *elmo3* knockout zebrafish lines were generated using the CRISPR/Cas9 system in the reporter line *Tg(fli1:EGFP)*. These transgenic lines were used to investigate the functions of Elmo1, Elmo2 and Elmo3 through the consequences of the loss of each protein. For each gene two fish lines with different mutations which lead to possible frameshifts were generated. One of these mutant lines was selected as working line for experiments. All generated results presented in this study were generated using this fish line if not mentioned separately. The other line was kept as backup. The induced frameshift mutations of the mutated fish lines resulted in an early stop codon in the mRNA sequence and therefore in a premature termination of the translation (Figure 2A,B,C). For the *elmo1*^{-/-} working line, a 10 base pair (bp) insertion (Figure 2A) and for the backup line a 19 bp deletion respectively in exon 2 were induced (Supplementary Figure 2A,D). For the *elmo2*^{-/-} working line, a 17 bp deletion (Figure 2B) and for the backup line a 10 bp deletion respectively in exon 9 were induced (Supplementary Figure 3A,D). For the *elmo3*^{-/-} working line, a 10 bp deletion (Figure 2C) and for the backup line a 5 bp deletion respectively in exon 2 were induced (Supplementary Figure 4A,D). The working line mutation in *elmo1* is predicted to lead to a 16 amino acids short version of the Elmo1 protein lacking all three known domains. The working line mutation in *elmo2* is predicted to lead to a 324 amino acids short version of the Elmo2 protein lacking the majority of the ELMO domain and the entire PH domain. The working line mutation in *elmo3* is predicted to lead to a 30 amino acids short version of the Elmo3 protein lacking all three domains. Therefore, the created premature-translation-termination codons in *elmo1*^{-/-}, *elmo2*^{-/-} and *elmo3*^{-/-} zebrafish led to remaining peptides which cannot be functional and result in the loss of the respective protein's function.

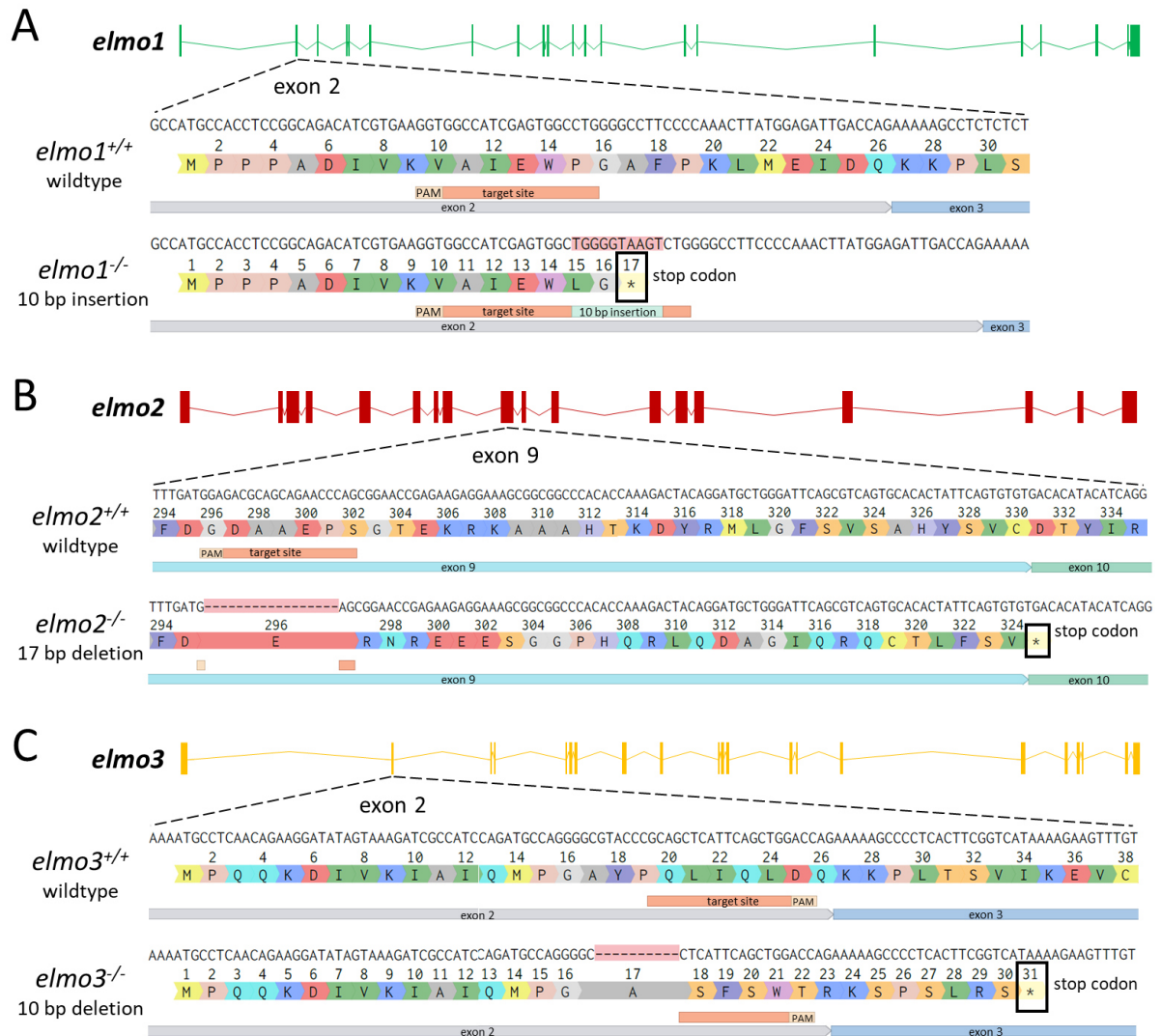


Figure 2. Generation of *elmo1*, *elmo2* and *elmo3* knockout zebrafish lines with the CRISPR/Cas9 system. (A) Exon map of the zebrafish *elmo1* gene (ensembl transcript ID: ENSDART00000172618.2) and the position of the CRISPR target site designed for zebrafish *elmo1* targeting exon 2. The cDNA sequence and the resulting amino acid sequence of *elmo1*^{+/+} and the generated *elmo1*^{-/-} line with a 10 bp insertion. The resulting stop codon is indicated with a star. **(B)** Exon map of the zebrafish *elmo2* gene (ensembl transcript ID: ENSDART00000162982.2) and the position of the CRISPR target site designed for zebrafish *elmo2* targeting exon 9. The cDNA sequence and the resulting amino acid sequence of *elmo2*^{+/+} and the generated *elmo2*^{-/-} line with a 17 bp deletion. The resulting stop codon is indicated with a star. **(C)** Exon map of the zebrafish *elmo3* gene (ensembl transcript ID: ENSDART00000061738.7) and the position of the CRISPR target site designed for zebrafish *elmo3* targeting exon 2. The cDNA sequence and the resulting amino acid sequence of *elmo3*^{+/+} and the generated *elmo3*^{-/-} line with a 10 bp deletion. The resulting stop codon is indicated with a star. PAM, protospacer adjacent motif.

2.3 Validation of *elmo1*^{-/-}, *elmo2*^{-/-} and *elmo3*^{-/-} zebrafish lines on DNA, RNA and protein level

All six mutations were verified by sequencing genomic DNA (Supplementary Figure 2-4). To prove the loss of the respective protein in the mutated lines, Western Blot analyses with antibody staining against zebrafish Elmo1, Elmo2 and Elmo3 were done with protein lysates of different organs from adult *elmo1*^{+/+}, *elmo1*^{-/-}, *elmo2*^{+/+}, *elmo2*^{-/-}, *elmo3*^{+/+} and *elmo3*^{-/-} zebrafish. The loss of the Elmo1 protein could be shown in the brain and the eyes of both *elmo1*^{-/-} zebrafish lines (Figure 3). Due to the fact that the used antibody was designed against a mouse epitope, the staining showed unspecific binding effects of the antibody which were visible as additional bands, which was also reported from Elliott *et al.* [53]. The antibody staining against Elmo2 and Elmo3 was not successful. Antibodies against all commercially available epitopes of ELMO2 and ELMO3 were used but most likely due to species differences, none of them bound against the respective zebrafish protein.

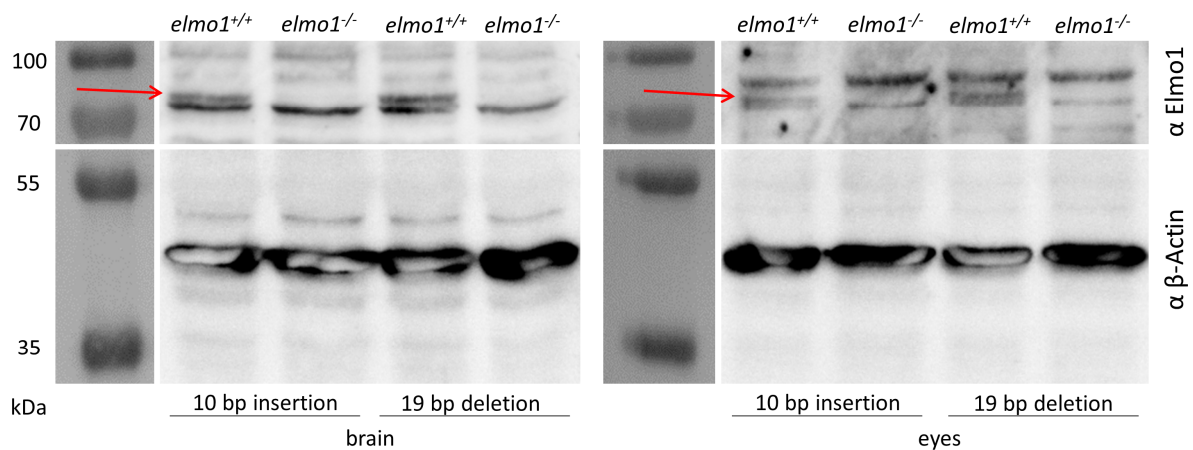


Figure 3. Validation of the loss of the Elmo1 protein in the *elmo1*^{-/-} zebrafish lines. Western Blot analyses with protein lysates of total brain (left) and eyes (right) with subsequent antibody staining against the Elmo1 (up) and the β -Actin (down) protein showed the loss of the Elmo1 protein in the 10 bp deletion and in the 19 bp deletion *elmo1*^{-/-} zebrafish lines. The protein masses of the Elmo1 isoforms are 83.9, 83.9 and 85.4 kDa. The protein mass of β -Actin is 41.8 kDa. Elmo1 protein bands are indicated with a red arrow. bp, base pair; kDa, kilodalton.

Because proving the loss of the Elmo2 protein in *elmo2*^{-/-} zebrafish and the Elmo3 protein in *elmo3*^{-/-} zebrafish was not possible, each working line mutation was additionally validated on RNA level by RT-PCR of the respective gene and its transcripts and subsequent gel electrophoretic segregation (Figure 4A,B,C).

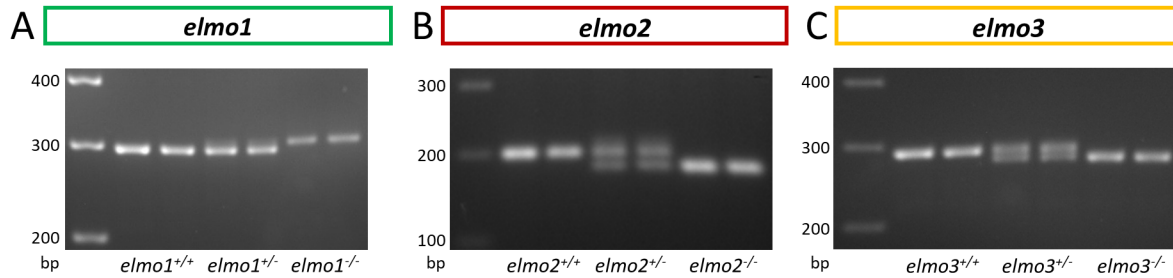


Figure 4. Validation of *elmo1*, *elmo2* and *elmo3* mutations in zebrafish lines at RNA level. (A) The 10 base pair insertion in *elmo1* was confirmed on RNA level by gel electrophoretic segregation of PCR products of cDNA which was synthesized from mRNA from *elmo1*^{+/+}, *elmo1*^{+/-} and *elmo1*^{-/-} larvae at 120 hpf. PCR product size: wild type 298 bp, homozygous 308 bp. **(B)** The 17 base pair deletion in *elmo2* was confirmed on RNA level by gel electrophoretic segregation of PCR products of cDNA which was synthesized from mRNA from *elmo2*^{+/+}, *elmo2*^{+/-} and *elmo2*^{-/-} larvae at 120 hpf. PCR product size: wild type 198 bp, homozygous 181 bp. **(C)** The 10 base pair deletion in *elmo3* was confirmed on RNA level by gel electrophoretic segregation of PCR products of cDNA which was synthesized from mRNA from *elmo3*^{+/+}, *elmo3*^{+/-} and *elmo3*^{-/-} larvae at 120 hpf. PCR product size: wild type 290 bp, homozygous 280 bp. bp, base pair; hpf, hours post fertilization; PCR, polymerase chain reaction. Data were jointly produced with Katrin Bennewitz.

2.4 The loss of *Elmo3* led to a decreased survival rate

In embryonic and larval development, gross morphology and viability of *elmo1*^{-/-}, *elmo2*^{-/-} and *elmo3*^{-/-} zebrafish appeared unaltered compared to their wild type littermates until 120 hours post fertilization (hpf) (Figure 5). Adult animals also showed no differences in their general morphology. Analysis of genotypes of heterozygous incrosses revealed the expected distribution equal to the Mendelian inheritance of *elmo3* larvae (120 hpf) and of adult (3 months post fertilization (mpf)) *elmo1* and *elmo2* animals (Figure 6A). However, *elmo3* adults (3 mpf) showed an altered genotype distribution with 32 % *elmo3*^{+/+}, 55 % *elmo3*^{+/-} and 13 % *elmo3*^{-/-} animals. This result observed in the *elmo3* working line (10 bp deletion) was supported by the *elmo3* backup line (5 bp deletion) which had a similar distribution with 31 % *elmo3*^{+/+}, 57 % *elmo3*^{+/-} and 12 % *elmo3*^{-/-}. A subsequent analysis starting from 3 mpf found a significant and progressive decrease in the survival rate of *elmo3*^{-/-} zebrafish (Figure 6B). In conclusion the analysis revealed a normal development and viability of *elmo1*^{-/-} and *elmo2*^{-/-} zebrafish, but a reduced viability of *elmo3*^{-/-} mutants in adulthood.

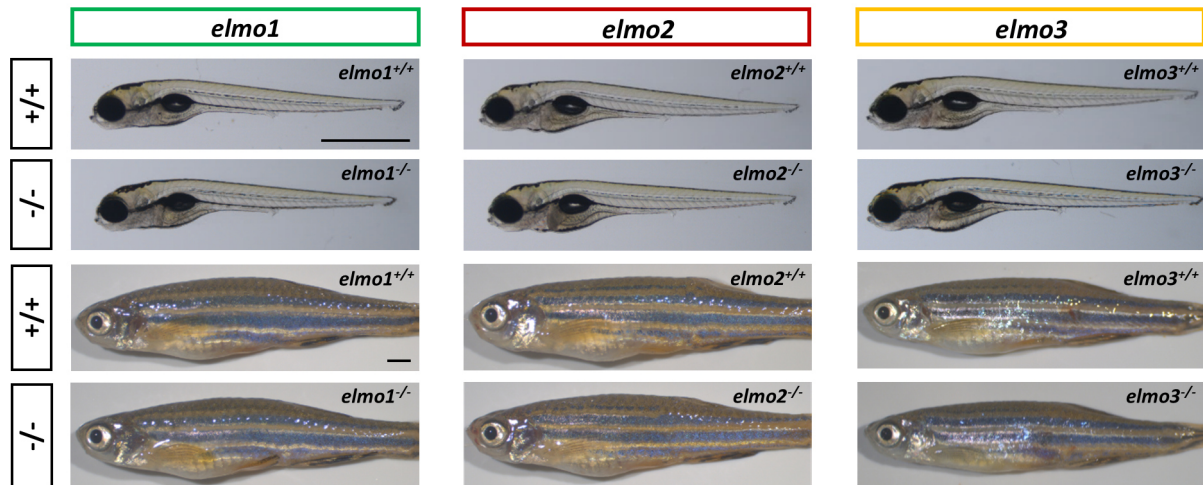


Figure 5. The general morphology was not changed between wild type and homozygous *elmo1*, *elmo2* and *elmo3* mutant zebrafish in larval and adult stage. Representative light microscopy pictures of larvae at 120 hpf and adults (8–13 mpf) of *elmo1*^{+/+}, *elmo1*^{-/-}, *elmo2*^{+/+}, *elmo2*^{-/-}, *elmo3*^{+/+} and *elmo3*^{-/-} zebrafish. Scale bar is 1 mm. hpf, hours post fertilization; mpf, months post fertilization.

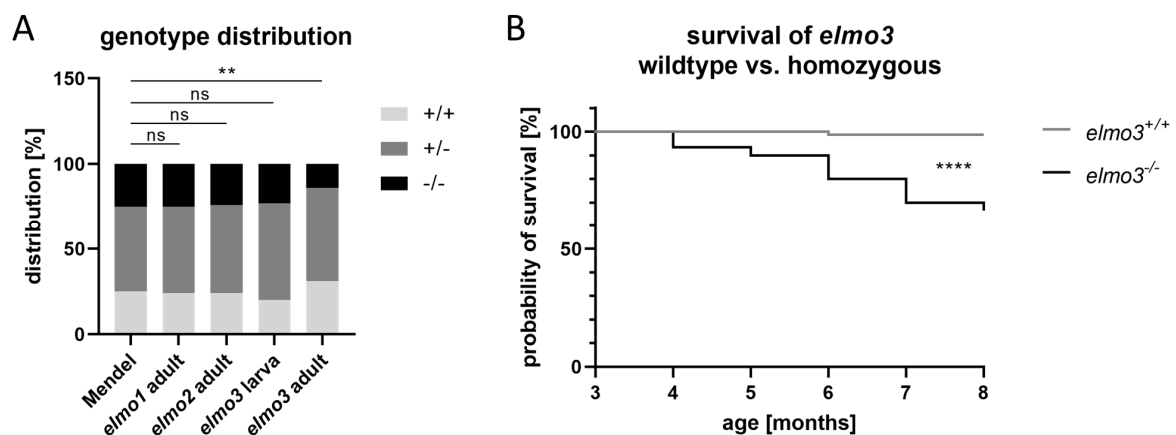


Figure 6. The loss of Elmo3 led to a reduced survivability of *elmo3*^{-/-} zebrafish. **(A)** Genotype distribution of Mendelian inheritance and the filial generation of *elmo1* ($n = 358$), *elmo2* ($n = 354$) and *elmo3* ($n_{\text{larva}} = 100$, $n_{\text{adult}} = 224$) after heterozygous *inter se* crossings. Age of adults was 3 mpf and age of larvae was 120 hpf. The genotype distribution in *elmo3* adults was altered to the Mendelian inheritance. **(B)** Reduced survival rate of adult *elmo3*^{-/-} ($n = 30$) compared to *elmo3*^{+/+} ($n = 74$) zebrafish over the age of 3 to 8 months. Statistical analysis was done with chi-square test and logrank test. ** $p < 0.01$, **** $p < 0.0001$. ns, not significant; bp, base pair; hpf, hours post fertilization; mpf, months post fertilization.

2.5 Analyses of the *elmo* expression patterns in wild type and *elmo1*^{-/-}, *elmo2*^{-/-} and *elmo3*^{-/-} zebrafish

Due to the homology within the Elmo protein family in zebrafish (Figure 1), RT-qPCR was applied to assess the expression of the *elmo* genes in developing larvae and in adult organs in wild types (Figure 7) and to examine if they compensate for each other in *elmo1*^{-/-}, *elmo2*^{-/-} and *elmo3*^{-/-} at 120 hpf, respectively (Figure 8). In wild type zebrafish larvae the expression of *elmo1* was over ten times higher than the expression of *elmo2* and over five times higher than the expression of *elmo3* over the first five days of development (Figure 7A). This was also measured in adult eyes and kidneys, where *elmo1* RNA levels were over twenty times higher than those of *elmo2* and *elmo3* in the eyes and over ten times higher in the kidney (Figure 7B). Likewise, the expression levels of *elmo2* and *elmo3* differ from each other in larvae at 24 and 48 hpf and in the adult eye and kidney. These differences between the expression levels of *elmo1*, *elmo2* and *elmo3* could be a possible indicator for varying functions of the three proteins in the early development as well as in adult organs. In *elmo1*^{-/-} mutant larvae *elmo1* RNA levels were decreased (Figure 8A) and in *elmo2*^{-/-} mutant larvae *elmo2* RNA levels were decreased at 120 hpf (Figure 8B), whereas *elmo3* RNA was not changed in *elmo3*^{-/-} mutant larvae (Figure 8C). Mutations which lead to a premature-translation-termination codon can cause transcript degradation by nonsense-mediated decay or reduced transcription by epigenetic silencing [177–179]. Likewise, the mutated RNA can be insensitive, escape or not trigger this event [180–182]. Remarkably, *elmo1* expression was increased in *elmo2*^{-/-} larvae (Figure 8B) which could indicate a compensatory mechanism of Elmo1 during a loss of Elmo2, hinting at a functional similarity.

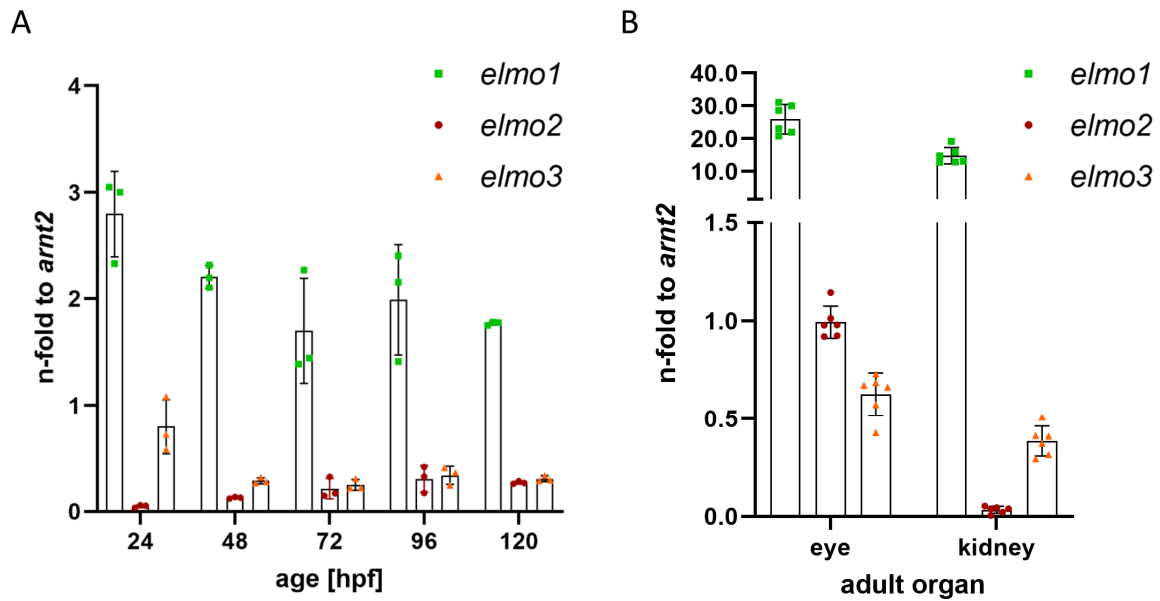


Figure 7. Differential expression of *elmo1*, *elmo2* and *elmo3* in development and in adult eyes and kidneys of wildtype zebrafish. (A) Over the first five days of development of wildtype zebrafish larvae, *elmo1* RNA levels were much higher than *elmo2* and *elmo3*. $n = 3$ samples per group, each containing 30 larvae. **(B)** In adult wildtype zebrafish eyes and kidneys (13 mpf) *elmo1*, *elmo2* and *elmo3* RNA levels differ from each other. $n = 6$ samples per organ type. RNA levels were quantified with RT-qPCR and compared with *arnt2*. hpf, hours post fertilization; mpf, months post fertilization. Data were jointly produced with David Wohlfart and Haozhe Qi.

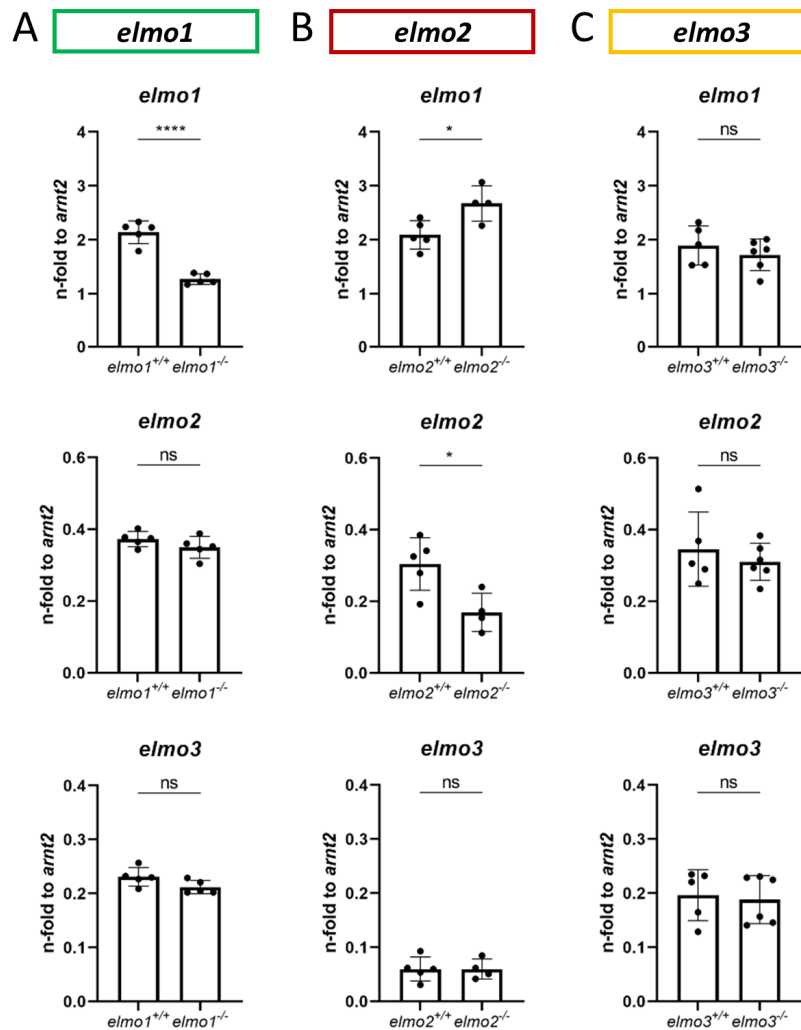


Figure 8. Indicated compensation of *elmo1* in *elmo2*^{-/-} zebrafish larvae due to increased *elmo1* RNA levels. (A) Quantification of RNA levels of *elmo1*, *elmo2* and *elmo3* at 120 hpf showed a decline of *elmo1* RNA levels in *elmo1*^{-/-} compared to *elmo1*^{+/+}. n = 5 samples per group, each containing 30 larvae. **(B)** Quantification of RNA levels of *elmo1*, *elmo2* and *elmo3* at 120 hpf showed an increase of *elmo1* RNA levels and a decrease of *elmo2* RNA levels in *elmo2*^{-/-} compared to *elmo2*^{+/+}. n = 5 samples per group, each containing 30 larvae. **(C)** Quantification of RNA levels of *elmo1*, *elmo2* and *elmo3* at 120 hpf showed no changes in *elmo3*^{-/-} compared to *elmo3*^{+/+}. n = 5-6 samples per group, each containing 30 larvae. RNA levels were quantified with RT-qPCR and compared with *arnt2*. Statistical analysis was done with t-test and Mann-Whitney test. * p < 0.05, **** p < 0.0001. ns, not significant; hpf, hours post fertilization.

2.6 Differential changes in vascular structures in *elmo1*^{-/-}, *elmo2*^{-/-} and *elmo3*^{-/-} zebrafish

Recent reports have shown that the Elmo1 mediated Rac1 activation during angiogenesis induces and maintains the formation of the zebrafish vasculature [46, 71]. Furthermore, RAC1 positively regulated angiogenesis and the loss of RAC1 led to strong vascular alterations in embryonic mice [102]. To address which impact a loss of Elmo1, Elmo2 or Elmo3 may have on the vasculature in zebrafish, the larval trunk vasculature (96 hpf) (Figure 9), the larval hyaloid vasculature (120 hpf) (Figure 10) and the adult retinal vasculature (9-15 mpf) (Figure 11) was analyzed in *elmo1*^{-/-}, *elmo2*^{-/-} and *elmo3*^{-/-} zebrafish. For this purpose, the mutant lines were generated using the *Tg(fli1:EGFP)* zebrafish line. This vascular reporter line is characterized by the expression of enhanced green fluorescent protein in endothelial cells which enables a visualization and analysis of vascular structures by fluorescent light [183].

The trunk vasculature in *elmo1*^{-/-}, *elmo2*^{-/-} and *elmo3*^{-/-} larvae (Figure 9A-D) appeared mostly unaltered. Solely the number of additional sprouts between the ISVs was decreased in *elmo1*^{-/-} compared to *elmo1*^{+/+} larvae (Figure 9B). However, at 32 hpf, *elmo1*^{-/-} zebrafish larvae displayed a developmental delay of the trunk vasculature compared to *elmo1*^{+/+}, which was expressed in ISV formation defects and additional sprouts (Supplementary Figure 5A-C) but not present anymore at 96 hpf.

The vasculature of the hyaloids, the precursor of the retinal vasculature [184], of *elmo1*^{-/-}, *elmo2*^{-/-} and *elmo3*^{-/-} larvae exhibited no changes in branching and sprouting respectively compared to *elmo1*^{+/+}, *elmo2*^{+/+} and *elmo3*^{+/+} (Figure 10). Interestingly, both *elmo1*^{-/-} and *elmo3*^{-/-} zebrafish revealed an increase in vessel diameter (Figure 10A,C,D,F).

In contrast, in the adult retinal vasculature (Figure 11A), branches and sprouts were decreased in *elmo1*^{-/-} zebrafish compared to *elmo1*^{+/+} (Figure 11B,C,H). In *elmo2*^{-/-} zebrafish, branches were unchanged, but sprouts were decreased compared to *elmo2*^{+/+} (Figure 11D,E,I). Contrary to the reduced vascular formation in *elmo1*^{-/-} retinae, in *elmo3*^{-/-} zebrafish, retinal branches increased and sprouts showed no change compared to *elmo3*^{+/+} (Figure 11F,G,J).

Additional analyses of the permeability of hyaloid vessels of *elmo2*^{+/+} and *elmo2*^{-/-} larvae at 120 hpf (Supplementary Figure 6) and of the vascular density in adult brains (Supplementary Figure 7) of *elmo2*^{+/+} and *elmo2*^{-/-} zebrafish showed no alterations.

Together, the data in the *elmo1*^{-/-}, *elmo2*^{-/-} and *elmo3*^{-/-} zebrafish mutants revealed different phenotypic alterations in the trunk, hyaloid and retinal vasculature, which suggests all three Elmo proteins as regulators of the vasculature modulating similar and diverse processes in vascular development and morphogenesis.

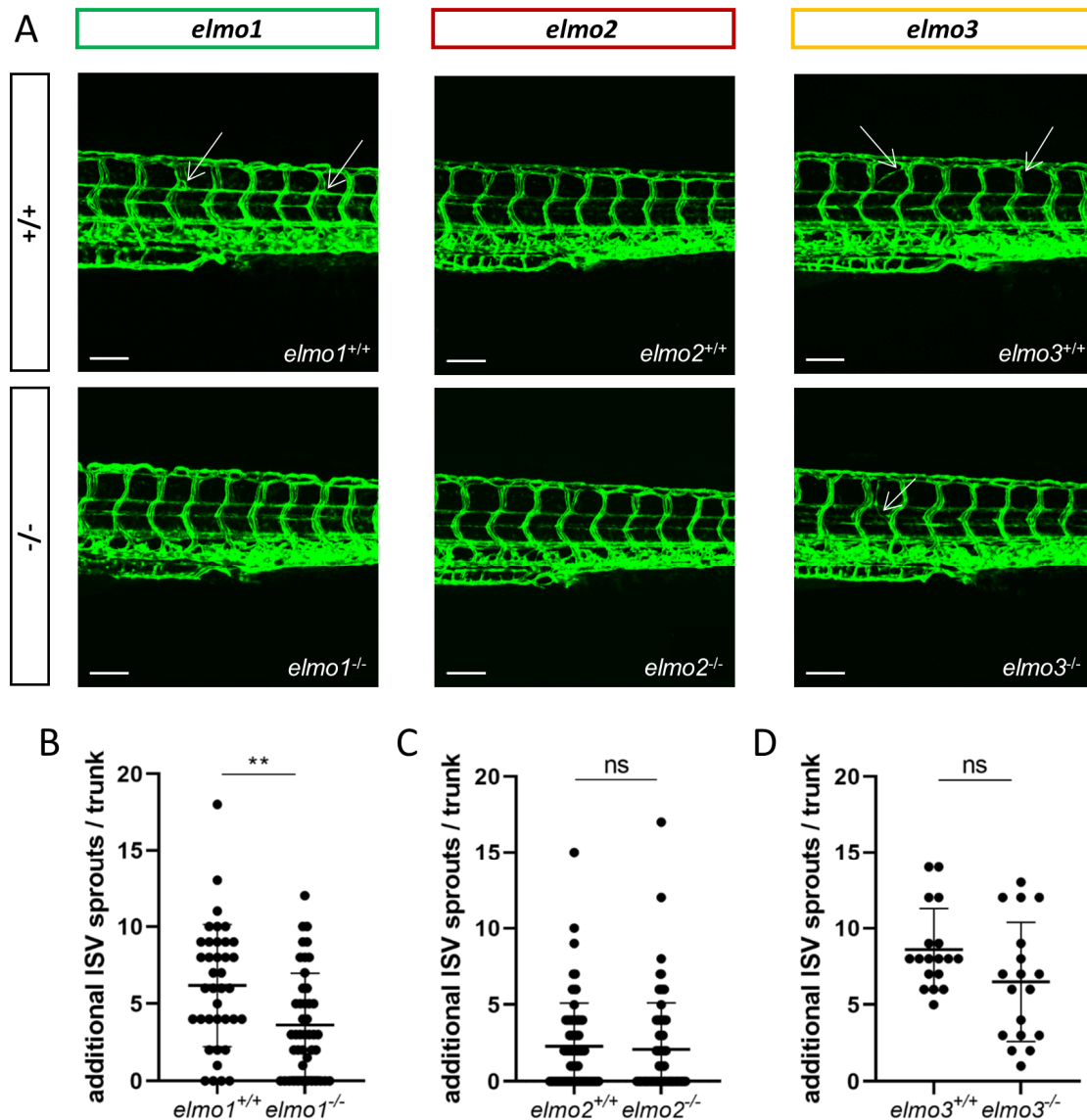


Figure 9. The loss of Elmo1 led to decreased sprouts in the larval trunk vasculature in zebrafish at 96 hpf. (A) Representative confocal microscopy images of the trunk vasculature of *elmo1*^{+/+} and *elmo1*^{-/-} (left), *elmo2*^{+/+} and *elmo2*^{-/-} (middle) and *elmo3*^{+/+} and *elmo3*^{-/-} (right) zebrafish larvae at 96 hpf. Additional ISV sprouts are indicated with a white arrow. Scale bar is 100 μ m. **(B)** Quantification of additional sprouts at trunk ISVs of larvae at 96 hpf showed decreased sprouts in *elmo1*^{-/-} compared to *elmo1*^{+/+}. n = 38-44 trunks per group. **(C)** Quantification of additional sprouts at trunk ISVs of larvae at 96 hpf showed no alterations in *elmo2*^{-/-} compared to *elmo2*^{+/+}. n = 69-82 trunks per group. **(D)** Quantification of additional sprouts at trunk ISVs of larvae at 96 hpf showed no alterations in *elmo3*^{-/-} compared to *elmo3*^{+/+}. n = 18 trunks per group. Statistical analysis was done with Mann-Whitney test. ** p < 0.01. ns, not significant; hpf, hours post fertilization; ISV, intersegmental vessel.

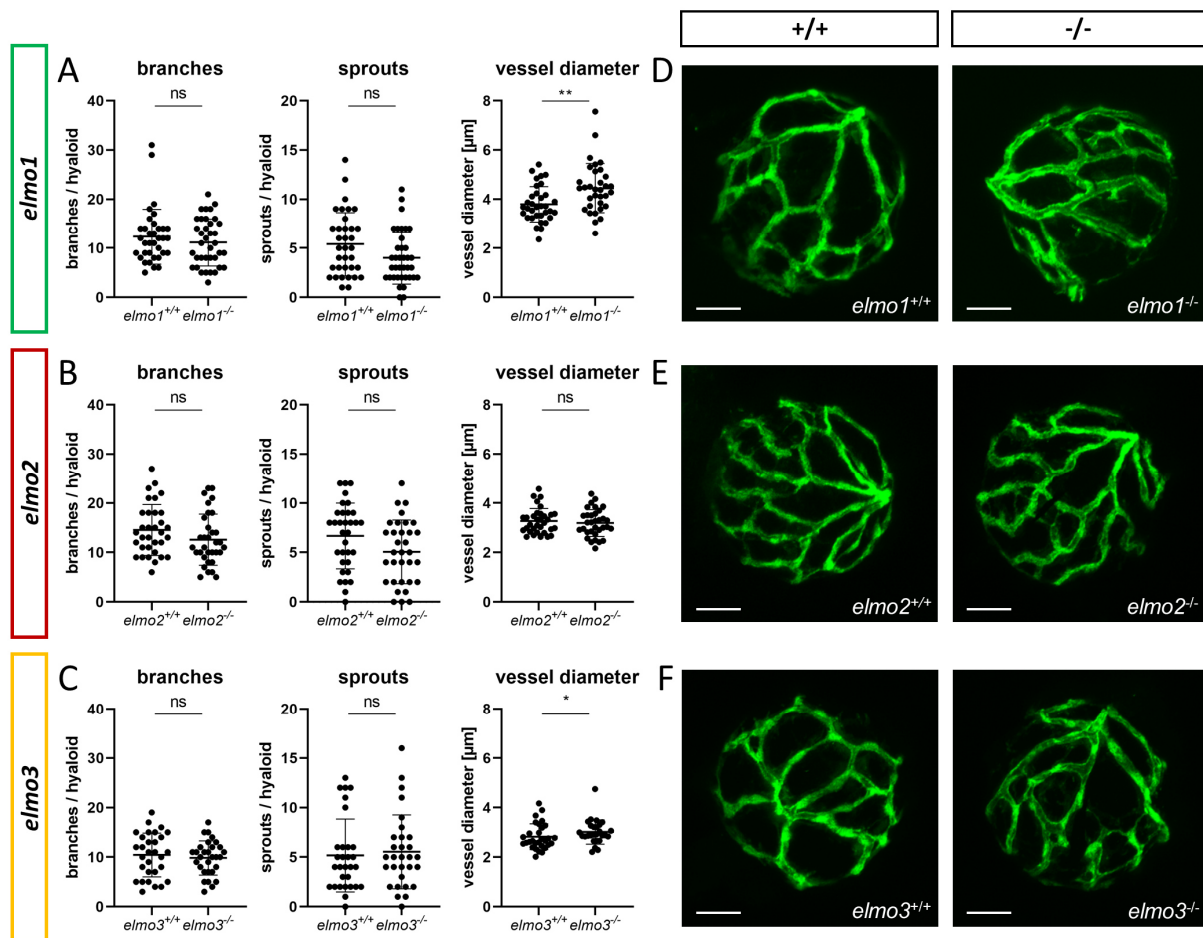


Figure 10. The loss of Elmo1 and Elmo3 respectively led to an increased diameter of hyaloid blood vessels in zebrafish larvae. (A) Quantification of larval hyaloid vasculature at 120 hpf showed no changes in branches and sprouts but an increase in the vessel diameter in *elmo1*^{-/-} compared to *elmo1*^{+/+}. n = 33-37 hyaloids per group. (B) Quantification of larval hyaloid vasculature at 120 hpf showed no changes in branches, sprouts and vessel diameter in *elmo2*^{-/-} compared to *elmo2*^{+/+}. n = 33 hyaloids per group. (C) Quantification of larval hyaloid vasculature at 120 hpf showed no changes in branches and sprouts but an increase in the vessel diameter in *elmo3*^{-/-} compared to *elmo3*^{+/+}. n = 27-31 hyaloids per group. (D-F) Representative confocal microscopy images of the hyaloid vasculature of *elmo1*^{+/+} and *elmo1*^{-/-} (D), *elmo2*^{+/+} and *elmo2*^{-/-} (E) and *elmo3*^{+/+} and *elmo3*^{-/-} (F) zebrafish larvae at 120 hpf. Scale bar is 50 μm. Statistical analysis was done with t-test and Mann-Whitney test. * p < 0.05, ** p < 0.01. ns, not significant; hpf, hours post fertilization.

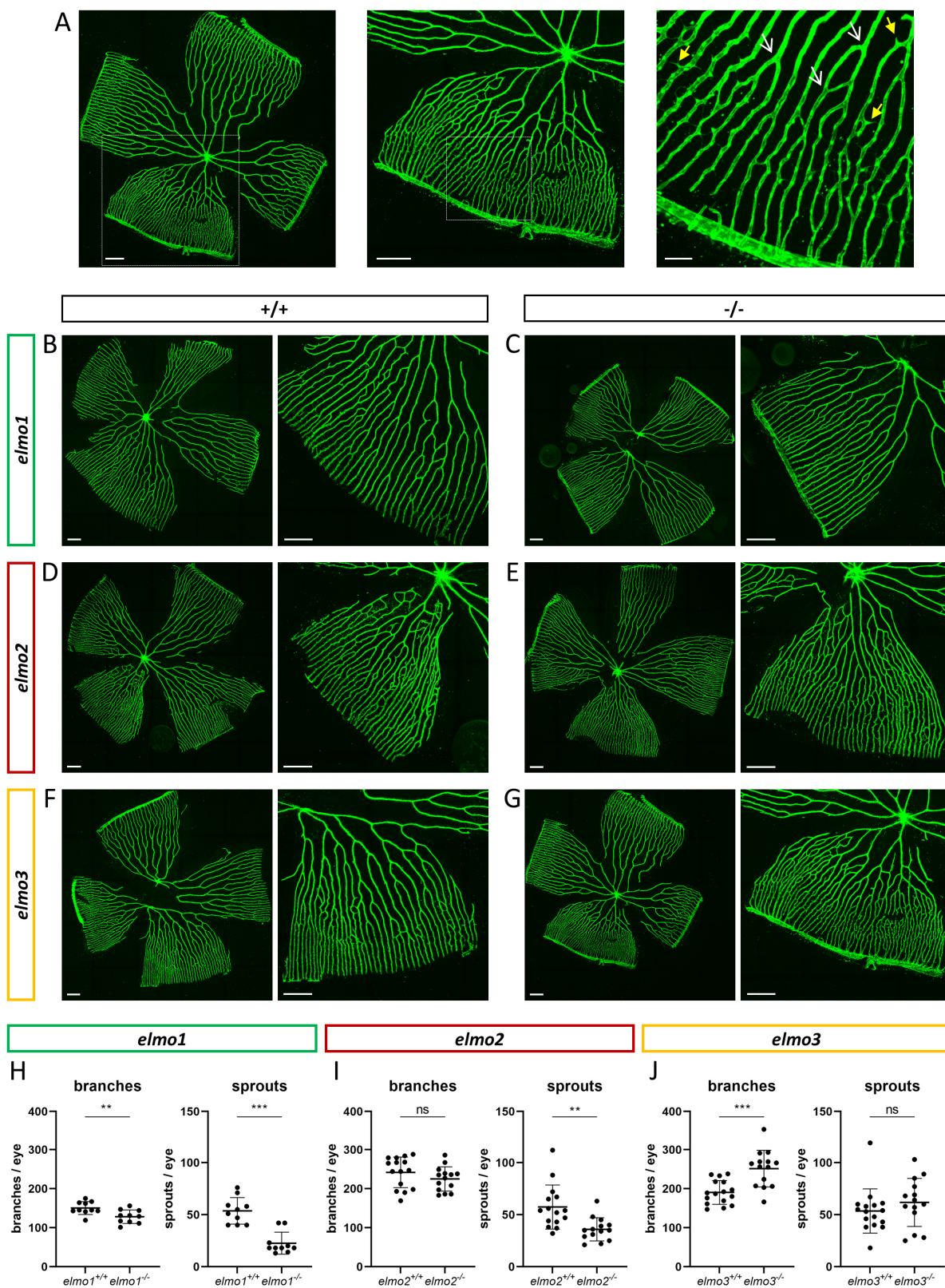


Figure 11. Different regulation of the retinal vasculature through Elmo1, Elmo2 and Elmo3 in adult zebrafish. (A) Exemplary pictures of a confocal scan of an adult zebrafish retinal vasculature. White squares each indicate the section of the image on the right. Scale bars are 200 μm (left, middle) and 50 μm (right). Representative vascular branches are indicated with a yellow arrow with a full arrowhead and sprouts are indicated with a white arrow with an open arrowhead. **(B-G)** Representative

confocal microscopy images of the retina vasculature of *elmo1*^{+/+} (B) and *elmo1*^{-/-} (C), *elmo2*^{+/+} (D) and *elmo2*^{-/-} (E) and *elmo3*^{+/+} (F) and *elmo3*^{-/-} (G) adult zebrafish. Scale bar is 200 μ m. (H) Quantification of the adult retina vasculature showed a decrease in branches and sprouts in *elmo1*^{-/-} compared to *elmo1*^{+/+}. n = 10 retinae per genotype. (I) Quantification of the adult retina vasculature showed no changes in branches and a decrease in sprouts in *elmo2*^{-/-} compared to *elmo2*^{+/+}. n = 14-15 retinae per genotype. (J) Quantification of the adult retina vasculature showed an increase in branches and no changes in sprouts in *elmo3*^{-/-} compared to *elmo3*^{+/+}. n = 14-16 retinae per genotype. Analyzed retinae were obtained from animals of 9-15 mpf. Statistical analysis was done with t-test and Mann-Whitney test. ** p < 0.01, *** p < 0.001. ns, not significant; mpf, months post fertilization.

2.7 Morphological analysis of adult *elmo1*^{-/-}, *elmo2*^{-/-} and *elmo3*^{-/-} zebrafish kidneys revealed different changes in glomerular structures

ELMO gene variants have been associated with diabetic kidney disease [62, 72–78]. Especially *ELMO1*, which promotes development of nephropathy in diabetic mice [61] and was suggested to promote the development of glomerular injury through dysregulation of the ECM [136].

To investigate if the three *Elmo* proteins have an essential function in kidney formation, it was analyzed whether adult *elmo1*^{-/-}, *elmo2*^{-/-} and *elmo3*^{-/-} zebrafish kidneys showed an altered morphology, with a special focus on the glomeruli. The overall structure of the kidney and the glomeruli were analyzed via PAS staining and cell number and the size of the glomeruli and their corresponding bowman space and capillary area were quantified. The gross morphology of the kidneys showed no abnormal alterations in *elmo1*^{-/-}, *elmo2*^{-/-} and *elmo3*^{-/-} zebrafish, respectively compared to *elmo1*^{+/+}, *elmo2*^{+/+} and *elmo3*^{+/+}. Furthermore, in *elmo1*^{-/-}, *elmo2*^{-/-} and *elmo3*^{-/-} the number of glomerular nuclei was unchanged compared to their wild type littermates (Figure 12A-D). Compared to *elmo1*^{+/+}, *elmo1*^{-/-} glomeruli exhibited an unchanged glomerulus size and capillary area, but an increased bowman space (Figure 12A,B). *elmo2*^{-/-} glomeruli also displayed an increased bowman space besides an increased glomerulus size, but no change in the capillary area, when compared to *elmo2*^{+/+} (Figure 12A,C). *elmo3*^{-/-} glomeruli showed no changes in the size of the glomeruli, the bowman space or the capillary area compared to *elmo3*^{+/+} (Figure 12A,D).

To analyze if parts of the filtration unit of the glomerulus, specifically the GBM was altered, electron microscopy (EM) images of the glomeruli were taken, analyzed and the thickness of the GBM was measured. The GBM thickness of *elmo1*^{-/-} and *elmo2*^{-/-} respectively showed no significant changes to the GBM thickness of *elmo1*^{+/+} (Figure 13A,D) and *elmo2*^{+/+} (Figure 13B,E) glomeruli. In contrast, the GBM thickness of

elmo3^{-/-} glomeruli was increased compared to *elmo3*^{+/+} (Figure 13C,F). In summary the loss of Elmo1, Elmo2 or Elmo3 respectively led to different changes in the glomerulus morphology, indicating a divergent impact of the three Elmo proteins on the development of the zebrafish kidney.

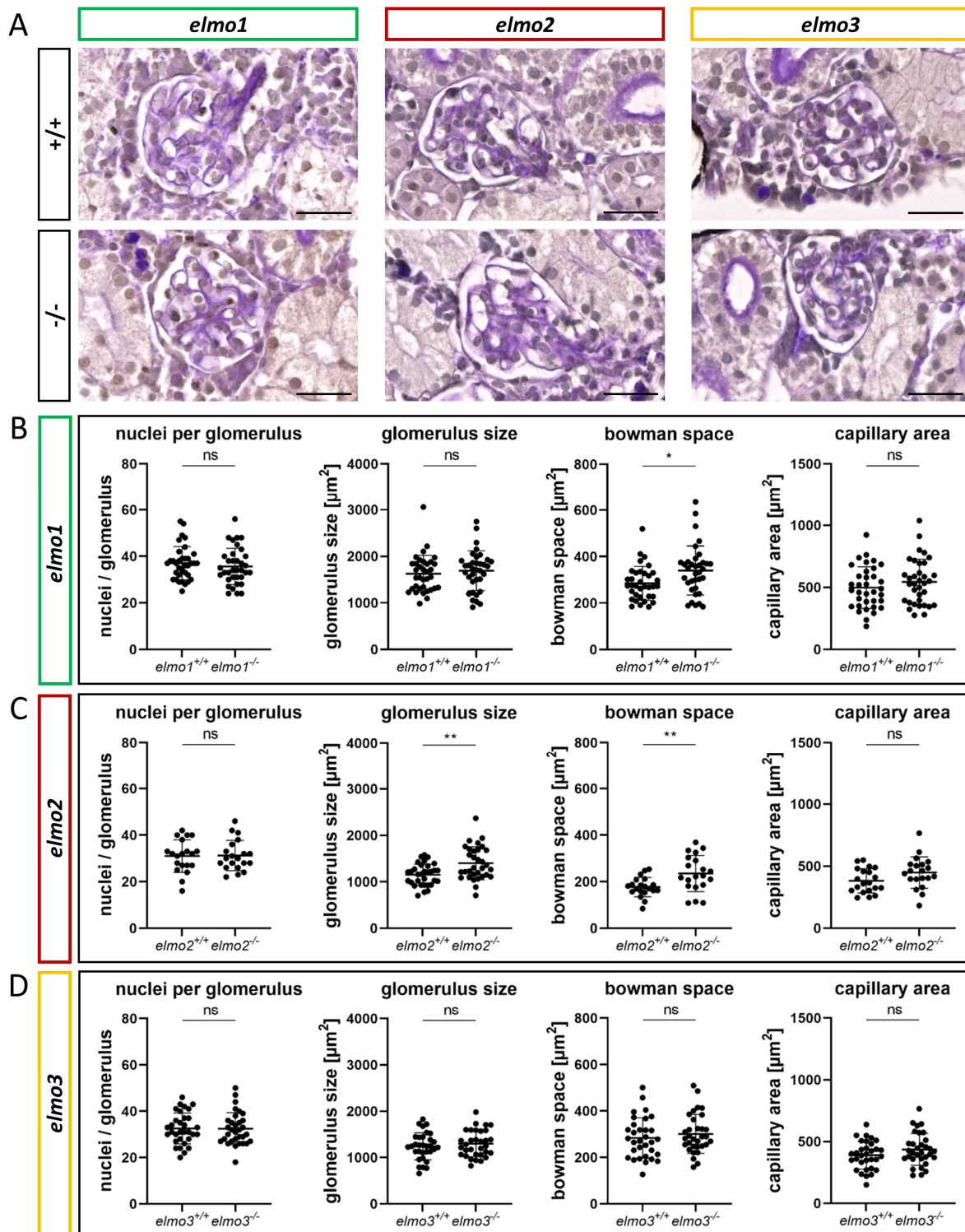


Figure 12. Different regulation of the glomerular structure through Elmo1, Elmo2 and Elmo3 in the kidney of adult zebrafish. (A) Representative light microscopy images of PAS stained sections of

glomeruli in the kidney of *elmo1*^{+/+} and *elmo1*^{-/-}, *elmo2*^{+/+} and *elmo2*^{-/-} and *elmo3*^{+/+} and *elmo3*^{-/-} adult zebrafish (9-13 mpf). Scale bar is 20 μ m. **(B)** Analysis of the glomerulus structure in adult zebrafish kidneys showed no changes in the number of nuclei, glomerulus size and capillary area but an increase in the bowman space in *elmo1*^{-/-} compared to *elmo1*^{+/+}. n = 35 glomeruli per genotype, 7 glomeruli per kidney. **(C)** Analysis of the glomerulus structure in adult zebrafish kidneys showed no changes in the number of nuclei and the capillary area but an increase in glomerulus size and bowman space in *elmo2*^{-/-} compared to *elmo2*^{+/+}. n = 20 glomeruli per genotype, 5 per kidney. **(D)** Analysis of the glomerulus structure in adult zebrafish kidneys showed no alterations in *elmo3*^{-/-} compared to *elmo3*^{+/+}. n = 32 glomeruli per genotype, 8 per kidney. Statistical analysis was done with t-test and Mann-Whitney test. * p < 0.05, ** p < 0.01. ns, not significant; mpf, months post fertilization.

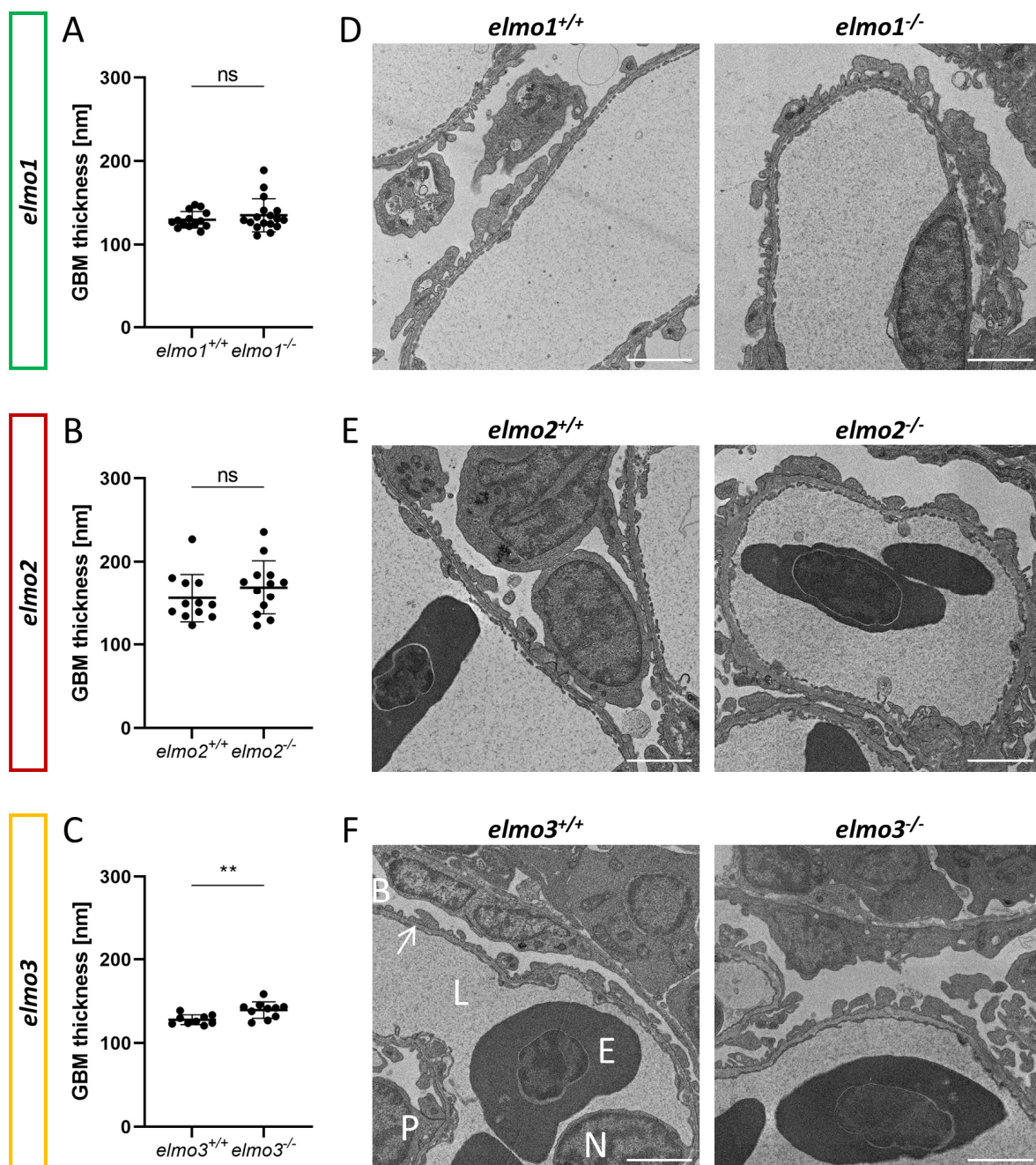


Figure 13. The loss of Elmo3 led to a thickened glomerular basement membrane in adult zebrafish kidneys. (A) Quantification of the thickness of the GBM in the adult kidney (9-15 mpf) showed no alterations in *elmo1*^{-/-} compared to *elmo1*^{+/+}. n = 14-17 per genotype. Each data point represents the mean thickness per one glomerulus. **(B)** Quantification of the thickness of the GBM in the adult kidney showed no alterations in *elmo2*^{-/-} compared to *elmo2*^{+/+}. n = 12-13 per genotype. Each data point represents the mean thickness per one glomerulus. **(C)** Quantification of the thickness of the GBM in the adult kidney showed an increase of the GBM thickness in *elmo3*^{-/-} compared to *elmo3*^{+/+}. n = 9-10 per group. Each data point represents the mean thickness per one glomerulus. **(D-F)** Representative electron microscopy images of glomerulus sections of adult kidneys of *elmo1*^{+/+} and *elmo1*^{-/-} **(D)**, *elmo2*^{+/+} and *elmo2*^{-/-} **(E)** and *elmo3*^{+/+} and *elmo3*^{-/-} **(F)** zebrafish. Exemplarily glomerulus compartments as GBM (arrow), Bowman space (B), endothelial cell nucleus (N), capillary lumen (L), podocyte (P) and erythrocyte (E) are indicated in white. Scalebar is 2 μ m. Statistical analysis was done with t-test and Mann-Whitney test. ** p < 0.01. ns, not significant; GBM, glomerular basement membrane; mpf, months post fertilization. Histological analysis and electron microscopy were performed by the Institute of Pathology IPH, EM Lab of the Heidelberg University Hospital.

2.8 Elmo1 regulates adult blood glucose in zebrafish

Previous studies have described the ELMO proteins as promoters for RAC1 activity [33, 35–38] and RAC1 was shown to be an important regulator of the glucose homeostasis by ensuring the vesicular insulin transport by organizing the pancreatic cytoskeleton during glucose induced insulin secretion [1, 153]. Furthermore, a lack of RAC1 is associated with insulin resistance in humans and rodents [154, 185, 186] and ELMO2 and RAC1, both regulate the insulin dependent membrane translocation of GLUT4 in muscle cells [79], both indicating a regulatory role of RAC1 and ELMO2 in glucose uptake. To address the question if Elmo1, Elmo2 or Elmo3 maintain glucose homeostasis in zebrafish, whole body glucose content of larval (120 hpf) and blood glucose levels of adult (7-15 mpf) *elmo1*^{-/-}, *elmo2*^{-/-} and *elmo3*^{-/-} zebrafish were measured (Figure 14). Interestingly, adult blood glucose levels of fasted *elmo1*^{-/-} zebrafish were decreased compared to *elmo1*^{+/+} (Figure 14B), whereas postprandial blood glucose levels were increased (Figure 14C). In *elmo2*^{-/-} and *elmo3*^{-/-}, adult blood glucose levels, both fasting and postprandial were unaltered respectively compared to *elmo2*^{+/+} (Figure 14E,F) and *elmo3*^{+/+} (Figure 14H,I) zebrafish. The whole body glucose between *elmo1*^{+/+} and *elmo1*^{-/-}, *elmo2*^{+/+} and *elmo2*^{-/-} and *elmo3*^{+/+} and *elmo3*^{-/-} larvae at 120 hpf showed no differences (Figure 14A,D,G). In conclusion, these data have identified an important impact of Elmo1 in maintaining the regulation of blood glucose levels in adult zebrafish, thereby functionally differentiating itself from Elmo2 and Elmo3.

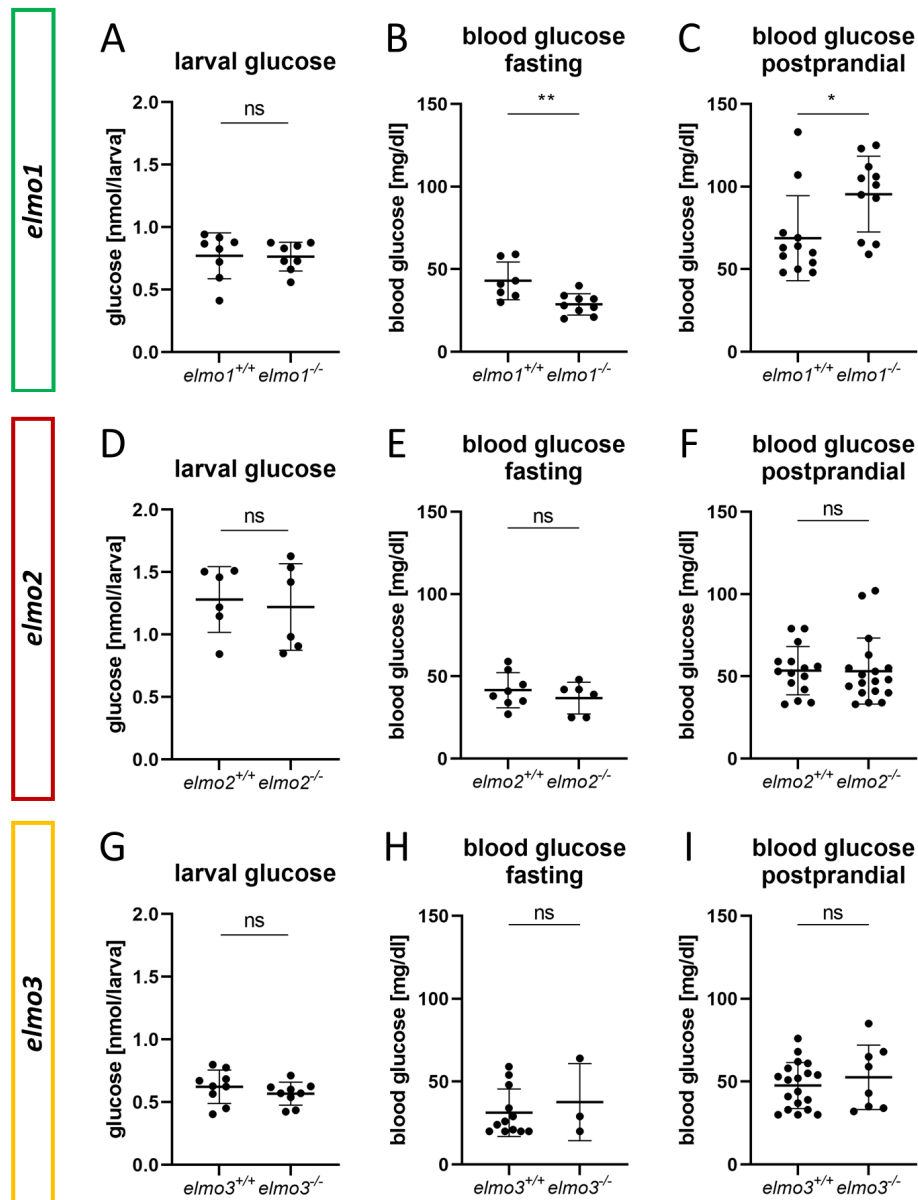


Figure 14. The loss of Elmo1 led to altered blood glucose levels in adult zebrafish. (A) Whole body glucose levels were not changed in *elmo1^{-/-}* compared to *elmo1^{+/+}* at 120 hpf. n = 8 samples per genotype, each containing 20 zebrafish larvae. **(B)** Fasting blood glucose levels were decreased in adult *elmo1^{-/-}* compared to *elmo1^{+/+}*. **(C)** Postprandial blood glucose levels were increased in adult *elmo1^{-/-}* compared to *elmo1^{+/+}*. **(D)** Whole body glucose levels were not changed in *elmo2^{-/-}* compared to *elmo2^{+/+}* at 120 hpf. n = 6 samples per group, each containing 20 zebrafish larvae. **(E,F)** Fasting and postprandial blood glucose levels were unaltered in adult *elmo2^{-/-}* compared to *elmo2^{+/+}*. **(G)** Whole body glucose levels were not changed in *elmo3^{-/-}* compared to *elmo3^{+/+}* at 120 hpf. n = 9 samples per group, each containing 20 zebrafish larvae. **(H,I)** Fasting and postprandial blood glucose levels were unaltered in adult *elmo3^{-/-}* compared to *elmo3^{+/+}*. Blood glucose was obtained from animals of 7-15 mpf. Statistical analysis was done with t-test and Mann-Whitney test. * p < 0.05, ** p < 0.01. ns, not significant; hpf, hours post fertilization; mpf, months post fertilization.

To investigate if the loss of Elmo1, Elmo2 or Elmo3 generally affects the regulation of glucose levels through the modulation of insulin production or insulin sensitivity in the early development of the organism, the expression of *preproinsulin* and *insulin receptor a* and *b* was measured. These genes showed no significant changes in their expression in 120 hpf zebrafish larvae (Figure 15A-C).

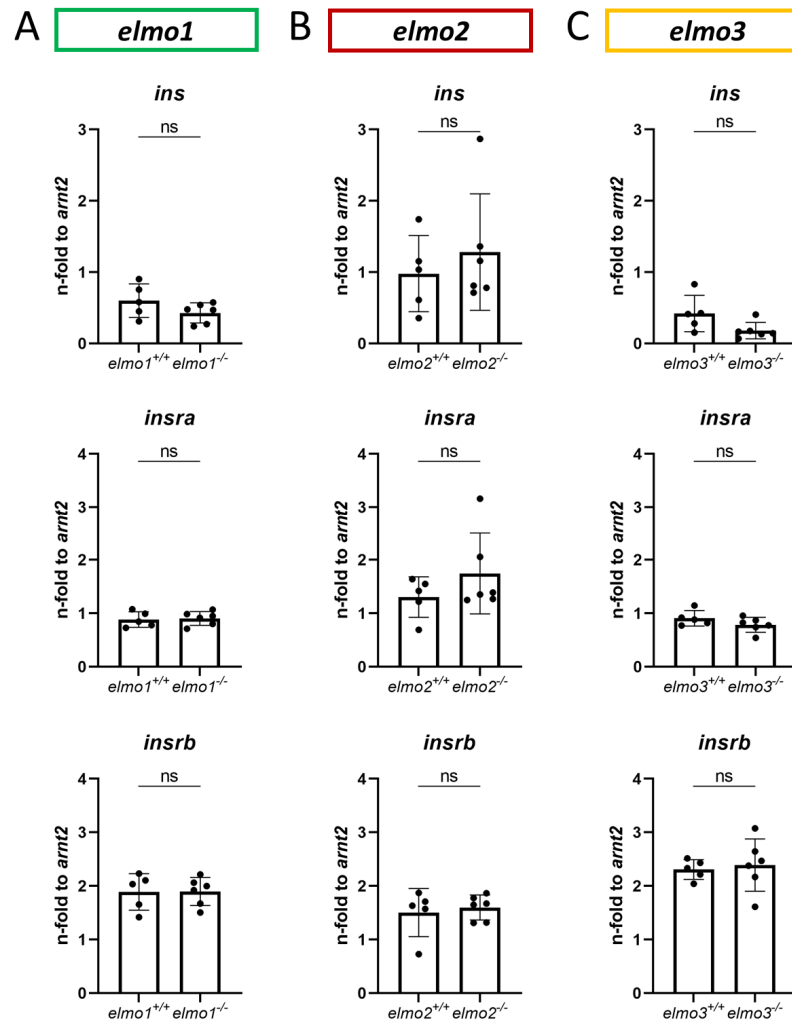


Figure 15. Unaltered expression of *preproinsulin* and *insulin receptor* genes in larval *elmo1*^{-/-}, *elmo2*^{-/-}, and *elmo3*^{-/-} zebrafish. Quantification of RNA levels of *preproinsulin* (*ins*), *insulin receptor a* and *b* showed no changes in *elmo1*^{-/-} (A), *elmo2*^{-/-} (B) and *elmo3*^{-/-} (C) respectively compared to *elmo1*^{+/+}, *elmo2*^{+/+} and *elmo3*^{+/+} zebrafish at 120 hpf. n = 5-6 samples per genotype, each containing 30 larvae. RNA levels were quantified with RT-qPCR and compared with *arnt2*. Statistical analysis was done with t-test and Mann-Whitney test. ns, not significant; hpf, hours post fertilization.

Due to changed blood glucose levels in adult *elmo1*^{-/-} zebrafish, it was analyzed if different factors of the glucose metabolism were transcriptionally regulated in postprandial livers of *elmo1*^{-/-} compared to *elmo1*^{+/+} zebrafish (Figure 16). Among the tested RNAs of genes responsible for several glucose transporters and regulators of

glycolysis and gluconeogenesis, *glucose transporter 1a (glut1a)* was significantly decreased and *glucose transporter 5 (glut5)* and *hexokinase 2 (hk2)* were significantly increased in *elmo1*^{-/-} compared to *elmo1*^{+/+} zebrafish livers. The RNA levels of the other tested factors showed no significant alterations.

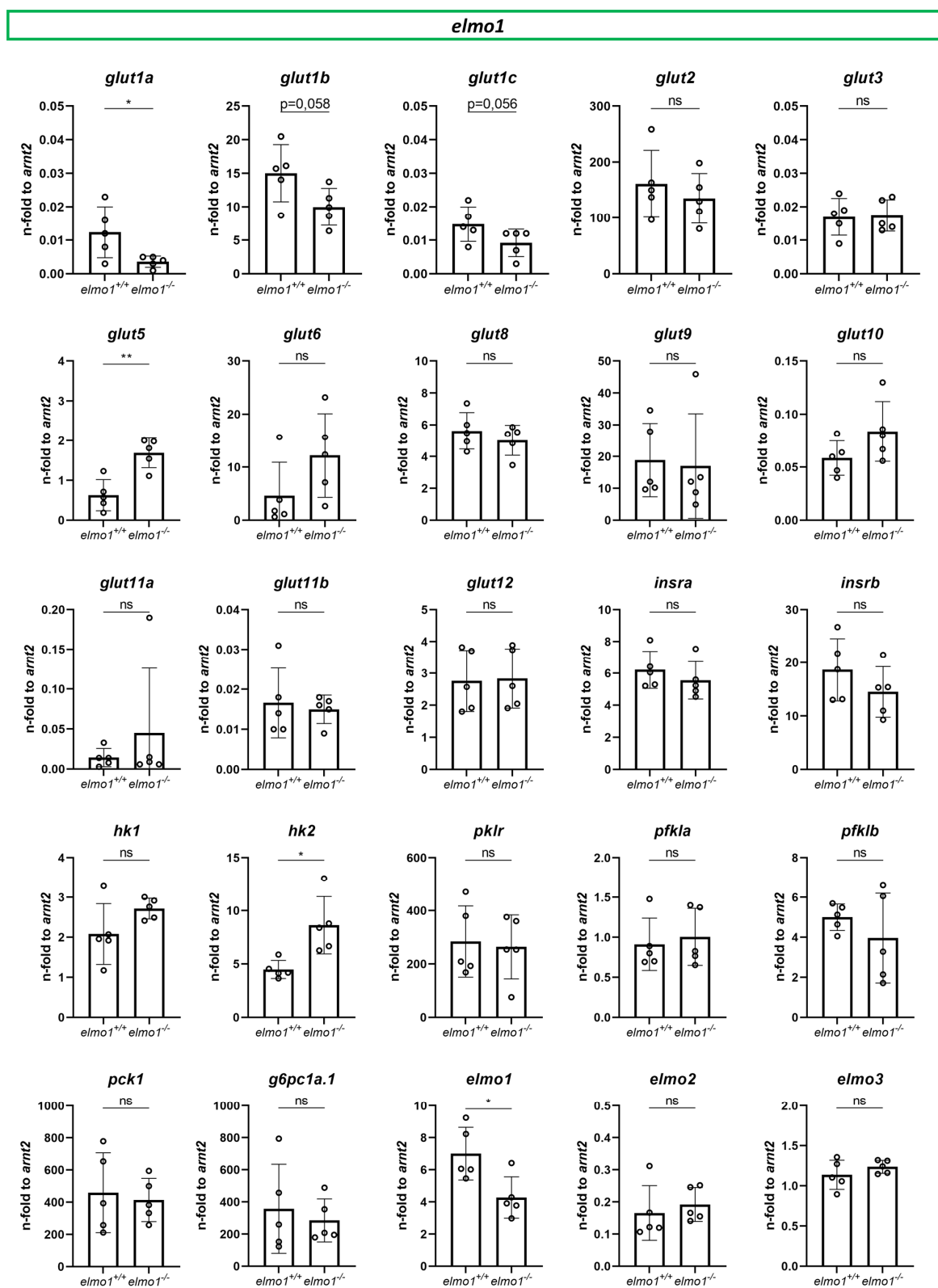


Figure 16. The loss of Elmo1 led to altered expression of individual glucose level regulating genes in adult postprandial zebrafish livers. Quantification of RNA levels of glucose transporter genes and genes associated with glycolysis and gluconeogenesis in adult postprandial livers of *elmo1*^{-/-} zebrafish showed a decrease of *glut1a* and an increase of *glut5* and *hk2* compared to *elmo1*^{+/+} zebrafish. n = 5-6 organ samples per genotype. RNA levels were quantified with RT-qPCR and compared with *arnt2*. Statistical analysis was done with t-test and Mann-Whitney test. * p < 0.05, ** p < 0.01. ns, not significant; hpf, hours post fertilization.

2.9 Transcriptome analyses of *elmo1*^{-/-}, *elmo2*^{-/-} and *elmo3*^{-/-} zebrafish larvae revealed that the Elmo proteins transcriptionally modulate vascular and neuronal development

To identify underlying pathways of the observed alterations in vasculature, kidney and glucose homeostasis in *elmo1*^{-/-}, *elmo2*^{-/-} and *elmo3*^{-/-} zebrafish and to reveal novel cellular mechanisms regulated by the Elmo proteins, the regulation of the transcriptome was analyzed with RNA sequencing. RNA was isolated from zebrafish larvae at 120 hpf and analyzed based on the Kyoto Encyclopedia of Genes and Genomes (KEGG) database for signaling pathways and based on the Gene Ontology Biological Process (GOBP) database for cell processes and mechanisms.

Table 1. The loss of Elmo3 led to more changes in the regulation of the transcriptome of zebrafish larvae than the loss of Elmo1 or Elmo2. Comparison of the regulation of signaling pathways in *elmo1*^{-/-}, *elmo2*^{-/-} and *elmo3*^{-/-} zebrafish larvae respectively compared to *elmo1*^{+/+}, *elmo2*^{+/+} and *elmo3*^{+/+} showed that more pathways are significantly regulated in *elmo3*^{-/-} (62) than in *elmo1*^{-/-} (11) or *elmo2*^{-/-} (9). 150 pathways were analyzed in total. Shown are pathways which are significantly regulated in at least one of the three comparisons. Kyoto Encyclopedia of Genes and Genomes (KEGG) based analysis of pathways of the transcriptome using RNA-sequencing data from zebrafish larvae at 120 hpf. n = 6 samples per genotype, each containing 30 larvae. Regulation of the gene sets is given as normalized enrichment score (NES). Green background marks downregulated pathways, red background marks upregulated pathways and blue background marks significantly regulated pathways. m.c., main category; 1. M, 1. Metabolism; 2. G, 2. Genetic Information Processing; 3. E, 3. Environmental Information Processing; 4. C, 4. Cellular Processes; 5. O, 5. Organismal Systems; 6. H, 6. Human Diseases. hpf, hours post fertilization; NES, normalized enrichment score. Library preparation and RNA-sequencing were performed by BGI (www.bgi.com; Shenzhen, China) and statistical analysis was done by Carsten Sticht from the Next-Generation Sequencing (NGS) Core Facility of the Medical Faculty Mannheim.

KEGG pathway	m. c.	sub category	elmo1 ^{-/-}		elmo2 ^{-/-}		elmo3 ^{-/-}	
			NES	adj. p-value	NES	adj. p-value	NES	adj. p-value
dre01100_Metabolic_pathways	1. M	1.0 Global and overview maps	-0.89	0.9967	-0.76	1.0000	-2.00	0.0009
dre01200_Carbon_metabolism	1. M	1.0 Global and overview maps	0.96	0.8633	0.75	1.0000	-2.13	0.0009
dre01212_Fatty_acid_metabolism	1. M	1.0 Global and overview maps	0.67	0.9967	-0.90	0.9610	-1.98	0.0009
dre00010_Glycolysis_Gluconeogenesis	1. M	1.1. Carbohydrate metabolism	0.84	0.9884	-0.73	1.0000	-1.93	0.0009
dre00040_Pentose_and_glucuronate_interconversions	1. M	1.1. Carbohydrate metabolism	-1.31	0.3632	0.74	1.0000	-2.52	0.0009
dre00052_Galactose_metabolism	1. M	1.1. Carbohydrate metabolism	0.99	0.7806	0.93	0.9610	-1.88	0.0041
dre00053_Ascorbate_and_aldarate_metabolism	1. M	1.1. Carbohydrate metabolism	-1.51	0.1958	-0.73	1.0000	-2.50	0.0009
dre00500_Starch_and_sucrose_metabolism	1. M	1.1. Carbohydrate metabolism	0.62	0.9967	-0.83	0.9669	-1.71	0.0175
dre00520_Amino_sugar_and_nucleotide_sugar_metabolism	1. M	1.1. Carbohydrate metabolism	-1.44	0.2188	-0.72	1.0000	-2.55	0.0009
dre00620_Pyruvate_metabolism	1. M	1.1. Carbohydrate metabolism	-0.62	0.9967	0.80	1.0000	-2.05	0.0009
dre00630_Glyoxylate_and_dicarboxylate_metabolism	1. M	1.1. Carbohydrate metabolism	-1.58	0.1343	0.90	0.9610	-2.07	0.0016
dre00640_Propanoate_metabolism	1. M	1.1. Carbohydrate metabolism	-0.71	0.9966	-0.61	1.0000	-1.84	0.0072
dre00650_Butanoate_metabolism	1. M	1.1. Carbohydrate metabolism	-1.14	0.5839	-0.50	1.0000	-1.70	0.0235
dre00190_Oxidative_phosphorylation	1. M	1.2. Energy metabolism	1.83	0.0088	1.23	0.2647	1.10	0.3730
dre00071_Fatty_acid_degradation	1. M	1.3. Lipid metabolism	-1.02	0.7460	-0.76	1.0000	-2.54	0.0009
dre00100_Steroid_biosynthesis	1. M	1.3. Lipid metabolism	-1.01	0.7632	0.81	0.9669	-2.13	0.0009
dre00120_Primary_bile_acid_biosynthesis	1. M	1.3. Lipid metabolism	-1.05	0.7208	-0.88	0.9610	-2.24	0.0009
dre00140_Steroid_hormone_biosynthesis	1. M	1.3. Lipid metabolism	-0.90	0.8776	-0.74	1.0000	-2.40	0.0009
dre00561_Glycerolipid_metabolism	1. M	1.3. Lipid metabolism	-0.74	0.9967	-1.07	0.7209	-1.81	0.0046
dre00565_Ether_lipid_metabolism	1. M	1.3. Lipid metabolism	-1.49	0.1873	-1.13	0.5960	-1.84	0.0059
dre00590_Arachidonic_acid_metabolism	1. M	1.3. Lipid metabolism	-1.06	0.6906	1.16	0.5235	-1.65	0.0235
dre00591_Linoleic_acid_metabolism	1. M	1.3. Lipid metabolism	-0.77	0.9884	1.43	0.2445	-1.76	0.0165
dre00600_Sphingolipid_metabolism	1. M	1.3. Lipid metabolism	0.80	0.9966	-1.22	0.4636	-1.62	0.0172
dre01040_Biosynthesis_of_unsaturated_fatty_acids	1. M	1.3. Lipid metabolism	1.17	0.5254	-1.22	0.4943	-1.74	0.0154
dre00260_Glycine_serine_and_threonine_metabolism	1. M	1.5. Amino acid metabolism	0.97	0.8235	1.26	0.4057	-2.24	0.0009
dre00270_Cysteine_and_methionine_metabolism	1. M	1.5. Amino acid metabolism	-0.91	0.8699	-0.73	1.0000	-1.69	0.0145
dre00280_Valine_leucine_and_ileucine_degradation	1. M	1.5. Amino acid metabolism	-1.40	0.2580	-1.16	0.5443	-2.26	0.0009
dre00330_Arginine_and_proline_metabolism	1. M	1.5. Amino acid metabolism	-0.94	0.8633	-0.62	1.0000	-2.06	0.0009
dre00340_Histidine_metabolism	1. M	1.5. Amino acid metabolism	-1.32	0.3632	-0.63	1.0000	-2.21	0.0009
dre00350_Tyrosine_metabolism	1. M	1.5. Amino acid metabolism	-1.03	0.7460	-1.61	0.1060	-1.62	0.0389
dre00380_Tryptophan_metabolism	1. M	1.5. Amino acid metabolism	1.01	0.7511	-0.77	1.0000	-2.40	0.0009
dre00410_beta-Alanine_metabolism	1. M	1.6. Metabolism of other amino acids	-1.28	0.3915	0.41	1.0000	-2.28	0.0009
dre00480_Glutathione_metabolism	1. M	1.6. Metabolism of other amino acids	-1.04	0.7208	1.03	0.7882	-2.25	0.0009
dre00510_N-Glycan_biosynthesis	1. M	1.7. Glycan biosynthesis and metabolism	-0.58	0.9967	-1.36	0.2445	-1.70	0.0086
dre00511_Other_glycan_degradation	1. M	1.7. Glycan biosynthesis and metabolism	-0.88	0.8720	-0.81	0.9669	-1.85	0.0062
dre00513_Various_types_of_N-glycan_biosynthesis	1. M	1.7. Glycan biosynthesis and metabolism	-0.67	0.9967	-1.01	0.8134	-1.94	0.0023
dre00770_Pantothenate_and_CoA_biosynthesis	1. M	1.8. Metabolism of cofactors and vitamins	-0.91	0.8688	-1.04	0.7998	-2.00	0.0023
dre00830_Retinol_metabolism	1. M	1.8. Metabolism of cofactors and vitamins	-1.15	0.5226	0.93	0.9610	-2.27	0.0009
dre00860_Porphyrin_and_chlorophyll_metabolism	1. M	1.8. Metabolism of cofactors and vitamins	0.94	0.8633	1.49	0.1616	-1.96	0.0016
dre01240_Biosynthesis_of_cofactors	1. M	1.8. Metabolism of cofactors and vitamins	-1.02	0.7280	1.23	0.2445	-2.17	0.0009
dre00980_Metabolism_of_xenobiotics_by_cytochrome_P450	1. M	1.11. Xenobiotics biodegradation and metabolism	-0.93	0.8688	0.87	0.9669	-2.76	0.0009
dre00982_Drug_metabolism	1. M	1.11. Xenobiotics biodegradation and metabolism	-0.97	0.8301	0.75	1.0000	-2.69	0.0009
dre00983_Drug_metabolism	1. M	1.11. Xenobiotics biodegradation and metabolism	1.19	0.4644	0.73	1.0000	-2.02	0.0009
dre03020_RNA_polymerase	2. G	2.1. Transcription	0.91	0.8688	-0.75	1.0000	1.71	0.0191
dre03040_Spliceosome	2. G	2.1. Transcription	-1.93	0.0078	-1.25	0.3122	0.84	0.9069
dre03008_Ribosome_biogenesis_in_eukaryotes	2. G	2.2. Translation	0.81	0.9966	-1.91	0.0141	1.32	0.1386
dre03010_Ribosome	2. G	2.2. Translation	2.13	0.0078	2.58	0.0141	1.45	0.0244
dre03015_mRNA_surveillance_pathway	2. G	2.2. Translation	-1.30	0.3031	-1.72	0.0227	0.88	0.8327
dre03018_RNA_degradation	2. G	2.3. Folding, sorting and degradation	0.80	0.9966	-1.15	0.5443	1.52	0.0235
dre03050_Proteasome	2. G	2.3. Folding, sorting and degradation	0.54	0.9967	-1.33	0.2987	-2.17	0.0009
dre04141_Protein_processing_in_endoplasmic_reticulum	2. G	2.3. Folding, sorting and degradation	-1.39	0.1166	-1.15	0.4943	-1.47	0.0101
dre03030_DNA_replication	2. G	2.4. Replication and repair	-1.47	0.2425	-1.64	0.0985	-1.82	0.0062
dre04010_MAPK_signaling_pathway	3. E	3.2. Signal transduction	-1.59	0.0088	-0.92	0.9669	1.12	0.2349
dre04068_FoxO_signaling_pathway	3. E	3.2. Signal transduction	-0.94	0.8688	1.24	0.2445	1.48	0.0170
dre04150_mTOR_signaling_pathway	3. E	3.2. Signal transduction	-0.82	0.9966	-1.27	0.2445	1.43	0.0174
dre04310_Wnt_signaling_pathway	3. E	3.2. Signal transduction	-1.72	0.0088	-1.61	0.0154	-0.83	0.9332
dre04330_Notch_signaling_pathway	3. E	3.2. Signal transduction	-1.00	0.7632	-1.55	0.1018	2.04	0.0011
dre04350_TGF-beta_signaling_pathway	3. E	3.2. Signal transduction	-1.25	0.3383	-1.60	0.0329	-0.94	0.7117
dre04512_ECM-receptor_interaction	3. E	3.3. Signaling molecules and interaction	-1.84	0.0096	-1.91	0.0141	-1.78	0.0027
dre04514_Cell_adhesion_molecules	3. E	3.3. Signaling molecules and interaction	-0.71	0.9967	-0.99	0.8393	-1.50	0.0198
dre04142_Lysosome	4. C	4.1. Transport and catabolism	1.44	0.1166	0.93	0.9610	-1.47	0.0182
dre04145_Phagosome	4. C	4.1. Transport and catabolism	-0.97	0.8301	-1.00	0.8134	-1.94	0.0009
dre04146_Peroxisome	4. C	4.1. Transport and catabolism	-1.47	0.1343	0.69	1.0000	-2.42	0.0009
dre04210_Apoptosis	4. C	4.2. Cell growth and death	-0.99	0.7840	1.55	0.0329	-1.19	0.2127
dre04510_Focal_adhesion	4. C	4.3. Cellular community - eukaryotes	-1.91	0.0078	-1.49	0.0257	-1.55	0.0027
dre04530_Tight_junction	4. C	4.3. Cellular community - eukaryotes	-1.58	0.0096	-0.99	0.8449	-1.71	0.0015
dre04810_Regulation_of_actin_cytoskeleton	4. C	4.5. Cell motility	-1.63	0.0078	-0.82	1.0000	-1.62	0.0015
dre04620_Toll-like_receptor_signaling_pathway	5. O	5.1. Immune system	-1.81	0.0204	1.19	0.4394	-1.06	0.4806
dre04622_RIG-I-like_receptor_signaling_pathway	5. O	5.1. Immune system	-1.74	0.0316	1.13	0.5443	-1.01	0.5724
dre03320_PPAR_signaling_pathway	5. O	5.2. Endocrine system	0.94	0.8688	-0.92	0.9610	-2.06	0.0009
dre04916_Melanogenesis	5. O	5.2. Endocrine system	-1.40	0.1400	-1.86	0.0141	0.96	0.6915
dre04744_Photorotransduction	5. O	5.7. Sensory system	1.25	0.4235	1.57	0.1188	1.79	0.0061
dre05132_Salmonella_infection	6. H	6.8. Infectious diseases: Bacterial	-1.37	0.0844	-0.94	0.9610	-1.76	0.0009

The KEGG based analysis revealed that out of 150 analyzed pathways, 11 were significantly regulated in *elmo1*^{-/-}, 9 in *elmo2*^{-/-} and 62 in *elmo3*^{-/-} mutants (Table 1). These results suggested a strong impact of Elmo3 on the transcriptional regulation and comparable weaker regulations through Elmo1 and Elmo2. Interestingly, only three pathways were found to be regulated in the same direction in all three *elmo* mutants (Ribosome – upregulated; ECM-receptor interaction – downregulated; Focal adhesion – downregulated). Comparing two *elmo* mutants only, exhibited four pathways regulated in the same direction in *elmo1* and *elmo2* (Wnt signaling pathway – down), five in *elmo1* and *elmo3* (Tight junction – down; Regulation of actin cytoskeleton – down) and three in *elmo2* and *elmo3*, indicating only minor functional similarities in the regulation of the larval transcriptome between Elmo1, Elmo2 and Elmo3.

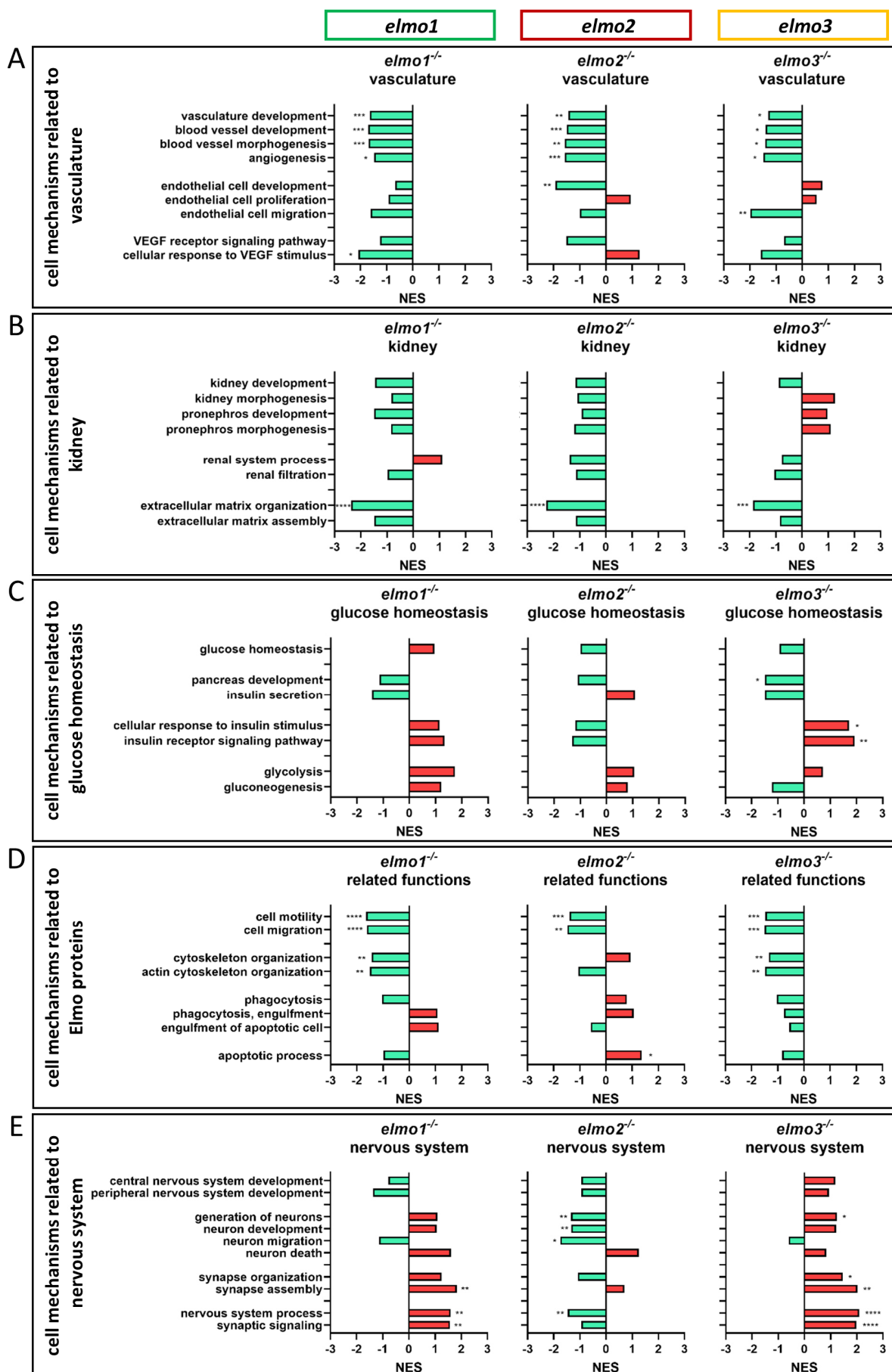


Figure 17. Regulation of the transcriptome in larval zebrafish after loss of Elmo1, Elmo2 or Elmo3 only showed limited similarities. Comparison of the regulation of cell mechanisms in *elmo1*^{-/-}, *elmo2*^{-/-} and *elmo3*^{-/-} in zebrafish larvae respectively compared to *elmo1*^{+/+}, *elmo2*^{+/+} and *elmo3*^{+/+}. Gene Ontology Biological Process (GOBP) based analysis of cell mechanisms of the transcriptome using RNA-sequencing data from zebrafish larvae at 120 hpf. n = 6 samples per genotype, each containing 30 zebrafish larvae. Regulation of the gene sets is given as normalized enrichment score (NES). **(A)** Cell mechanisms related to vascular development were generally downregulated in *elmo1*^{-/-}, *elmo2*^{-/-} and *elmo3*^{-/-} respectively compared to *elmo1*^{+/+}, *elmo2*^{+/+} and *elmo3*^{+/+}. **(B)** Cell mechanisms related to kidney development and function showed a downregulation of extracellular matrix organization in *elmo1*^{-/-}, *elmo2*^{-/-} and *elmo3*^{-/-} respectively compared to *elmo1*^{+/+}, *elmo2*^{+/+} and *elmo3*^{+/+}. **(C)** Cell mechanisms related to glucose homeostasis were differently regulated in *elmo3*^{-/-}. **(D)** Cell mechanisms related to further functions of Elmo proteins showed a general downregulation in *elmo1*^{-/-} and *elmo3*^{-/-} and different changes in *elmo2*^{-/-}. **(E)** Cell mechanisms related to the nervous system were generally upregulated in *elmo1*^{-/-} and *elmo3*^{-/-} and downregulated in *elmo2*^{-/-}. hpf, hours post fertilization; NES, normalized enrichment score. Library preparation and RNA-sequencing were performed by BGI (www.bgi.com; Shenzhen, China) and statistical analysis was done by Carsten Sticht from the Next-Generation Sequencing (NGS) Core Facility of the Medical Faculty Mannheim.

GOBP based analyses (Figure 17) showed a downregulation of the vascular development, blood vessel development, blood vessel morphogenesis and angiogenesis mechanisms (Figure 17A) in the transcriptomes of *elmo1*^{-/-}, *elmo2*^{-/-} and *elmo3*^{-/-} zebrafish larvae, indicating that the transcriptional regulation of the vasculature overlaps in early development. These results correlated with the data of Elmo1 as a promoting factor of the trunk vasculature [46, 71] and the retinal vasculature (Figure 11) and suggested novel vascular functions of Elmo2 and Elmo3. However, mechanisms related to early kidney formation and function were not significantly regulated in any direction in *elmo1*^{-/-}, *elmo2*^{-/-} and *elmo3*^{-/-} zebrafish larvae (Figure 17B), albeit the data revealed an impact of the three Elmo proteins on the organization of the ECM, which is of major structural importance for the glomeruli and its GBM [187]. The mechanisms related to glucose homeostasis were not significantly changed in larval *elmo1*^{-/-} and *elmo2*^{-/-} zebrafish (Figure 17C). Surprisingly, the *elmo3*^{-/-} larval data exhibited a downregulated cellular response to insulin and pancreas development. Mechanisms related to functions which were already linked to Elmo1 and partially to Elmo2 and Elmo3, showed a common downregulation of cell motility and cell migration in *elmo1*^{-/-}, *elmo2*^{-/-} and *elmo3*^{-/-}, a downregulation of the cytoskeleton organization in *elmo1*^{-/-} and *elmo3*^{-/-} and an upregulation of the apoptotic process in *elmo2*^{-/-} zebrafish larvae (Figure 17D). Lastly, the transcriptome data revealed a transcriptional regulation

of the three Elmo proteins on the nervous system process and neuronal development, which were upregulated in *elmo1*^{-/-} and *elmo3*^{-/-} (Figure 17E). This again correlated with known data of the ELMO proteins to regulate [33, 36, 55, 56, 58–60] and inhibit [54] neuronal development and revealed again a divergent function of Elmo1 and Elmo3 to Elmo2 in these processes.

In conclusion, these transcriptome analyses revealed that the individual Elmo proteins affect similar as well as different pathways and mechanisms on a transcriptional level, identified Elmo3 as an important transcriptional regulator in zebrafish larvae and highlighted the three Elmo proteins as promotive factors for vascular development and regulators of the nervous system.

2.10 Metabolome analyses of *elmo1*^{-/-}, *elmo2*^{-/-} and *elmo3*^{-/-} zebrafish larvae revealed an increase of amino acids due to the loss of Elmo1 and an increase of fatty acids due the loss of Elmo2

Because the transcriptome analysis exhibited several regulated pathways related to metabolic processes in *elmo3*^{-/-} larvae (Table 1) and to assess if the metabolome is generally affected by the loss of Elmo1, Elmo2 or Elmo3, amino acids (Figure 18), fatty acids (Figure 19), adenosines (Figure 20) and glutathione (Figure 21) were measured in *elmo1*^{+/+}, *elmo2*^{+/+}, *elmo3*^{+/+}, *elmo1*^{-/-}, *elmo2*^{-/-} and *elmo3*^{-/-} larvae at 96 hpf. Surprisingly, the metabolome of *elmo3*^{-/-} larvae just showed few changes and did not correlate with the transcriptional data. ADP and ATP were decreased in *elmo3*^{-/-} compared to *elmo3*^{+/+} larvae (Figure 20C) which was also the case in *elmo1*^{-/-} compared to *elmo1*^{+/+} larvae (Figure 20A), suggesting a similar role in the regulation of the larval energy maintenance. However, *elmo1*^{-/-} exhibited an increase of nine amino acids (Asp, Glu, Asn, Thr, Ala, Pro, Val, Ile, Leu) compared to *elmo1*^{+/+} larvae (Figure 18A), whereas *elmo2*^{-/-} larvae showed an increase in one (Ala) (Figure 18B) and *elmo3*^{-/-} larvae no changes in amino acids (Figure 18C). Measuring fatty acids exhibited an increase of eight fatty acids in *elmo2*^{-/-} (C16:0, C20:4n6, C20:5n3, C20:2, C20:1n9, C22:6n3, C22:1n9, C24:1n9) compared to *elmo2*^{+/+} larvae (Figure 19B), while in *elmo1*^{-/-} one fatty acid (C14:0) was increased (Figure 19A) and no fatty acid changed in *elmo3*^{-/-} larvae (Figure 19C). Both results indicate that Elmo1, Elmo2 and Elmo3 functionally diverge. The ratio of GSH to GSSG was assessed as one parameter of redox status and oxidative stress [188]. These measurements showed no changes in *elmo1*^{-/-}, *elmo2*^{-/-} and *elmo3*^{-/-} larvae at 96 hpf (Figure 21A-C). Overall, the

metabolome analyses of the *elmo1*^{-/-}, *elmo2*^{-/-} and *elmo3*^{-/-} larvae have not identified the Elmo proteins as major metabolic regulators.

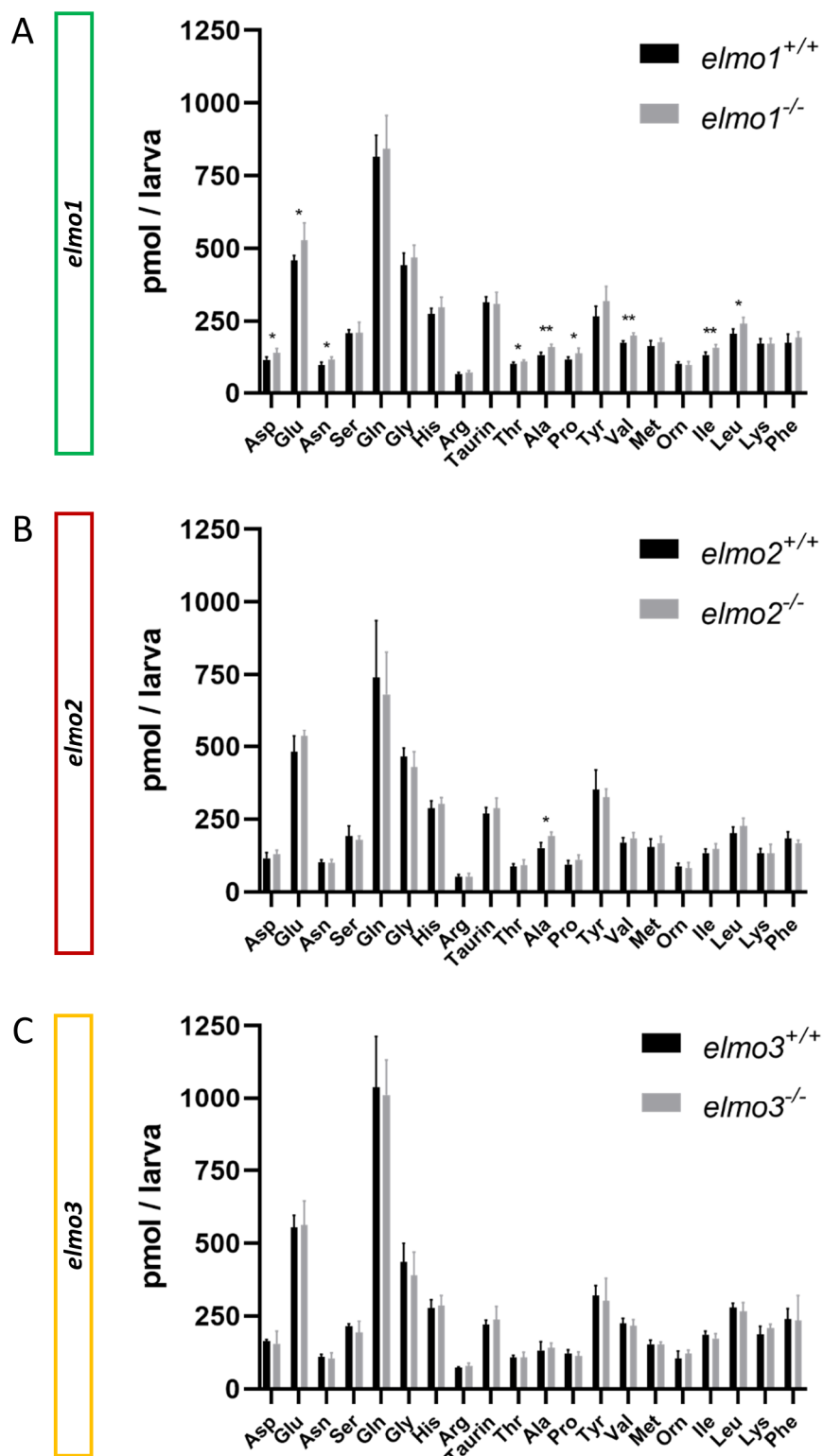


Figure 18. The loss of Elmo1 led to an increase of amino acids in zebrafish larvae. **(A)** Quantification of amino acids showed an increase of several amino acids in *elmo1*^{-/-} compared to *elmo1*^{+/+}. n = 5 samples per genotype, each containing 40 larvae at 96 hpf. **(B)** Quantification of amino acids showed an increase of one amino acid in *elmo2*^{-/-} compared to *elmo2*^{+/+}. n = 6 samples per

genotype, each containing 40 larvae at 96 hpf. **(C)** Quantification of amino acids showed no alterations between *elmo3^{-/-}* and *elmo3^{+/+}*. n = 5 samples per genotype, each containing 40 larvae at 96 hpf. Statistical analysis was done with t-test and Mann-Whitney test. * p < 0.05, ** p < 0.01. Data are listed as numbers in Supplementary Table 1. Ala, alanine; Arg, arginine; Asp, aspartic acid; Gln, glutamine; Glu, glutamic acid; Gly, glycine; His, histidine; Ile, isoleucine; Leu, leucine; Lys, lysine; Met, methionine; Orn, ornithine; Phe, phenylalanine; Pro, proline; Ser, serine; Thr, threonine; Tyr, tyrosine; Val, valine; hpf, hours post fertilization. Measurements were performed by the Metabolomics Core Technology Platform of the Centre of Organismal Studies Heidelberg.

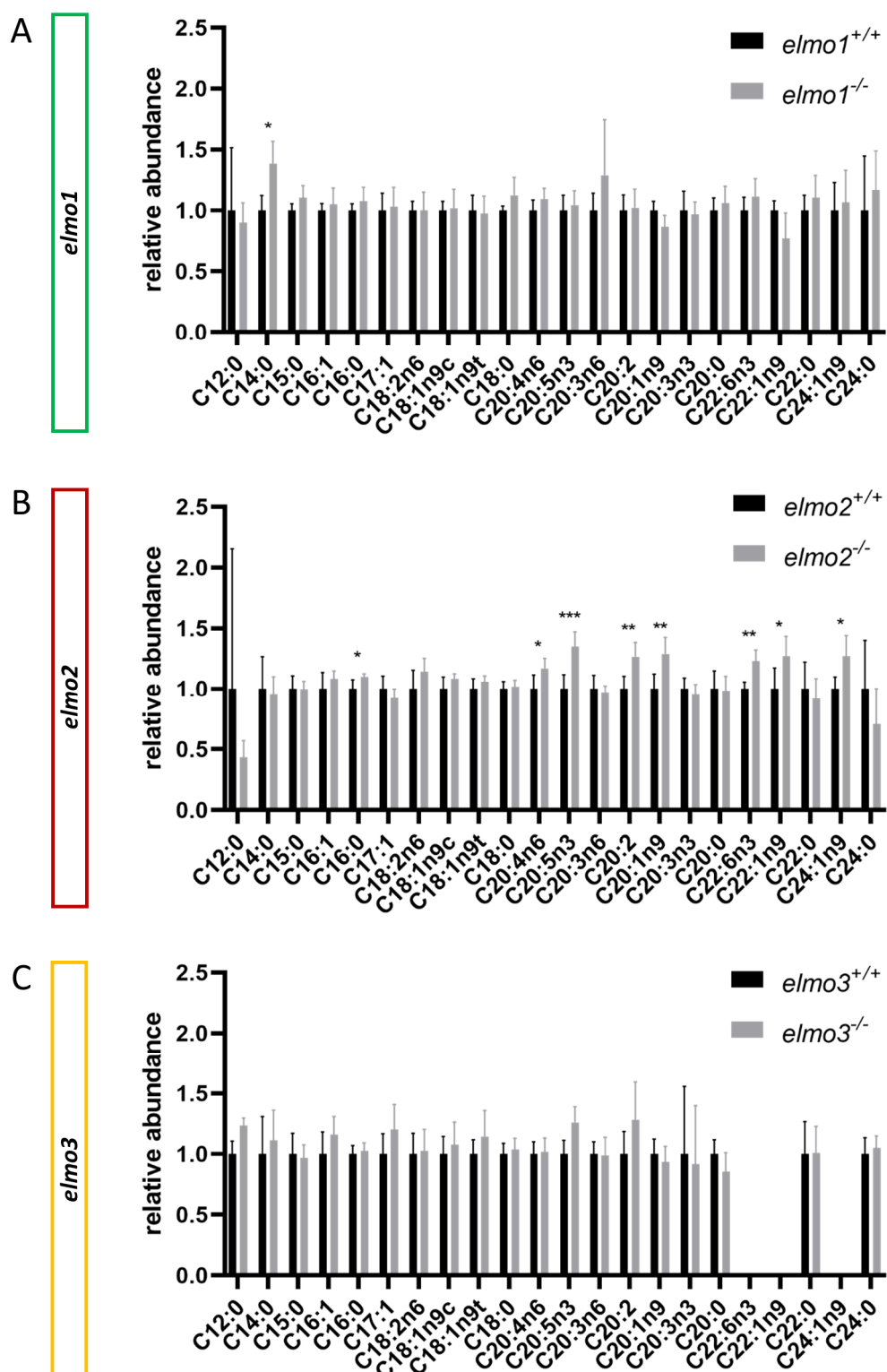


Figure 19. The loss of Elmo2 led to an increase of fatty acids in zebrafish larvae. (A) Quantification of fatty acids showed an increase of one fatty acid in *elmo1*^{-/-} compared to *elmo1*^{+/+}. n = 4 samples per genotype, each containing 40 larvae at 96 hpf. **(B)** Quantification of fatty acids showed an increase of several fatty acids in *elmo2*^{-/-} compared to *elmo2*^{+/+}. n = 5-7 samples per genotype, each containing 40 larvae at 96 hpf. **(C)** Quantification of fatty acids showed no alterations between *elmo3*^{-/-} and *elmo3*^{+/+}. n = 5 samples per genotype, each containing 40 larvae at 96 hpf. Statistical analysis was done with

t-test and Mann-Whitney test. * $p < 0.05$, ** $p < 0.01$, *** $p < 0.001$. Data are listed as numbers in Supplementary Table 2. hpf, hours post fertilization. Measurements were performed by the Metabolomics Core Technology Platform of the Centre of Organismal Studies Heidelberg.

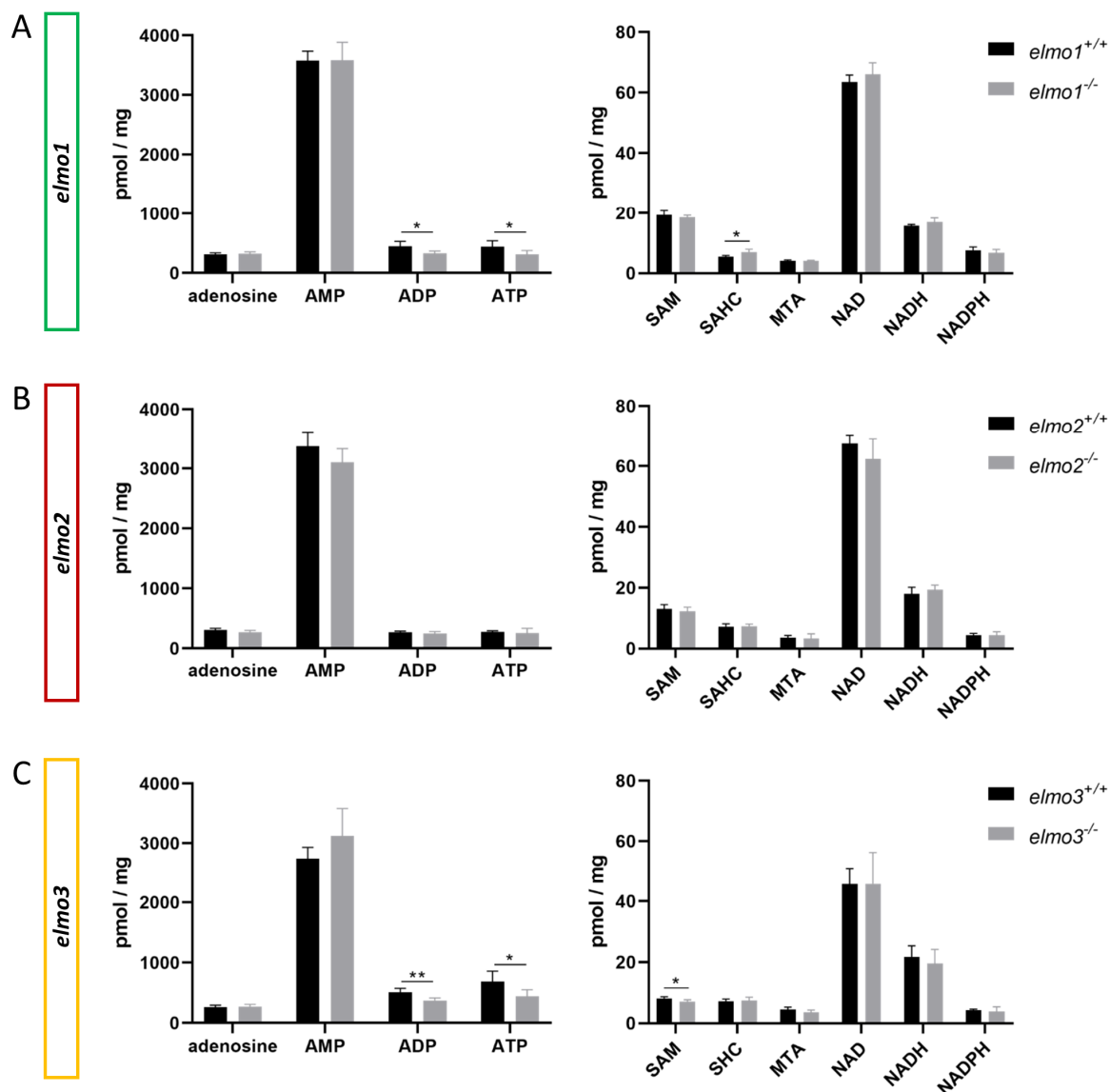


Figure 20. The loss of Elmo1 and Elmo3 respectively led to decreased ADP and ATP levels in zebrafish larvae. (A) Quantification of adenosines showed decreased ADP and ATP levels and an increased SAHC level in *elmo1*^{-/-} compared to *elmo1*^{+/+}. n = 5 samples per genotype, each containing 40 larvae at 96 hpf. **(B)** Quantification of adenosines showed no alterations between *elmo2*^{-/-} and *elmo2*^{+/+}. n = 6 samples per genotype, each containing 40 larvae at 96 hpf. **(C)** Quantification of adenosines showed decreased ADP, ATP and SAM levels in *elmo3*^{-/-} compared to *elmo3*^{+/+}. n = 5 samples per genotype, each containing 40 larvae at 96 hpf. Statistical analysis was done with t-test and Mann-Whitney test. * $p < 0.05$, ** $p < 0.01$. Data are listed as numbers in Supplementary Table 3. ADP, adenosine diphosphate; AMP, adenosine monophosphate; ATP, adenosine triphosphate; MTA, methylthioadenosine; NAD/NADH, nicotinamide adenine dinucleotide; NADPH, nicotinamide adenine dinucleotide phosphate; SAHC/SHC, S-adenosylhomocystein; SAM, S-adenosyl-methionine; hpf, hours

post fertilization. Measurements were performed by the Metabolomics Core Technology Platform from the Centre of Organismal Studies Heidelberg.

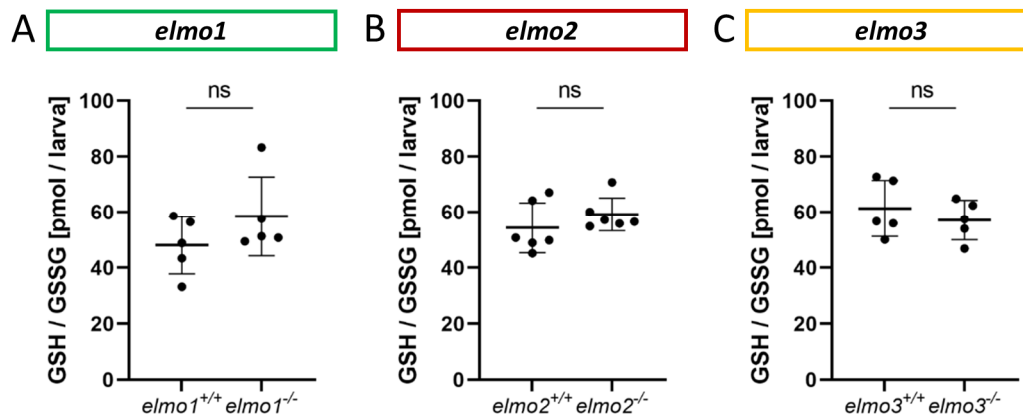


Figure 21. No alterations in glutathione ratios in *elmo1*^{-/-}, *elmo2*^{-/-} and *elmo3*^{-/-} zebrafish larvae.

(A) Comparisons of the ratio of reduced to oxidized glutathione showed no alterations in *elmo1*^{-/-} compared to *elmo1*^{+/+}. n = 5 samples per genotype, each containing 40 larvae at 96 hpf. (B) Comparisons of the ratio of reduced (GSH) to oxidized (GSSG) glutathione showed no alterations in *elmo2*^{-/-} compared to *elmo2*^{+/+}. n = 6 samples per genotype, each containing 40 larvae at 96 hpf. (C) Comparisons of the ratio of reduced to oxidized glutathione showed no alterations in *elmo3*^{-/-} compared to *elmo3*^{+/+}. n = 5 samples per genotype, each containing 40 larvae at 96 hpf. Statistical analysis was done with t-test and Mann-Whitney test. ns, not significant; hpf, hours post fertilization. Measurements were performed by the Metabolomics Core Technology Platform from the Centre of Organismal Studies Heidelberg.

In summary the comprehensive comparison of the phenotypic changes in organ morphology, transcriptome and metabolome of *elmo1*^{-/-}, *elmo2*^{-/-} and *elmo3*^{-/-} zebrafish (Figure 22) revealed multiple phenotypical similarities, but also several distinct changes in all analyzed areas.

			<i>elmo1</i> ^{-/-}	<i>elmo2</i> ^{-/-}	<i>elmo3</i> ^{-/-}
vasculature	larval	trunk sprouting	↕	—	—
		hyaloid branching	—	—	—
		hyaloid sprouting	—	—	—
		hyaloid diameter	↑	—	↑
	adult	retina branching	↓	—	↑
		retina sprouting	↓	↓	—
kidney	adult	glomerular nuclei	—	—	—
		glomerulus size	—	↑	—
		bowman space	↑	↑	—
		capillary area	—	—	—
		GBM thickness	—	—	↑
glucose homeostasis	larval	whole body glucose	—	—	—
	adult	blood glucose fasting	↓	—	—
		blood glucose postprandial	↑	—	—
transcriptome	larval	vasculature	↓	↓	↓
		kidney	—	—	—
		glucose homeostasis	—	—	↕
		related functions	↓	↕	↓
		nervous system	↑	↓	↑
metabolome	larval	amino acids	↑	—	—
		fatty acids	—	↑	—
		ADP, ATP	↓	—	↓
		glutathiones	—	—	—

Figure 22. Comparison of *elmo1*^{-/-}, *elmo2*^{-/-} and *elmo3*^{-/-} phenotype in zebrafish indicates different functions of Elmo1, Elmo2 and Elmo3. Overview and comparison of the results of the phenotypical analysis of *elmo1*^{-/-}, *elmo2*^{-/-} and *elmo3*^{-/-} zebrafish in larval and adult stages indicate that Elmo1, Elmo2 and Elmo3 have not the same role in the regulation of the organism. Listed are the fields which were analyzed in this study and their outcome in the specific zebrafish line. Results are visualized with arrows and bars. Arrow up (red) indicates an increase, arrow down (green) indicates a decrease, one arrow up and one arrow down at once indicate different changes, bar (grey) indicates no change. GBM, glomerular basement membrane.

2.11 *elmo1*^{-/-}, *elmo2*^{-/-} double knockout zebrafish exhibit no stronger alterations than single knockout lines

Because *elmo1* expression was increased in *elmo2*^{-/-} larvae, indicating a possible compensation between Elmo1 and Elmo2, the consequences of a loss of both proteins should be investigated. *elmo1*^{-/-} and *elmo2*^{-/-} single knockout animals were crossed to initiate the generation of double knockout animals. Their double heterozygous filial generation was crossed *inter se*, to obtain among others the *Tg(fli:EGFP) elmo1*^{-/-}, *elmo2*^{-/-} double knockout and the *elmo1*^{+/+}, *elmo2*^{+/+} control group zebrafish.

It should be analyzed if the double knockout zebrafish show an aggravation of the phenotypical changes which were observed in the single knockouts. Therefore, the retina vasculature, the GBM thickness and the values of blood sugar were measured and compared between adult *elmo1*^{-/-}, *elmo2*^{-/-} and *elmo1*^{+/+}, *elmo2*^{+/+} zebrafish.

elmo1^{-/-}, *elmo2*^{-/-} zebrafish showed a decreased branching and sprouting of the adult retina vasculature compared to *elmo1*^{+/+}, *elmo2*^{+/+} (Figure 23), which comprised the phenotypical changes observed in *elmo1*^{-/-} and *elmo2*^{-/-} zebrafish (Figure 11).

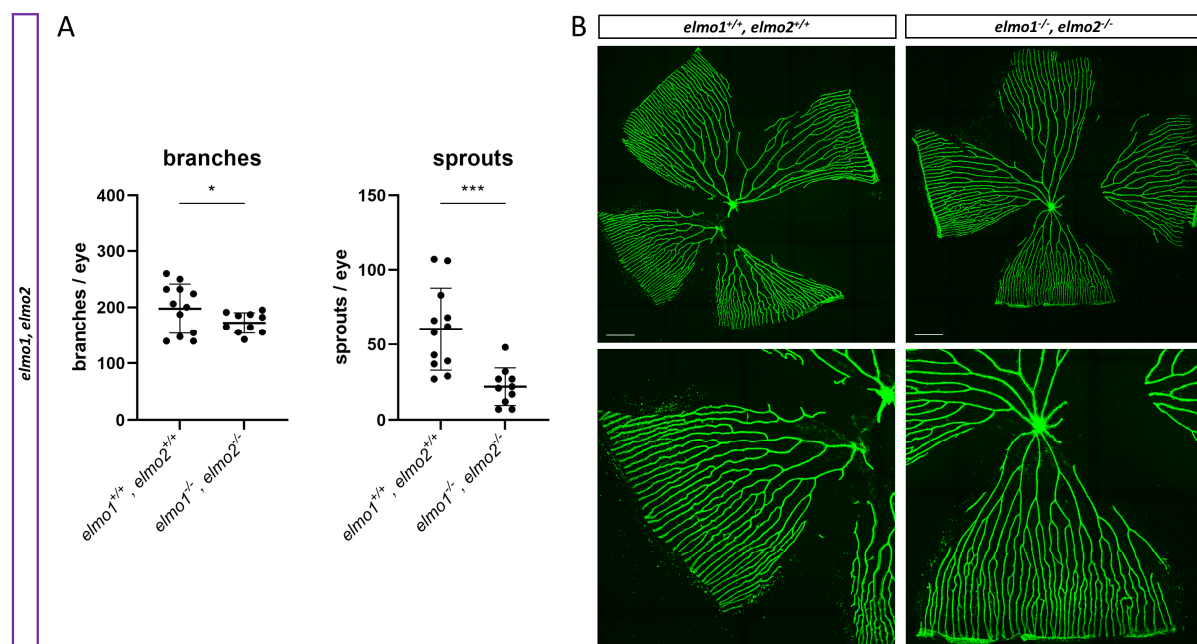


Figure 23. The loss of Elmo1 and Elmo2 led to a downregulation of the retinal vasculature in adult zebrafish. (A) Quantification of the adult retina vasculature showed a decrease in branches and sprouts in *elmo1*^{-/-}, *elmo2*^{-/-} compared to *elmo1*^{+/+}, *elmo2*^{+/+} zebrafish. n = 10-12 retinae per genotype. **(B)** Representative confocal microscopy images of the retina vasculature of adult *elmo1*^{+/+}, *elmo2*^{+/+} and *elmo1*^{-/-}, *elmo2*^{-/-} zebrafish. Scale bar is 300 μm. Analyzed retinae were obtained from animals of 8.5 mpf. Statistical analysis was done with t-test and Mann-Whitney test. * p < 0.05, *** p < 0.001. mpf, months post fertilization.

The GBM thickness in kidneys of *elmo1*^{-/-}, *elmo2*^{-/-} zebrafish was not significantly changed compared to kidneys of *elmo1*^{+/+}, *elmo2*^{+/+} (Figure 24A,B). This was also the case in the comparison of *elmo1*^{-/-} to *elmo1*^{+/+} and *elmo2*^{-/-} to *elmo2*^{+/+} (Figure 13).

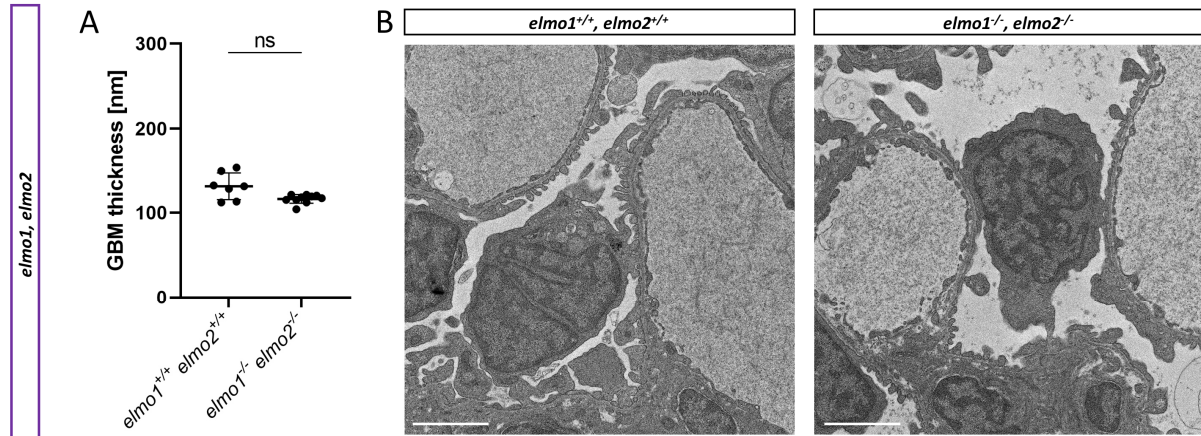


Figure 24. Unaltered glomerular basement membrane thickness in kidneys of adult *elmo1*^{-/-}, *elmo2*^{-/-} zebrafish. (A) Quantification of the thickness of the GBM in the adult kidney showed no alterations in *elmo1*^{-/-}, *elmo2*^{-/-} compared to *elmo1*^{+/+}, *elmo2*^{+/+} zebrafish (8.5 mpf). n = 7-10 per genotype. Each data point represents the mean thickness per one glomerulus. (B) Representative electron microscopy images of glomerulus sections of adult kidneys of *elmo1*^{+/+}, *elmo2*^{+/+} and *elmo1*^{-/-}, *elmo2*^{-/-} zebrafish. Scalebar is 2 μ m. Statistical analysis was done with Mann-Whitney test. ns, not significant; GBM, glomerular basement membrane; mpf, months post fertilization. Histological analysis and electron microscopy were performed by the Institute of Pathology IPH, EM Lab of the Heidelberg University Hospital.

The loss of Elmo1 led to decreased fasting and increased postprandial blood glucose levels in adult zebrafish (Figure 14). The loss of Elmo2 led to no such changes. Interestingly, the loss of both proteins also led to decreased fasting values but not to increased postprandial values (Figure 25).

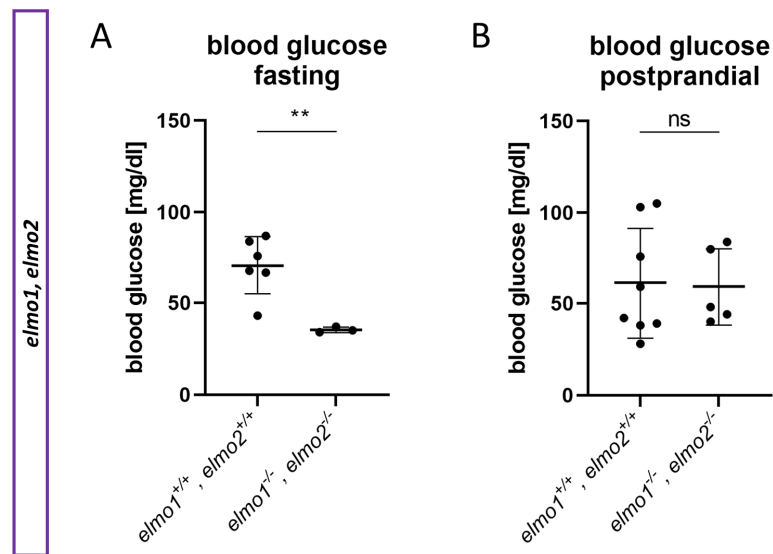


Figure 25. The loss of Elmo1 and Elmo2 led to decreased fasting blood glucose levels in adult zebrafish. (A) Fasting blood glucose levels were decreased in adult *elmo1^{-/-}, elmo2^{-/-}* compared to *elmo1^{+/+}, elmo2^{+/+}* zebrafish. **(B)** Postprandial blood glucose levels were unaltered in adult *elmo1^{-/-}, elmo2^{-/-}* compared to *elmo1^{+/+}, elmo2^{+/+}* zebrafish. Blood glucose was obtained from animals of 8.5 mpf. Statistical analysis was done with t-test and. ** $p < 0.01$. ns, not significant; mpf, months post fertilization.

In summary *elmo1^{-/-}, elmo2^{-/-}* double knockout zebrafish exhibited most of the phenotypical changes observed in *elmo1^{-/-}* or *elmo2^{-/-}* single knockout zebrafish lines but did not show a reinforcement of the changes or additional phenotypical alterations in the observed areas.

3 Discussion

Parts of this chapter have been published in the following publication in *Frontiers in Cell and Developmental Biology* in 2022 and have been originally written by myself.

Comparative morphological, metabolic and transcriptome analyses in *elmo1*^{-/-}, *elmo2*^{-/-} and *elmo3*^{-/-} zebrafish mutants identified a functional non-redundancy of the Elmo proteins

Mike Boger, Katrin Bennewitz, David Philipp Wohlfart, Ingrid Hausser, Carsten Sticht, Gernot Poschet, Jens Kroll

In this project, I established *elmo1*, *elmo2* and *elmo3* knockout zebrafish lines and performed morphological, metabolic and transcriptome analyses to compare the observed phenotypes between the three lines and to assess the functional homogeneity within the Elmo protein family. The results of these experiments are summarized in Figure 22 and showed that despite few similarities, *elmo1*^{-/-}, *elmo2*^{-/-}, and *elmo3*^{-/-} zebrafish exhibited several different morphologic, metabolic and transcriptional alterations, demonstrating a functional divergence between the three Elmo proteins.

3.1 Vascular changes in *elmo1*^{-/-}, *elmo2*^{-/-} and *elmo3*^{-/-} zebrafish indicate shared and varying regulatory functions within the Elmo protein family

Elmo1 is known to regulate and promote the early vascular development. Specifically, zebrafish studies have shown that *elmo1* is strongly expressed in the vasculature during embryogenesis and that it facilitates angiogenesis and the formation of blood vessels [46, 71]. By exhibiting an impaired vascular sprouting in the larval trunk and in the adult retina additional to a decreased vascular formation in the adult retina of *elmo1*^{-/-} zebrafish, the data of this study support this role of Elmo1 as a promotor of vascular formation and strengthen it by showing not only changes in developing larvae but also changes in vascular structures of adults.

An increased vessel thickness in larval hyaloids of *elmo1*^{-/-} zebrafish further suggests an impact of Elmo1 on vessel size, which would expand its regulatory capability in the vasculature, since vasodilation is caused differently than angiogenesis. Vasodilation is caused by the relaxation of smooth muscle cells of the blood vessels which can be triggered by different factors [96, 189]. The most prominent is the elevated presence

of the endothelial relaxation factor nitric oxide (NO) which is mainly produced from arginine [190, 191]. Arginine was measured and showed a non-significant increase of nine percent in *elmo1*^{-/-} compared to *elmo1*^{+/+} larvae. *elmo3*^{-/-} larvae also exhibited an increased hyaloid vessel diameter and a non-significant increase of arginine of about nine percent, compared to *elmo3*^{+/+} larvae. Further research is necessary to identify the underlying mechanism of the hyaloid vessel dilation of these two lines but based on these data an arginine-derived increase of NO as a possible cause can not be excluded.

The knockout of *elmo1* did not result in vascular malformations in the larval trunk at 96 hpf, as it was described in a transient morpholino based knockdown in zebrafish larvae at 56 hpf [46] which had implied an essential function of Elmo1 in the formation of blood vessels. Kok *et al.* already failed to detect structural changes in the larval trunk of a permanent *elmo1* knockout zebrafish [192]. But the permanent knockout in this study led to a developmental delay with ISV formation defects and additional sprouts in *elmo1*^{-/-} larvae at 32 hpf. A reason why these changes were not present anymore at 96 hpf could not be determined but might be explained through a compensation mechanism. The strong compensatory abilities of zebrafish are a widely discussed topic in zebrafish research. El-Brolosy *et al.* demonstrated that a permanent gene knockout can lead to significantly weaker consequences than an abrupt knockdown due to compensations [177, 178]. Consequently, these results raise the question of how much of the observed changes in the phenotype of the knockout lines the direct results of the loss of the proteins' functions are and how much of the protein's functions already have been compensated. Furthermore, the results emphasize how much the phenotypical changes depend on the observed time point.

However, the trunk vasculature of *elmo1*^{-/-} larvae did reveal a decreased number of sprouts at intersegmental vessels at 96 hpf. In a previous study in zebrafish larvae, it was suggested that Elmo1 stabilizes newly formed blood vessels and sprouts and promotes the survival of endothelial cells by protecting them from apoptosis [71]. The loss of this putative function in the knockout might be a possible cause for the reduced trunk sprouting, besides the option of a reduction of angiogenic signals due to the lost proangiogenic function of Elmo1 [46, 71].

The function of Elmo1 to promote vascular formation was further supported by the larval transcriptome data showing the downregulation of vascular developmental processes in *elmo1*^{-/-} larvae at 120 hpf. Interestingly, *elmo2*^{-/-} and *elmo3*^{-/-} zebrafish

larvae both exhibited a similar transcriptional regulation of the vasculature as seen in *elmo1*^{-/-}, indicating a functional homogeneity of the three proteins in the transcriptional regulation of the vascular development.

Additionally, some phenotypical changes were observed in two out of the three knockout lines, such as decreased vascular sprouting in adult retinae in *elmo1*^{-/-} and *elmo2*^{-/-} zebrafish and an increased vessel diameter in the hyaloid vasculature of *elmo1*^{-/-} and *elmo3*^{-/-} larvae, indicating that individual functions are shared just in two out of three proteins of the Elmo family.

The adult retina vasculature of *elmo3*^{-/-} was increased, revealing the opposing change to *elmo1*^{-/-} zebrafish. It needs further investigations addressing the cause of this development. One possible reason could be an increase of stress. *elmo3*^{-/-} zebrafish showed a reduced viability which is associated with stress reactions and various stress reactions were shown to lead to a dysregulated angiogenesis and an increased vascular formation [193–196].

These findings of the vascular phenotypes in *elmo1*^{-/-}, *elmo2*^{-/-} and *elmo3*^{-/-} zebrafish indicate partially overlapping functions of the three Elmo proteins in vascular development, even though the underlying mechanisms are unidentified. However, the observed varieties also demonstrate clear differences of the three proteins in the regulation of the vascular morphogenesis.

3.2 Elmo1, Elmo2 and Elmo3 regulate the ECM and affect the glomerular morphogenesis

Despite a physiologically healthy structure of the adult kidney tissue in *elmo1*^{-/-}, *elmo2*^{-/-} and *elmo3*^{-/-} zebrafish, the performed analyses identified an impact of Elmo1, Elmo2 and Elmo3 on the morphogenesis of glomerular structures. Changes in the form of an increased bowman space in *elmo1*^{-/-}, an increased bowman space and glomerular hypertrophy in *elmo2*^{-/-} and an increased GBM thickness in *elmo3*^{-/-} zebrafish were observed. Although the loss of each protein only led to small alterations, these changes are all associated with pathologic kidney development. Glomerular hypertrophy and the general volume increase of glomerulus compartments can indicate hypertension and were reported in the early stages of renal diseases [197–199]. An increased GBM thickness is caused by an imbalance between the synthesis and the degradation of ECM constituents and a subsequent ECM accumulation in the glomerulus and its GBM [200–202]. It is commonly associated with a reduced glomerular filtration rate [203] and

is one of the hallmarks in the development of diabetic nephropathy [152]. The transcriptomes of *elmo1*^{-/-}, *elmo2*^{-/-}, and *elmo3*^{-/-} zebrafish larvae exhibited no changes in the regulation of processes associated with kidney development and function, revealing no possible explanation for the observed structural changes. However, in the larval transcriptomes, the process of ECM organization and the ECM-receptor interaction pathway were strongly downregulated when Elmo1, Elmo2 or Elmo3 were absent. This might affect organs depending on a correctly regulated ECM and could be a cause for structural changes as observed in the glomeruli of *elmo1*^{-/-}, *elmo2*^{-/-} and *elmo3*^{-/-} zebrafish. Because the GBM and a significant part of the glomeruli consist of ECM, a correct ECM organization is a crucial determinant of glomerulus structure and function [114, 115]. Although the *elmo1*^{-/-} zebrafish only exhibited an increased bowman space area and a strongly transcriptional downregulated ECM, these findings fit to results of previous studies which have shown that manipulated *ELMO1* expression is linked to the dysregulation of ECM proteins, resulting in structural changes in glomeruli and the GBM in particular [61, 136]. Shimazaki *et al.* showed that an overexpression of *ELMO1* in COS cells led to an aggravated expression of ECM components as collagen and fibronectin and to an attenuated expression of matrix metalloproteases, important for ECM modulation and reorganization [62, 201]. Remarkably, Hathaway *et al.* pointed out that a temporarily overexpression of *ELMO1* in diabetic mice aggravated the severity of DN structurally and functionally [61]. Whereas a reduced *ELMO1* expression led to less severe diabetic complications and almost abolished the pathological features of DN. These results and the finding of elevated *ELMO1* in tubular and glomerular cells in the kidneys of diabetic mice [62] showed that *ELMO1* promotes the progression of DN, especially when overexpressed. Several studies reporting about diabetic patients with *ELMO1* gene variants having a susceptibility to develop DN [62, 72–76, 78] indicate that a changed or reduced function of *ELMO1* also promotes the development of DN. In this study, the loss of *Elmo1* also affects the organization of the ECM, the glomerular morphogenesis and dysregulates the adult blood glucose levels which all could contribute to the emergence of DN. Taken together, the combination of all this data implies that a dysregulated *ELMO1/Elmo1/elmo1* expression, independently whether up or down, is disadvantageous for the health of the kidney and could ultimately promote the development of renal disease.

3.3 Elmo1 as a novel blood glucose regulator

This study identified Elmo1 as a novel regulator of glucose homeostasis. Specifically, *elmo1*^{-/-} zebrafish exhibited a disturbed adult blood glucose regulation by showing decreased fasting and increased postprandial blood glucose levels.

Altered insulin levels as possible cause for the changed blood glucose levels could not be investigated, since the amount of blood, receiving from an adult zebrafish is not sufficient for current test systems.

The RT-qPCR analyses of the transcriptional regulation of proteins involved in glucose homeostasis in postprandial adult *elmo1*^{-/-} livers revealed just few significant changes, since *glut1a* expression was decreased and *glut5* and *hk2* expression was decreased. In humans and rodents, GLUT1 is responsible to sustain the low basal glucose level in all cells and its amount in the cytoplasm and at the cell membrane is therefore inverted to the present glucose level [204–206]. Zebrafish have three paralogs of *glut1*: *glut1a*, *glut1b* and *glut1c*. Although not significantly for *glut1b* and *glut1c*, the observed reduced expression of all three *glut1* genes could be a direct consequence of the high blood glucose levels present in postprandial *elmo1*^{-/-} zebrafish.

GLUT5 is the main fructose transporter, solely transporting fructose [207–209]. Its expression increased in diabetic human muscles [210] and decreased in adipocytes of diabetic rats [211]. *GLUT5* expression was described to be dependent on the serum fructose level, which is elevated in diabetic states [212]. Serum fructose was not determined but a high fructose level parallel to the high glucose level cannot be excluded as possible cause for elevated *glut5* expression in postprandial *elmo1*^{-/-} zebrafish.

HK2 facilitates the first step of glycolysis, phosphorylating glucose converting it to glucose-6-phosphate [213]. *HK2* expression increases in response to insulin to maintain glucose concentrations [214] and reduced expression of *HK2* was reported in skeletal muscles in insulin resistant diabetic rats [215]. Because it is neither known what the serum level of insulin, nor what the intracellular glucose levels in postprandial livers of the investigated *elmo1*^{-/-} zebrafish was, a cause for the increased expression of *hk2* cannot be determined.

In *elmo1*^{-/-} zebrafish larvae whole body glucose levels as well as the expression of insulin signaling genes and mechanisms related to insulin secretion and glucose homeostasis in the larval transcriptome remained unaltered, revealing no potential mechanism for an explanation of the altered blood glucose levels in adults. It further

indicates that the loss of Elmo1 is not relevant to the larval developmental stages regarding glucose metabolism and causes a disturbed blood glucose regulation solely in the adult stage through a so far unknown mechanism. One hypothetical explanation for the mechanism is based on the function of Rac1 facilitating the glucose induced insulin secretion through the reorganization of the pancreatic cytoskeleton [1, 153]. If Elmo1's function as GEF is crucial for a correct Rac1 activation in this process, the insulin secretion would be Elmo1 dependent and consequently disturbed through its loss.

Based on the phenotypical changes of the three knockout mutants, Elmo2 and Elmo3 functionally differ from Elmo1, as the adult blood glucose levels in *elmo2*^{-/-} as well as in *elmo3*^{-/-} zebrafish were unchanged in fasting and postprandial states.

Due to no changes in larval and adult blood glucose levels, as well as no transcriptional changes of genes and mechanisms related to glucose homeostasis in *elmo2*^{-/-} zebrafish, no regulatory role of Elmo2 can be diminished in the process of glucose metabolism. In cell culture ELMO2 was described to regulate the insulin dependent translocation of GLUT4 in human muscle cells and adipocytes [79], suggesting ELMO2 to be involved in the glucose uptake through skeletal muscles and fat tissue. This hypothesis was not tested in organisms yet. If zebrafish Elmo2 possess a comparable function as well, the influence of its loss would have been either not strong enough to cause consequences or to detect them in this study. Furthermore, zebrafish do not possess the *glut4* gene or Glut4 protein, nor a functional equivalent is known so far, which impedes a transmission of this mechanism to zebrafish.

Besides unaltered glucose levels in larvae and in adult blood of *elmo3*^{-/-} zebrafish, the larval transcriptome exhibited changes, such as in glycolysis and gluconeogenesis and in the cellular response to insulin stimulus. This indicates a regulatory role of Elmo3 in mechanisms involved in glucose homeostasis but leaves it unclear to which extend.

Altogether, these data revealed an important role of Elmo1 in the regulation of the adult blood glucose without giving a potential explanation for the underlying mechanism but attributing a functional difference of Elmo1, Elmo2 and Elmo3 in the regulation of the glucose metabolism.

3.4 Elmo1 is a potential risk factor for the development of diabetes and DN

The results of this study did not identify Elmo1, Elmo2 or Elmo3 to be involved in the development of diabetes or its complications, but they report an impact of the individual Elmo proteins in important systems which are affected by the pathogenesis of diabetes. Adult *elmo1*^{-/-} zebrafish showed a dysregulated blood glucose, as fasting levels were decreased, and postprandial levels were increased. This is comparable to a diabetic state in humans in which untreated patients often develop hypoglycemia during fasting state and hyperglycemia after food intake [216–220]. As already discussed, if Elmo1 is one of the GEFs regulating the Rac1 dependent insulin secretion, a loss of Elmo1 could result in hypoinsulinemia and the disturbance of the blood glucose regulation.

elmo1^{-/-} zebrafish exhibited an unexpected correlation of changes, as they have postprandial hyperglycemia but a decreased vascular density in the retina, opposite to hyperglycemia that was observed to lead to or correlate with retinopathy in diabetes in humans [144, 221, 222]. This discrepancy might be explained through the function of Elmo1 as a basic promotor of vascular development [46, 71]. The consequence of a loss of this function might be stronger or interfere with a potential angiogenic signal resulting from hyperglycemia induced damaging of the vasculature.

Although pathways and mechanisms of the glucose homeostasis were not significantly regulated in the *elmo1*^{-/-} larval transcriptome, the larval metabolome revealed changes comparable to as in diabetes. These were for example an increase in branched-chain amino acids (valine, leucine and isoleucine), alanine, aspartic acid and glutamic acid which has been associated with diabetes and diabetic risk [223–225]. Additionally, the energy sources ATP and ADP were decreased, which has also been associated with diabetes and insulin resistance [226–228].

Observed increase in glomerular structures, as an increase in the bowman space in *elmo1*^{-/-} and *elmo2*^{-/-} and a glomerular hypertrophy in *elmo2*^{-/-} was reported in the early stages of nephropathy [197–199] and the GBM thickening, observed in *elmo3*^{-/-} zebrafish, is a hallmark of diabetic nephropathy [200–202]. But whether these changes are part of a pathological development or just a structural difference, based on the functions of the individual Elmo proteins in the morphogenesis of the glomeruli, could not be determined.

Because of these findings and because this study is mostly descriptive, focusing on the phenotypical comparison of *elmo* mutants, no mechanisms leading to the development of diabetes or DN were identified, but fundamental insights into the

proteins' functions were discovered which build the basis for new hypotheses and further research questions. Based on the results of this study, two hypotheses can be made, aiming at a possible explanation for the frequently reported susceptibility of diabetic patients with *ELMO* gene variants to develop diabetic nephropathy [62, 72–76, 78]:

- 1) Due to the putative function of ELMO1 to regulate the blood glucose level, diabetic patients with *ELMO1* gene variants and a subsequent impaired function of the ELMO1 protein might have more difficulties to keep the blood glucose under control and therefore have a susceptibility to develop diabetic complications as nephropathy. A loss of parts or the whole function of ELMO1 might be an additional risk factor for individuals to develop diabetes in the first place.
- 2) In 2005 Shimazaki *et al.* already prognosed the promotion of the development of DN or glomerular injury through a dysregulated ECM in glomerular structures caused by dysregulated ELMO1 and a subsequent effect on glomerular function and health [62]. Diabetes patients who face this problem could have a higher risk to develop nephropathy. As ECM is transcriptionally and glomeruli morphologically changed in *elmo1^{-/-}*, *elmo2^{-/-}*, and *elmo3^{-/-}* zebrafish in this study, this theory could be applied to ELMO2 and ELMO3 explaining why their variants are also associated with the development of DN [77, 78].

A combination of both hypotheses would increase the risk factors for getting nephropathy and would possibly explain why there are far more findings about diabetic patients developing DN with gene variants of *ELMO1* than with gene variants of *ELMO2* and *ELMO3*.

In conclusion, Elmo1 could be a potential risk factor, not only for developing diabetic nephropathy, as often described, but also for the development of diabetes itself. Further investigations will be needed to understand the mechanisms underlying the disturbed blood glucose regulation caused by the loss of Elmo1, if this leads to metabolic changes comparable as in diabetes and if these results can be transferred to humans. Furthermore, it needs to be investigated what exact roles Elmo1, Elmo2 and Elmo3 have in the regulation of the ECM and if the loss of these functions increases the risk of developing nephropathy in diabetes.

3.5 The larval transcriptome is unequally regulated in *elmo1*^{-/-}, *elmo2*^{-/-} and *elmo3*^{-/-} zebrafish

Consistent with the morphological findings in vasculature and kidney, transcriptome analyses revealed phenotypical parallels as well as several differences between *elmo1*^{-/-}, *elmo2*^{-/-} and *elmo3*^{-/-} zebrafish.

Comparing the regulation of GOBP based biological processes (Figure 17), multiple transcriptional patterns were shared between *elmo1*^{-/-}, *elmo2*^{-/-} and *elmo3*^{-/-} zebrafish larvae. For example, cell motility, vascular development and extracellular matrix organization were equally downregulated. Furthermore, individual processes were similarly regulated only between *elmo1*^{-/-} and *elmo3*^{-/-}, whereas *elmo2*^{-/-} showed no or opposite changes, as in cytoskeleton organization or nervous system process. This further supports the idea of functional similarities just between two of the three Elmo proteins. Additionally, this analysis revealed multiple distinct findings of the individual Elmo proteins, such as the increased apoptotic process in *elmo2*^{-/-} or the increased response to insulin stimulus in *elmo3*^{-/-} larvae, suggesting independent functions.

Considering the total transcriptional regulation of KEGG based signaling pathways (Table 1), similarities appeared only as exceptions as most pathways showed different regulation patterns in *elmo1*^{-/-}, *elmo2*^{-/-} and *elmo3*^{-/-} zebrafish. Only three pathways showed a similar regulation. Especially the dysregulation of one third of the analyzed pathways in the larval transcriptome of *elmo3*^{-/-} zebrafish demonstrated a functional difference between the three Elmo proteins and revealed Elmo3 as an important factor to sustain the correct transcriptional regulation in the larval state. The enormous dysregulation of the larval transcriptome of *elmo3*^{-/-} zebrafish could be a possible cause for its reduced viability.

3.6 Elmo proteins fulfill common, but mainly individual functions

The conclusion of the morphologic and transcriptomic investigation was further supported by the metabolome analyses, revealing a common ADP and ATP decrease in *elmo1*^{-/-} and *elmo3*^{-/-} but different changes in amino acid and fatty acid amounts in *elmo1*^{-/-}, *elmo2*^{-/-} and *elmo3*^{-/-} zebrafish larvae. The investigation of the *elmo1*^{-/-}, *elmo2*^{-/-} double knockout zebrafish line also reinforces the idea that each Elmo protein fulfills individual functions. The phenotypical changes observed in the *elmo1*^{-/-} and *elmo2*^{-/-} single knockout lines were largely reproduced but not enhanced in the double knockout line. Uneven expression patterns among *elmo1*, *elmo2* and *elmo3* in wild

type zebrafish organs and larvae in this and other studies [35, 46], as well as in mice organs support the hypothesis of a functional divergence [229, 230].

The results of previous studies, addressing the question of the functional uniformity within the ELMO protein family, also fit to the conclusion of common and divergent functions. Whereas ELMO1 and ELMO2 were shown to function similarly in maintaining myoblast fusion in mouse derived myoblasts and they both are required for axon guidance [51, 59], Stevenson *et al.* stated that ELMO2 cannot rescue T cell migration in *ELMO1*^{-/-} mice [29]. Protein binding studies reported overlapping and different preferences of the three ELMO proteins to different binding partners [29, 52, 79]. Furthermore, some findings imply an inconsistent compensation potential between the ELMO proteins. Elliott *et al.* suggested a compensation of ELMO1 by ELMO2 in mouse macrophages but not in Sertoli cells [53], and in this study, an increase of *elmo1* RNA in *elmo2*^{-/-} larvae was observed, whereas *elmo2* RNA was unaltered in *elmo1*^{-/-} larvae.

Taken together, the data of the morphological, metabolic and transcriptomic analyses of the three *elmo* mutant zebrafish lines, combined with the results from previous studies, show that Elmo proteins share multiple functions and when knocked out, partially lead to similar changes in the phenotype. However, they also demonstrate that Elmo1, Elmo2 and Elmo3 have strong functional differences, as they regulate diverse mechanisms and lead to a multitude of different phenotypical alterations in the described gene knockout organisms. This leads to the conclusion that there is no vast majority of shared functions within the Elmo protein family, but the individual Elmo proteins largely perform distinct functions and regulate diverging mechanisms.

3.7 Conclusion

This study identified several new functions of the Elmo proteins in zebrafish, amongst others the modulation of survival, morphology, metabolome and transcriptome. Since it is mainly a phenotypical comparison and screening, the results of this study build a basis to develop new research questions and for further necessary investigations addressing the understanding of the underlying mechanisms.

Findings in the glucose homeostasis and the glomeruli as well as in the metabolome and the transcriptome in the knockout animals indicate a promotive role of the loss of Elmo1 for the development of diabetes. The loss of each of the three Elmo proteins was identified as a promotive factor for the development of renal alterations and could

be one part of the answer to the question, why diabetic patients with *ELMO* gene variants have a susceptibility to develop nephropathy.

The main finding of this study is that the three Elmo proteins have various individual functions which they do not share. Even though Elmo1, Elmo2 and Elmo3 exhibit similarities in protein amino acid sequences, are GEFs for Rac1 promoting its activity and share functions, this phenotypical comparison led to the conclusion that they mainly fulfill different functions and do not work redundantly. Therefore, this study is important for the understanding of the Elmo protein family and demonstrates that Elmo1, Elmo2 and Elmo3 can no longer be considered as a functional unity.

4 Material and Methods

Parts of this chapter have been published in the following publication in *Frontiers in Cell and Developmental Biology* in 2022 and have been originally written by myself.

Comparative morphological, metabolic and transcriptome analyses in *elmo1*^{-/-}, *elmo2*^{-/-} and *elmo3*^{-/-} zebrafish mutants identified a functional non-redundancy of the Elmo proteins

Mike Boger, Katrin Bennewitz, David Philipp Wohlfart, Ingrid Hausser, Carsten Sticht, Gernot Poschet, Jens Kroll

4.1 Material

4.1.1 Equipment

Product	Company
Table centrifuge	Carl Roth
Microcentrifuge Mikro 200R	Hettich
Benchtop centrifuge Rotina 420R	Hettich
Vertical micropipette puller P30	Sutter Instruments
Dry cabinet UNB 300	Memmert
Incubation shaking cabinet Certomat IS	Sartorius
Magnetic stirrer and heater	IKA
Vortex-Genie 2	Scientific Industries
Balance 440-47N and ABS	Kern
Heating and shaking block	HLC
See saw rocker	Stuart
Water bath AQUAline AL12	Lauda
pH-meter ProfiLine 197i	WTW ProfiLine
Pneumatic PicoPump PV 820	World Precision Instruments
Compressor Jun-Air 3-4	Jun-Air
Hamilton syringe Gastight 1705	Hamilton
Pipettes	Eppendorf
Drigalski spatula	Marienfeld
Glucometer Freedom Lite	Abbott

Pipet device accu-jet pro	Brand
BioPhotometer D30	Eppendorf
µCuvette G1.0	Eppendorf
Thermal cycler T100	BioRad
qPCR – cycler Quantstudio 3	Thermo Fischer Scientific
Western Blot system	BioRad
Chemi – Smart 5000	PeqLab
Agarose gel chamber	Peqlab Biotechnologie
Electrophoresis power supply	Consort
UV transilluminator and imager	INTAS
Leica HI1210 water bath	Leica
Leica RM2235 microtome	Leica
Leica CM 1950 cryostat	Leica
Zeiss Axio Scan.Z1	Zeiss
Plate reader Infinite M200	Tecan
Microscope MZ 10 F	Leica
Upright scanner TCS SP5 DS	Leica
Confocal microscope DM6000 B	Leica
UV-lamp EL 6000	Leica
Upright microscope BX51	Olympus Life Science
Camera XC10	Olympus Life Science

4.1.2 Software

Software	Usage
Leica Application Suite X 3.4.2.18368	Imaging and image analysis
Leica Application Suite V4.8	Imaging
Leica Application Suite V4.13	Imaging
ImageJ 1.48v	Image analysis
Inkscape 1.1.1	Image generation
IntasGelCaptureEntry	Imaging
Microsoft Office Professional Plus 2016	Documentation, analysis, writing
GraphPad Prism Version 9.4.0 (673)	Basic statistical analysis
ZiFiT Targeter Version 4.2	CRISPR target site planning
Citavi 6.11	Documentation, citation

Yost tools Poly Peak Parser	Sequencing analysis
Benchling	Sequencing analysis

4.1.3 Consumables

Product	Company
Safe-Lock tubes (0.5, 1.5, 2.0, 5.0 mL)	Eppendorf
Reaction tubes (1.5 mL)	Greiner bio one
PP culture tube (14 mL)	Greiner bio one
Conical tubes (15 mL, 50 mL)	Falcon
PCR tubes (0.2 mL)	Star Labs
Quantitative PCR 96-well reaction plates	Life Technologies
Plates (6-, 12-, 24-, 96-well)	Greiner
Petri dishes (10 cm)	Greiner
Pipette tips (1000, 200, 10 µL)	TipOne Star Labs
Pipette filter tips (1000, 100, 20 and 10 µL)	Nerbe plus
Combitips advanced (0.2 mL)	Eppendorf
Serological pipettes (5, 10, 25 and 50 mL)	Falcon
Pasteur Pipettes	Hirschmann
Cannula (25G – 27G x 3/4-1")	BD Microlance
Syringes (1 mL)	BD Plastipak
Syringe filter Rotilabo (0.45 µm)	Carl Roth
Stainless steel beads (5 mm)	Qiagen
Microscope slides	Marienfeld
Superfrost ultra plus microscope slides	Thermo Scientific
Cover slips (22x22 mm)	Menzel Gläser
Cover slips (24x50 mm)	Marienfeld
Capillary thin-wall (4", 1.0 mm)	Precision Instruments
Blood glucose test-strips (Lite)	FreeStyle Lite
Dumont Tweezers	NeoLabs
Disposable scalpel	NeoLabs
Whatman filter paper	Sigma-Aldrich
Nitrocellulose membrane 0.22 µm	Whatman
Tissue-Tek Cryomold (15x15x5 mm)	Sakura Finetek
Microtome blade 34°/80mm	Thermo Scientific

pH-Fix 0-14	Macherey-Nagel
Parafilm	Biozym
Adhesive Optical Film	Biozym

4.1.4 Chemicals

If not indicated otherwise, all chemicals used were purchased from following companies:

Carl Roth GmbH

Merck AG Roche

Diagnostics GmbH

SERVA Electrophoresis GmbH

Sigma-Aldrich Chemie GmbH

Thermo Fisher Scientific Inc.

4.1.5 Solutions

Solution	Components
10x PBS	400 g NaCl 10 g KCl 72,09 g Na ₂ HPO ₄ * H ₂ O 10 g KH ₂ PO ₄ ad 5 L Milli-Q water
50x TAE	242 g TrisBase 57.1 mL conc. Acetic acid 100 mL 0.5 M EDTA pH 8.6 ad 1 L Milli-Q water
10x ERM	20 g NaCl 0.6 g KCl 0.54 g CaCl ₂ *6H ₂ O 3.2 g MgSO ₄ *7H ₂ O 0.01 g Methylene blue ad 1 L Milli-Q water
5x PTU	304 g PTU

	ad 1L Milli-Q water
Tricaine	400 mg Tricaine powder 97.9 mL Milli-Q water 2.1 mL 1 M TRIS (pH 9) ad to pH 7 and 100 mL Milli-Q water
Lysis buffer	133 μ L of 1.5 M TRIS/HCl, pH 8 40 μ L 0.5 M EDTA 60 μ L Tween 60 μ L Glycerol ad 20 mL Milli-Q water
NP40 lysis buffer	0.87 g NaCl 5 mL 1M TRIS/HCl, pH 7.4 1.8 mL 0.5 M Na ₂ EDTA, pH 8 1 bottle Proteinase inhibitor cocktail 10 mL 10 % Nonidet P40 solution 10 mL Glycerol ad 100 ml Milli-Q water
5x Laemmli buffer	8.34 mL TRIS/HCl, pH 6.8 5 g SDS 0.25 g Bromophenol blue 25 mL Glycerol 3.45 g DTT ad 50 mL Milli-Q water
4 % PFA	10 mL 10x PBS 80 mL Milli-Q water 4 g PFA ad 100 mL Milli-Q water
1 % periodic acid solution	1 g Periodic acid ad 100 mL Milli-Q water
Hematoxylin staining solution	1 g Hematoxylin

	0.2 g Sodium iodate (NaIO_3)
	50 g Potassium alum ($\text{KAl}(\text{SO}_4)_2 \cdot 12 \text{H}_2\text{O}$)
	50 g Chloral hydrate ($\text{C}_2\text{H}_3\text{Cl}_3\text{O}_2$)
	1 g Citric acid ($\text{C}_6\text{H}_8\text{O}_7$)
	ad 1 L Milli-Q water
Sulfurous water	600 mL Milli-Q water
	30 mL 1 M HCl
	36 mL 10 % Sodium metasilphite ($\text{Na}_2\text{S}_2\text{O}_5$)
10x electrophoresis buffer	144 g Glycine
	30 g TRIS
	10 g SDS
	ad 1 L Milli-Q water
10x blotting buffer	30.28 g TRIS
	106.6 g Glycine
	ad 1 L Milli-Q water
TRIS/HCl pH 7.8	90.86 g TRIS
	pH 7.8
	ad 500 mL Milli-Q water
LB medium	20 mL LB-Broth
	ad 1 L Milli-Q water
LB Amp medium	20 mL LB-Broth
	ad 1 L Milli-Q water
	100 mg Ampicillin
LB agar	35 g LB Agar
	ad 1 L Milli-Q water
LB Amp agar	35 g LB Agar
	ad 1 L Milli-Q water
	100 mg Ampicillin

4.1.6 Further materials

Product	Company
Great Salt Lake artemia cysts	Sanders
TetraMin fish flake food	Tetra
GoTaq Green Master Mix	Promega
PowerSybr Green PCR Master Mix	Thermo Fisher Scientific
DNA loading dye (6x)	Thermo Fisher Scientific
Gene Ruler DNA ladder mix	Thermo Fisher Scientific
Page ruler plus	Thermo Fisher Scientific
Supersignal horseradish peroxidase substrate	Thermo Fisher Scientific
Tissue-Tek OCT Compound	Sakura Finetek
Tissue-Clear	Sakura Finetek
Fluoromount-G mounting medium	Thermo Fisher Scientific
DPX mounting medium	Thermo Fisher Scientific
Quick-hardening mounting medium	Sigma-Aldrich
Paraplast Plus (paraffin)	Sigma-Aldrich
Antonia Red Dextran 4 (M _w 3000-5000)	Sigma-Aldrich
Gibco Trypsin-EDTA (10x, 0.5 %)	Thermo Fisher Scientific
QIAzol Lysis Reagent	Qiagen
Purified BSA (100x)	New England Biolabs
GoTaq Green Master Mix	Promega
PowerSYBR Green PCR Master Mix	Thermo Fisher Scientific
Illustra plasmidPrep Mini Spin Kit	GE Healthcare
Plasmid Midi Kit	Qiagen
QIAquick PCR Purification Kit	Qiagen
RNeasy Mini Kit	Qiagen
miRNeasy Mini Kit	Qiagen
Pierce BCA Protein Assay Kit	Thermo Fisher Scientific
MAK263-1KT Glucose Assay Kit	Sigma Aldrich
Maxima First strand cDNA Synthesis Kit	Thermo Fisher Scientific
MEGAscript T7 Transcription Kit	Thermo Fisher Scientific
mMESSAGE mMachinE T7 Kit	Thermo Fisher Scientific

4.1.7 Antibodies

Primary antibody	Company (catalogue number)
β -Actin antibody (1:1000 dilution; mouse; monoclonal)	Santa Cruz Biotechnology (sc-47778)
ELMO1 antibody (1:1000 dilution; goat; unknown)	Everest Biotech (EB05297)
ELMO2 antibody (1:1000 dilution; goat; polyclonal)	abcam (ab2240)
ELMO2 antibody (1:500 dilution; mouse; monoclonal)	Santa Cruz Biotechnology (sc-365739)
ELMO3 antibody (1:500 dilution; goat; polyclonal)	abcam (ab 219791)
ELMO3 antibody (1:500 dilution; mouse; monoclonal)	Santa Cruz Biotechnology (sc-166364)
Secondary antibody	Company (catalogue number)
anti-goat immunoglobulins/HRP (1:1000 dilution; rabbit; polyclonal)	DAKO, Agilent Technologies (P0160)
anti-mouse immunoglobulins/HRP (1:1000 dilution; rabbit; polyclonal)	DAKO, Agilent Technologies (P0260)

4.1.8 Enzymes and buffers

Product	Company
NEBuffer 3	New England Biolabs
NEBuffer 3.1	New England Biolabs
Cut Smart Buffer	New England Biolabs
BsmBI	New England Biolabs
BglII	New England Biolabs
Sall	New England Biolabs
BamHI	New England Biolabs
XbaI	New England Biolabs
T4 DNA Ligase Buffer	New England Biolabs
T4 Ligase	New England Biolabs
Proteinase K, recombinant PCR Grade	Sigma-Aldrich

4.1.9 Plasmids

Plasmid	Company
pT7-gRNA	Addgene
pT3TS-nCas9n	Addgene

4.1.10 Oligonucleotides

All oligonucleotides were designed using the NCBI primer blast (<https://www.ncbi.nlm.nih.gov/tools/primer-blast/>) and purchased from Sigma Aldrich.

CRISPR constructs

Gene	Oligonucleotide name	Sequence (5' to 3')
<i>elmo1</i>	ELMO1-CRISPR-for#1	TAGGTGGCCATCGAGTGGCCTG
<i>elmo1</i>	ELMO1-C1-rev-new	AAACCAGGCCACTCGATGGCCA
<i>elmo2</i>	Elmo2-CRISPR#2-for	TAGGAGACGCAGCAGAACCCAG
<i>elmo2</i>	Elmo2-CRISPR#2-rev	AAACCTGGGTTCTGCTGCGTCT
<i>elmo3</i>	Elmo3-CRISP#3-for	TAGGTCCAGCTGAATGAGCTGC
<i>elmo3</i>	Elmo3-CRISP#3-rev	AAACGCAGCTCATTGAGCTGGA

Genotyping by sequencing

Gene	Oligonucleotide name	Sequence (5' to 3')
<i>elmo1</i>	Elmo1-C1-gen-for2	CCTCTGTCTCCTACTACAGGCT
<i>elmo1</i>	Elmo1-C1-gen-rev2	GAAAGTTTAAATGATTGTGCAACCC
<i>elmo2</i>	Elmo2-genotyping#4-for	CTGTCCGCTCATGTTCAACACA
<i>elmo2</i>	Elmo2-genotyping#2-rev	GTGTGCACTGACGCTGAATC
<i>elmo3</i>	Elmo3-C3-gen-for1	AATCATTGTGACTATTGCGTGCC
<i>elmo3</i>	elmo3-gen-short-rev-four	ACATCCTCTTTATGACAGGAAGTGC

Genotyping by gel electrophoresis

Gene	Oligonucleotide name	Sequence (5' to 3')
<i>elmo1</i>	Elmo1-C1-gen-for2	CCTCTGTCTCCTACTACAGGCT
<i>elmo1</i>	Elmo1-C1-gen-rev2	GAAAGTTTAAATGATTGTGCAACCC
<i>elmo2</i>	elmo2-gen-short#for-three	GAGCTGCGCAGGATTGCGTT
<i>elmo2</i>	Elmo2-genotyping#2-rev	GTGTGCACTGACGCTGAATC
<i>elmo3</i>	Elmo3-C3-gen-for1	AATCATTGTGACTATTGCGTGCC

<i>elmo3</i>	elmo3-gen-short-rev-four	ACATCCTCTTTATGACAGGAAGTGC
--------------	--------------------------	---------------------------

RT-PCR

Gene	Oligonucleotide name	Sequence (5' to 3')
<i>elmo1</i>	elmo1 cDNA for d	TCTCTCTGTCTTTCTTGCCGCTT
<i>elmo1</i>	elmo1 cDNA rev a	CAATCTCCATAAGTTTGGGGAAGGC
<i>elmo2</i>	Elmo2-auf-Exon8-cDNA#1-for	GTGCTGACCTTTAACCTTCTGGA
<i>elmo2</i>	Elmo2-genotyping#2-rev	GTGTGCACTGACGCTGAATC
<i>elmo3</i>	elmo3 cDNA for 5	TTCCCGCTTTTAACAGGCTCTCA
<i>elmo3</i>	elmo3 cDNA rev 6	AGCGGCCTGGTGCTTTGGTT

RT-qPCR

Gene	Oligonucleotide name	Sequence (5' to 3')
<i>arnt2</i>	arnt2_qPCR_Left	AGCCAGACAGAGGTCTTCCA
<i>arnt2</i>	arnt2_qPCR_Right	CCGAGGTCAGCAAAGTCTTC
<i>elmo1</i>	elmo1-qPCR-1for	GGGACACTTTCTCTGTGGCCTT
<i>elmo1</i>	elmo1-qPCR-1rev	TCTTGAGCCACCTTCTGGTAGAGA
<i>elmo2</i>	elmo2-qPCR-1for	GACGCGGGTGCTGTGTGATATT
<i>elmo2</i>	elmo2-qPCR-1rev	CGTGTGTGAAGAACATGGGGTGG
<i>elmo3</i>	elmo3-qPCR-1for	AGCTCACACTCATCCTGTGCG
<i>elmo3</i>	elmo3-qPCR-1rev	GGTCCTGAGCGAAGAAGATCGG
<i>ins</i>	2-INS_qPCR_Left	GGTCGTGTCCAGTGTAAGCA
<i>ins</i>	2-INS_qPCR_Right	GGAAGGAAACCCAGAAGGGG
<i>insra</i>	Insra qPCR left	AGAGGCCAGCGAGCTCTAC
<i>insra</i>	Insra qPCR right	CACTTGTGTGGGGGCTCT
<i>insrb</i>	Insrb qPCR left	GCCTCTGCGGATCACTACAT
<i>insrb</i>	Insrb qPCR right	CTCCTGCGTGGTCTTGAAC
<i>glut1a</i>	glut1a_RT-PCR_Left	TGACCGGCCCATACGTTTTTC
<i>glut1a</i>	glut1a_RT-PCR_Right	ATCATCTCGGTTATATTTATCTGCC
<i>glut1b</i>	glut1b_RT-PCR_Left	CCATTTCTCCTGGGCTTTACCTTTA
<i>glut1b</i>	glut1b_RT-PCR_Right	CAGATTTGGCTTTGCTTTCTCGTT
<i>glut1c</i>	glut1c_RT-PCR_Left	CATCCGTAATATTCAGGTGCTAGTG
<i>glut1c</i>	glut1c_RT-PCR_Right	ATTTTCAGCAGAGGTGGAAAGAG
<i>glut2</i>	glut2_rt-pcr_Left	GCAGAAGAACCCTCACTC

<i>glut2</i>	glut2_rt-pcr_Right	TCTCCGCCACAATAAACC
<i>glut3</i>	glut3_RT-PCR_Left	TCGTCAATGTCTTGGCTCTG
<i>glut3</i>	glut3_RT-PCR_Right	CAACATACATTGGCGTGAGG
<i>glut5</i>	glut5_RT-PCR_Left	TCTCTGGTTGCTGGATTTGGT
<i>glut5</i>	glut5_RT-PCR_Right	CAAGAGGGTGAGGAGATTGTCC
<i>glut6</i>	glut6_RT-PCR_Left	TTGCTATTGCAGCCAGTTTG
<i>glut6</i>	glut6_RT-PCR_Right	CAGGCCGTCTGTTAGGGTAA
<i>glut8</i>	glut8_RT-PCR_Left	CATTTTGTCTGGTGTCTCATGT
<i>glut8</i>	glut8_RT-PCR_Right	CCTGCAATGAAAAAGCCCAT
<i>glut9</i>	glut9a_RT-PCR_Left	GAGGCCGGAGCAGAGAAAGCGTTC
<i>glut9</i>	glut9a_RT-PCR_Right	AGCATTTCAGTCCACACAGCTGATA
<i>glut10</i>	glut10_RT-PCR_Left	GCACTTCAGTAGGACCGCAT
<i>glut10</i>	glut10_RT-PCR_Right	GTGCCACATTAAGCAGTTGA
<i>glut11a</i>	glut11a_RT-PCR_Left	CCCTGGGAACTATCCCTCAT
<i>glut11a</i>	glut11a_RT-PCR_Right	TCCACTGATTGCCAACACAT
<i>glut11b</i>	glut11b_RT-PCR_Left	AAGGATGAGTACTGGCCGATCCTC
<i>glut11b</i>	glut11b_RT-PCR_Right	AATGCCGAGAGCGCTGACCCTTTC
<i>glut12</i>	Glut12_RT-PCR_Left	GGGACAATCCTGGACCACTA
<i>glut12</i>	Glut12_RT-PCR_Right	ACATCCCAACCAGCATTCTC
<i>hk1</i>	hk1_qPCR_Left	ATGATAGCGGCACAGCTTCT
<i>hk1</i>	hk1_qPCR_Right	GTTGGTGTCTCGTGCCAATC
<i>hk2</i>	hk2_qPCR_Left	TGAGGTCAGTCTCGTCCAGT
<i>hk2</i>	hk2_qPCR_Right	TCTTAATCGACAGGCCACCG
<i>gck</i>	gck_qPCR_Left	AATCACCGCTGACCTGCTAT
<i>gck</i>	gck_qPCR_Right	GCCACTTCACATACGCAATG
<i>pklr</i>	PK-L_qPCR_Left	TCCTGGAGCATCTGTGTCTG
<i>pklr</i>	PK-L_qPCR_Right	GTCTGGCGATGTTTCATTCT
<i>pfkla</i>	PFKla_qPCR_Left	ACTGCCACTCCAGCGTTAAA
<i>pfkla</i>	PFKla_qPCR_Right	CAGAGCTGGAGTTCACCCTC
<i>pfklb</i>	PFK Lb 2_qPCR_Left	GCCGTTCAACATTCACGACC
<i>pfklb</i>	PFK Lb 2_qPCR_Right	TGCAGTCGAACACTCCTTGG
<i>pck1</i>	cPEPCK_qPCR_Left	ATCACGCATCGCTAAAGAGG
<i>pck1</i>	cPEPCK_qPCR_Right	CCGCTGCGAAATACTTCTTC
<i>g6pc1a.1</i>	G6Pase_qPCR_Left	TCACAGCGTTGCTTTCAATC

g6pc1a.1 G6Pase_qPCR_Right

AACCCAGAAACATCCACAGC

4.1.11 Bacterial strains

For generation of the CRISPR constructs the *E. coli* *stabl3* strain was used for cloning.

4.1.12 Zebrafish transgenic lines

All experimental procedures on animals were approved by the local government authority, the Regierungspräsidium Karlsruhe (license no.: G-98/15 and I-19/02) and carried out in accordance with the approved guidelines. Zebrafish (*Danio rerio*) embryos and adults of the line *Tg(fli1:EGFP)* were used in this study.

4.1.13 Gene and transcript sequences

Genomic and complementary DNA and transcript sequences were obtained from the databank ensembl genome browser 106 (<https://www.ensembl.org/>).

Gene	Gene ID	Transcript ID
<i>elmo1</i>	ENSDARG00000098753	ENSDART00000172618.2
<i>elmo2</i>	ENSDARG00000063527	ENSDART00000162982.2
<i>elmo3</i>	ENSDARG00000042126	ENSDART00000061738.7

4.2 Methods

4.2.1 Zebrafish husbandry

The zebrafish line *Tg(fli1:EGFP)* [183] was used and raised as described [160] in normal husbandry environment. *Tg(fli1:EGFP)* was chosen because of its EGFP expressing endothelial cells. Embryos and larvae until 120 hpf were kept in egg water at 28.5 °C with or without PTU (0.003 %) to suppress pigmentation. Larvae older than 120 hpf and adult zebrafish were held in a 13-hour light / 11-hour dark cycle. Zebrafish older than 90 days are referred to as adults. Adults were fed twice a day, fresh *Artemia Salina* in the morning and fish flake food at midday.

4.2.2 Mutant generation

To use the CRISPR/Cas9 system to generate mutations, guide RNA (gRNA) to target the zebrafish genes *elmo1* (ensembl transcript ID: ENSDART00000172618.2; exon 2), *elmo2* (ensembl transcript ID: ENSDART00000162982.2; exon 9) and *elmo3* (ensembl transcript ID: ENSDART00000061738.7; exon 2) had to be designed. The respective oligonucleotides of the designed target site had to be annealed and ligated into the pT7-gRNA plasmid vector. Cloning was performed according to Jao *et al.* with modifications [166].

4.2.2.1 Target site design

Target sites and respective oligonucleotides which were used to generate the CRISPR constructs were designed with ZiFiT Targeter Version 4.2.

4.2.2.2 Oligonucleotide annealing

Annealing mix:

Oligonucleotide forward 100 μ M	2 μ L
Oligonucleotide reverse 100 μ M	2 μ L
NEBuffer 3	2 μ L
Milli-Q water	14 μ L

Annealing program:

95 °C	5 min
cool 0.1 °C per sec	
50 °C	10 min
cool 1 °C per sec	
4 °C	infinite

4.2.2.3 CRISPR plasmid generation

Digestion and ligation reaction mix:

annealed oligonucleotides	1 μ L
pT7-gRNA plasmid	400 ng
NEBuffer 3	1 μ L
T4 DNA Ligase Buffer	1 μ L
BsmBI	0.5 μ L
BgIII	0.3 μ L

Sall	0.3 μ L
T4 Ligase	0.5 μ L
Milli-Q water	ad 10 μ L

Digestion and ligation program:

(37 °C	60 min, 16 °C	45 min) 3x
37 °C	30 min	
55 °C	30 min	
80 °C	15 min	
4 °C	infinite	

4.2.2.4 Transformation of *Escherichia coli*

50 μ L of competent *Escherichia coli* (*E. coli*) stabl3 strain were thawed on ice. The ligated CRISPR plasmid (complete) was added to *E. coli* and the mixture was incubated on ice for 20 min. The mixture was incubated at 42 °C for exact 90 sec and subsequently put on ice for at least 90 sec. 1 mL LB was added and shaken in an incubation shaking cabinet (Sartorius) for 45 min at 37 °C and 220 rpm. Afterwards bacteria were centrifuged for 5 min at 6000 rpm (at max) at 4 °C. 900 μ L of the supernatant was removed and the residue of the supernatant was used to resuspend the bacterial pellet. The bacteria were plated on a LB Amp agar plate and incubated overnight at 37 °C.

4.2.2.5 Plasmid mini preparation

Single colonies from the LB Amp agar plates were picked with a pipette tip and used to inoculate 3 mL LB Amp medium in culture tubes (Greiner bio one). These were shaken overnight at 37 °C with 220 rpm. Plasmid DNA was isolated with the Illustra plasmidPrep Mini Spin Kit (GE Healthcare) according to the manufacturer's protocol. The isolated plasmid DNA was eluted with 30 μ L Milli-Q water. Used culture tubes with residual bacteria were stored for further procedure.

4.2.2.6 Identification of successful ligated CRISPR constructs

50-100 ng isolated plasmid DNA from each bacteria culture was sequenced by Eurofins Genomics with sanger sequencing with the manufacturer's primer mix M13rev-19. The sequences were analyzed with the software benchling

(benchling.com) and bacteria culture from which plasmids including the annealed CRISPR oligonucleotides were used for further procedure.

4.2.2.7 Plasmid midi preparation

10 µL from the used culture tubes (from 4.2.2.5) which contained successful ligated CRISPR plasmids were used to inoculate 3 mL LB Amp medium. These were shaken overnight at 37 °C with 220 rpm. 100 µL of each culture were used to inoculate 100 mL LB Amp in Erlenmeyer flasks and incubated overnight at 37 °C with 220 rpm. For culture backups, 800 µL from each culture were mixed with 200 µL sterile glycerol and stored at -80 °C. The residual bacterial cultures were used with the Plasmid Midi Kit (Qiagen) according to the manufacturer's protocol to isolate plasmid DNA. The isolated plasmid DNA was eluted with 75 µL Milli-Q water.

4.2.2.8 *In vitro* transcription of CRISPR gRNA and Cas9 mRNA

The pT7-gRNA and pT3TS-nCas9n plasmid vectors were linearized with BamHI and XbaI, respectively and purified with the PCR purification Kit (Qiagen) according to the protocol of the manufacturer. To generate the respective CRISPR gRNAs and the Cas9 mRNA, a subsequent *in vitro* transcription was performed using the T7 MEGAShortscript Kit (Invitrogen) and the mMEASSAGE MACHINE Kit (Invitrogen) according to the protocols of the manufacturers, respectively. The produced gRNAs were purified using the miRNeasy Mini Kit (Qiagen) and Cas9 mRNA was purified using the RNeasy Mini Kit (Qiagen) according to the protocols of the manufacturers, respectively. Until injection, RNAs were stored at -80 °C.

4.2.2.9 CRISPR/Cas9 injection

Freshly laid eggs of *Tg(fli1:EGFP)* zebrafish were arranged in a 1 % agarose ramp in ERM and with a Pneumatic PicoPump PV 820 (World Precision Instruments) 1 nL KCl (0.1 M) solution containing gRNA (250 pg/nL) and Cas9 mRNA (200 pg/nL) was injected into the cell of single cell stadium embryos [166].

4.2.2.10 Germline transmission and further breeding

The genotypes of the injected F0 fish were analyzed by Sanger sequencing by Eurofins Genomics and chimeric mutated individuals were crossed with wild type *Tg(fli1:EGFP)* zebrafish to generate heterozygous mutants. Promising mutations were selected and

respective individuals with the same mutation were crossed to generate homozygous mutants and wild type control fish.

4.2.2.11 Generation of a double gene knockout mutant zebrafish line

To generate a zebrafish line with knockout mutations in the *elmo1* and in the *elmo2* gene, single knockout *Tg(fli1:EGFP) elmo1^{-/-}* and *Tg(fli1:EGFP) elmo2^{-/-}* zebrafish were crossed to get a *Tg(fli1:EGFP) elmo1^{+/-}, elmo2^{+/-}* filial generation. These were crossed *inter se* to obtain among other genotypes the *Tg(fli1:EGFP) elmo1^{-/-}, elmo2^{-/-}* double knockout and the *Tg(fli1:EGFP) elmo1^{+/+}, elmo2^{+/+}* control zebrafish.

4.2.3 Preparation of adult zebrafish organs and blood glucose measurement

For experiments with animals with a gene knockout, littermates were always used as control. Adult zebrafish were put into single boxes in the afternoon the day before preparation. Blood glucose measurement was either done after 21-23 hours fasting or postprandial after feeding 1 hour with 0.5 g flakes following 1 hour in fresh water without food. Before blood glucose measurement and preparation fish were euthanized in an ice-cold water bath for 2 min. Blood was directly taken from the caudal vessel and measured with a glucometer (Freestyle Abbott) [231]. Subsequently, fish were decapitated and transferred into ice-cold PBS for organ isolation. Organs were either snap frozen in liquid nitrogen for RNA isolation and protein extraction or put in 4 % PFA/PBS for 24 h for visualization via confocal microscopy and periodic acid-Schiff (PAS) staining or in 3 % glutaraldehyde in cacodylate (0.1 M, pH 7.4) for visualization via electron microscopy or embedded in Tissue-Tek OCT Compound (Sakura Finetek) and frozen in liquid nitrogen cooled isopentane for visualization of brain sections via confocal microscopy.

4.2.4 Western Blot analysis

4.2.4.1 Protein lysate generation

100 μ L NP40 lysis buffer was added to each organ sample. After shaking on ice for 10 min, samples were homogenized with a 5 mm steel bead in a TissueLyser II (Qiagen) (2x, 2 min, 25 Hz). Afterwards samples were again incubated on ice for 15 minutes before the transferred lysate was centrifuged 10 min at 14000 rpm and 4 °C resulting in the supernatant as the final protein lysate.

4.2.4.2 Determination of protein concentration

The protein concentration of lysates was measured with a Pierce BCA Protein Assay Kit (Thermo Fisher Scientific) following the protocol of the manufacturer. Colorimetric detection was achieved with a plate reader (Tecan Infinite M200).

4.2.4.3 SDS-PAGE and Western Blot

1:5 Laemmli buffer was added to protein lysates. The lysates were heated for 5 min at 95 °C and approximately 60 µg of each lysate was loaded into a polyacrylamide gel (5 % stacking gel, 10 % separating gel) in a blotting system (Biorad). Proteins were separated by SDS-PAGE at 80 V for 25 min followed by 110 V for 90 min. Afterwards the separation gel including the separated proteins was transferred on a nitrocellulose membrane and the proteins were blotted from the gel onto the membrane at 100 V for 2 h in continuously cooled blotting buffer.

4.2.4.4 Immunohistochemistry

After blotting, the membrane was cut separating the different protein containing parts for antibody staining and incubated in Pierce Protein-Free blocking buffer (Thermo Fisher Scientific) for 1 h while shaking. Afterwards the membrane was incubated with the respective primary antibody diluted in blocking buffer in the respective concentration overnight at 4 °C while shaking. At the next day, the membrane was washed with PBST (3x, 5 min) and subsequently incubated with the respective second antibody for 30 min while shaking. Residual secondary antibody was washed away with PBST (3x, 5 min). Visualization was acquired by enhanced chemiluminescence by incubation with Supersignal horseradish peroxidase substrate (Thermo Fisher Scientific) and the Chemi – Smart 5000 (PeqLab).

4.2.5 Microscopy and analysis of vascular structures

Vascular structures of zebrafish larvae and adult organs were imaged with the confocal fluorescence microscope (Leica DM6000 B) with a scanner (Leica TCS SP5 DS) using a 20 x 0.7 objective. Images were analyzed with Leica Application Suite X and ImageJ.

4.2.5.1 Analysis of the larval trunk

For analysis of the larval trunk vasculature, larvae at 32 and 96 hpf were anaesthetized in 0.003 % tricaine and observed with a Leica MSV269. The first 6 intersegmental

vessels (ISVs) were skipped. The next 17 ISVs on both sides of the larva were observed for deformations and additional sprouts. Imaging was done as described above.

4.2.5.2 Analysis of the larval hyaloid

For analysis of the hyaloid vasculature, larvae at 120 hpf were anaesthetized in 0.003% tricaine and fixated in 4 % PFA/PBS for 24 hours. Afterwards fixated larvae were incubated in 0.25 % Trypsin/EDTA solution buffered with TRIS HCl (1.5 M, pH 7.8) for 80 min at room temperature during gentle movement on a shaker. Subsequently, larvae were washed three times for 10 min with PBS and stored in PBS at 4 °C until preparation. Hyaloids were isolated on an agarose plate and placed on an object slide in a drop of water. Imaging was done as described above.

4.2.5.3 Analysis of the larval hyaloid vessel permeability

For hyaloid vessel permeability analysis, larvae at 120 hpf were anaesthetized in 0.003% tricaine and 84 ng Antonia Red Dextran 4 (Merck) diluted in 0.1 M KCl was injected in the sinus venosus. Larvae were mounted into 1 % low melt agarose and imaged 30 and 50 min after injection. Imaging was done as described before through the lens of the larval eye. Quantification was done with the ratio of extravascular to intravascular fluorescence intensity of the hyaloid vessels and with the Measure and with the Threshold tool of the software ImageJ.

4.2.5.4 Analysis of the adult retina

Analysis of the adult retina vasculature was done as described [232]. In brief, for preparation, the fixated eye was transferred into cold PBS on an agarose plate for dissection. The retina was isolated and put on PBS on an object slide, cut and covered in Fluoromount-G mounting medium (Thermo Fisher Scientific) with a cover slip. Imaging was done as described above.

4.2.5.5 Analysis of the adult brain

For analysis of the adult brain vasculature, the brain was fixated in 4 % PFA/PBS over night at 4 °C. Afterwards the brain was washed with PBS (3x, 5 min), transferred into a cryomold (Sakura Finetek) and covered with Tissue-Tek OCT Compound (Sakura Finetek). The cryomold was put into a liquid nitrogen cooled cup, filled with isopentane,

for 5 sec until the OCT Compound hardened. The block was stored at -80 °C until it was cut with a Leica CM 1950 cryostat in 10 µm sections which were put on an object slide and stored at -20 °C until imaging. Imaging was done at the same day as cryosectioning and as described before. For analysis the software ImageJ was used. Area size measurements were done with the Measure and with the Threshold tool.

4.2.6 Microscopy and analysis of the kidney morphology

4.2.6.1 Paraffin embedding and PAS staining

For analysis of the adult glomerular structure, dissected kidneys were fixated in 4 % PFA/PBS in preparation for PAS staining. Fixated kidneys were embedded in paraffin and cut in 4 µm thick sections with a Leica RM2235 microtome and placed on an object slide. After deparaffinization, sections were put in 1 % periodic acid for 10 min, washed in distilled water and put in Schiff's reagent for 20 min, followed by three times in SO₂ water for 2 min. Afterwards sections were rinsed in running tap water, stained in hematoxylin solution and rinsed again, each for 5 min. Stained sections were dehydrated with ethanol solutions and mounted with mounting medium. Brightfield imaging was done with a Zeiss Axio Scan.Z1 slide scanner. Analysis of glomerular structure was done as described previously [174]. In brief, just sections were used at the point or near the point where the arterioles go into or out of the glomerulus to thereby try to analyze the glomerulus at its most concentric point as possible to obtain maximal comparability. For analysis the software ImageJ was used. Area size measurements were done with the Measure and with the Threshold tool. Nuclei numbers were counted manually.

4.2.6.2 Fixation and electron microscopy analysis

Fixation, electron microscopy and subsequent analysis of the images were performed in collaboration with Dr. Ingrid Haußer, Andrea Döbler and Ulrike Ganserer at the Institute of Pathology IPH, EM Lab of the Heidelberg University Hospital. For analysis of the glomerular basement membrane, kidneys were fixated in 3 % glutaraldehyde in cacodylate (0.1 M, pH 7.4), cut in 1 mm³ pieces and postfixed in 1 % aqueous osmium tetroxide for 1 hour at 4 °C. Subsequently, they were rinsed with water, dehydrated using ethanol solutions, transferred into propylene oxide and embedded in epoxy resin (glycidether 100). With an ultramicrotome (Reichert Ultracut E) semithin (1 µm) and

ultrathin sections (60-80 nm) were cut. To identify the glomeruli, the semithin sections were stained with methylene blue and analyzed under a light microscope (Olympus) at 200 X magnification. Ultrathin sections were treated with uranyl acetate and lead citrate and examined with a transmission electron microscope (JEM 1400), equipped with a 2k TVIPS CCD camera (TemCam F216) at 3000-10000 X magnification. Analysis was done with EMMeasure.

4.2.7 Collection of zebrafish larval samples

If not described differently, zebrafish larvae were anaesthetized in 0.003 % tricaine, collected and snap frozen in liquid nitrogen. Homogenization was achieved with a 1 mL syringe and a 25 G cannula.

4.2.8 Whole body glucose measurement in larvae

20 larvae at 120 hpf were collected per sample. Samples were homogenized in assay buffer with a 25G cannula and a 1 mL syringe. Glucose assay (MAK263, Sigma-Aldrich) was performed to determine the glucose levels following the protocol of the manufacturer. Fluorometric detection was achieved with a plate reader (Tecan Infinite M200).

4.2.9 Isolation of genomic DNA

For genomic DNA isolation, cut fin parts of adult zebrafish or whole larvae (72-120 hpf) were put in 20 μ L lysis buffer and incubated for 10 min at 98 °C. 10 μ L of proteinase K (10 mg/mL) were added following an incubation for at least 6 h. Afterwards DNA samples were heated up for 10 min at 98 °C and then either directly used or stored at -20 °C.

4.2.10 RNA purification

4.2.10.1 Larvae samples

30 larvae were collected per sample. Samples were homogenized in 350 μ L 1 % 2-mercaptoethanol in RLT lysis buffer (Qiagen) using a 25G cannula and a 1 mL syringe. Total RNA was isolated with the RNeasy Mini Kit (Qiagen) following the protocol of the manufacturer. The isolated RNA was eluted with 30 μ L nuclease-free water and stored at -80 °C until usage.

4.2.10.2 Organ samples

Total RNA from organ samples was extracted following the miRNeasy (Qiagen) handbook “Purification of total RNA, including small RNAs from animal tissue” and the appendix C “Disruption and homogenization of tissue using the TissueLyser II” using the RNeasy Mini Kit (Qiagen). In brief, organ samples were homogenized in 700 μL QIAzol lysis reagent (Qiagen) with a 5 mm steel bead in a TissueLyser II (Qiagen) (2x, 2 min, 20 Hz). After 5 min of incubation at RT, 140 μL chloroform were added. Afterwards, the samples were shaken vigorously for 15 sec and again incubated at RT for 3 min. Homogenates were centrifuged for 15 min at maximum speed at 4 °C. The upper phase of the homogenate was transferred into a new tube and mixed with 1.5 volumes (500 μl) 100 % ethanol by pipetting. 650 μl of the mixture was pipetted into a column and was centrifuged (15 sec, RT, max speed). This was repeated with the residual mixture. The column was washed with 650 μl buffer RW1 (15 sec, RT, max speed), 500 μl buffer RPE (15 sec, RT, max speed) and 500 μl buffer RPE (2 min, RT, max speed). RNA was eluted with 30 μl nuclease-free water (1 min, RT, max speed).

4.2.11 Polymerase chain reaction (PCR)

A PCR reaction mix contained 6.5 μL Milli-Q water, 2 μl forward primer (100 μM), 2 μL reverse primer (100 μM), 12.5 μL GoTaq Green Master Mix (Promega) and 2 μL of DNA sample. PCR was performed with a Thermal cycler T100 (BioRad) with the following cycles:

95 °C	5 min
(95 °C	30 sec,
individual annealing temperature	30 sec,
72 °C	45 sec) 32x
72 °C	10 min
4 °C	infinite

PCR products were either used directly or stored at -20 °C.

4.2.12 Reverse-transcription PCR (RT-PCR)

cDNA was synthesized from 1 μg RNA with the Maxima First Strand cDNA Synthesis Kit (Thermo Fisher Scientific) according to the protocol of the manufacturer. Standard PCRs were applied with the generated cDNA. Mutations (deletion and insertion) were

made visible by gel electrophoretic separation of PCR products. PCR products were either directly used or stored at -20 °C.

4.2.13 Reverse-transcription quantitative PCR (RT-qPCR)

cDNA was synthesized from 1 µg RNA with the Maxima First Strand cDNA Synthesis Kit (Thermo Fisher Scientific) according to the protocol of the manufacturer. For RT-qPCR Power SYBR™ Green PCR Master Mix Kit (Thermo Fisher Scientific) and 96 well reaction plates were used with a QuantStudio 3 Real-Time PCR System (Thermo Fisher Scientific). The reaction mix contained 1 pmol/µl forward and reverse primer respectively, 2 ng/µl cDNA, both diluted in Milli-Q water and 5 µl Power SYB Green PCR Master Mix in a total volume of 10 µl per well.

4.2.14 RNA-sequencing and transcriptome analysis

Quality control of total larvae RNA was performed in collaboration with Dr. Carolina Torre at the Next-Generation Sequencing (NGS) Core Facility of the Medical Faculty Mannheim with a Bioanalyzer (Agilent). Library construction and RNA-sequencing were performed by the Beijing Genomic Institution (BGI) (www.bgi.com; Shenzhen, China) with a BGISEQ-500. Sequencing analysis was performed in collaboration with Dr. Carsten Sticht at the Next-Generation Sequencing (NGS) Core Facility of the Medical Faculty Mannheim. The main procedure was done with R and Bioconductor using the NGS analysis package systempipeR [233]. Quality control of raw sequencing reads was performed using FastQC (Babraham Bioinformatics). Low-quality reads were removed using trim_galore (version 0.6.4). Resulting reads were aligned to zebrafish genome version danRer11 from UCSC and counted using Kallisto version 0.46.1 [234]. The count data were transformed to log₂-counts per million (logCPM) using the voom-function from the limma package [235]. Differential expression analysis was performed using the limma package in R. As the level of significance a false positive rate of $\alpha = 0.05$ with FDR correction was taken. Using the ggplot 2 package (version 2.2.1), the GOplot (version 1.0.2) [236] and the complexHeatmap (version 2.0.0) [237], volcano plots, chord plot and heatmaps were created. Raw RNA-sequencing data are available at GEO (Gene Expression Omnibus, NCBI) under the accession number: GSE197827.

4.2.15 Metabolome analyses

Metabolite analyses of amino acids, fatty acids, adenosine compounds and glutathiones were performed in collaboration with Dr. Gernot Poschet, Dr. Michael Büttner, Dr. Elena Heidenreich and Dr. Katja Machemer-Noonan at the Metabolomics Core Technology Platform at the Centre for Organismal Studies from the University of Heidelberg. For sample collection, zebrafish larvae at 96 hpf were anaesthetized in 0.003 % tricaine, collected and snap frozen in liquid nitrogen. 40 larvae were collected per sample. Measurements of amino acids, fatty acids, adenosine compounds and glutathione were performed by the Metabolomics Core Technology Platform from the Centre of Organismal Studies Heidelberg with either ultra-performance liquid chromatography with fluorescence detection (UPLC-FLR) or semi-targeted GC-MS as described from Lodd *et al.* [238].

4.2.16 Genotyping

Genotyping genomic zebrafish DNA was performed by PCR amplifying the area of a putative mutation and by subsequent gel electrophoretic separation or Sanger sequencing, which was performed by Eurofins Genomics (www.eurofinsgenomics.eu; Ebersberg). Sequencing results were analyzed with benchling (benchling.com) and PolyPeakParser [239].

4.2.17 Protein sequence alignment

Amino acid sequence alignment was achieved with the UniProt Align tool (<https://www.uniprot.org/align/>) with zebrafish Elmo1 (UniProt ID: Q6NV39), Elmo2 (UniProt ID: A0A0G2KRJ3) and Elmo3 (UniProt ID: F1QSV8) and human ELMO1 (UniProt ID: Q92556), ELMO2 (UniProt ID: Q96JJ3) and ELMO3 (UniProt ID: Q96BJ8).

4.2.18 Statistics

Data are given as mean with standard deviation. For the comparison of two groups of data, datasets were tested for Gaussian distribution. Then statistical significance between those groups was analyzed with the t-test (if data was normally distributed) or with the Mann-Whitney test (if data was not normally distributed). To determine the statistical significance between more than two groups with two categorical independent variables, a two-way ANOVA was applied. To determine statistical significance between the genotype distribution of zebrafish lines and the mendelian inheritance, the

chi square test was applied. To determine statistical significance between the survival of zebrafish lines, a logrank test was applied. p-values were given as: * $p < 0.05$, ** $p < 0.01$, *** $p < 0.001$, **** $p < 0.0001$. GraphPad Prism 9.3.1 was used for statistical analyses.

Appendix

Parts of this chapter have been published in the following publication in *Frontiers in Cell and Developmental Biology* in 2022 and have been originally written by myself.

Comparative morphological, metabolic and transcriptome analyses in *elmo1*^{-/-}, *elmo2*^{-/-} and *elmo3*^{-/-} zebrafish mutants identified a functional non-redundancy of the Elmo proteins

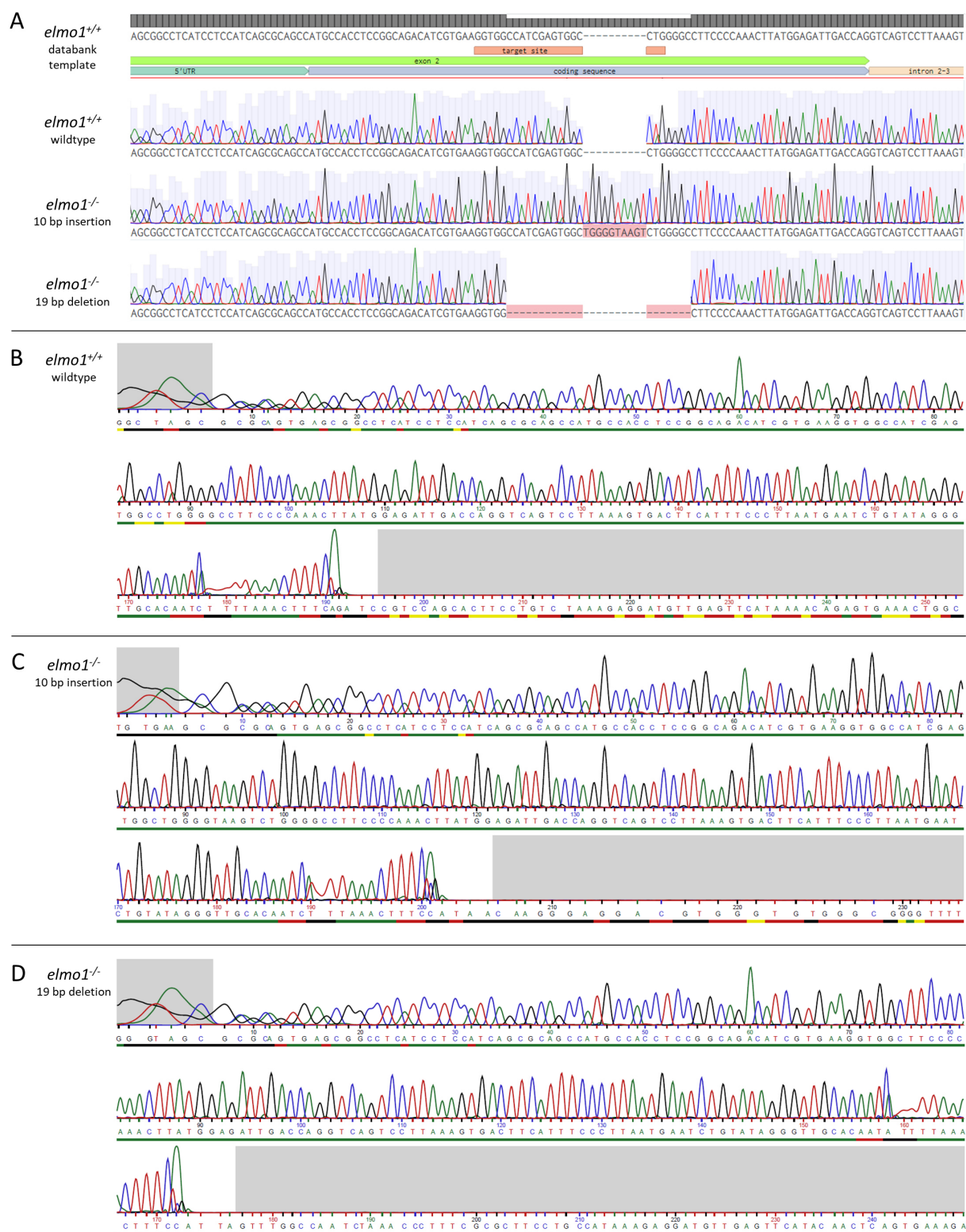
Mike Boger, Katrin Bennewitz, David Philipp Wohlfart, Ingrid Hausser, Carsten Sticht, Gernot Poschet, Jens Kroll

Supplementary Figure List

Supplementary Figure 1. Human ELMO1, ELMO2 and ELMO3 showed 45 % identity in amino acid sequence.	83
Supplementary Figure 2. Visualization and sequencing results of the target site area of wildtype zebrafish <i>elmo1</i> and the two generated <i>elmo1</i> ^{-/-} mutant lines.....	84
Supplementary Figure 3. Visualization and sequencing results of the target site area of wildtype zebrafish <i>elmo2</i> and the two generated <i>elmo2</i> ^{-/-} mutant lines.....	85
Supplementary Figure 4. Visualization and sequencing results of the target site area of wildtype zebrafish <i>elmo3</i> and the two generated <i>elmo3</i> ^{-/-} mutant lines.....	87
Supplementary Figure 5. The loss of Elmo1 delayed ISV and sprout formation in larval trunk vasculature in zebrafish at 32 hpf.....	88
Supplementary Figure 6. Unaltered hyaloid vessel permeability of <i>elmo2</i> ^{-/-} zebrafish larvae at 120 hpf.....	89
Supplementary Figure 7. Unaltered vascular density in adult brains of <i>elmo2</i> ^{-/-} zebrafish.	90
Supplementary Figure 8. The loss of Elmo1, Elmo2 and Elmo3 led to different intensities of changes in the regulation of the transcriptome of zebrafish larvae.	90

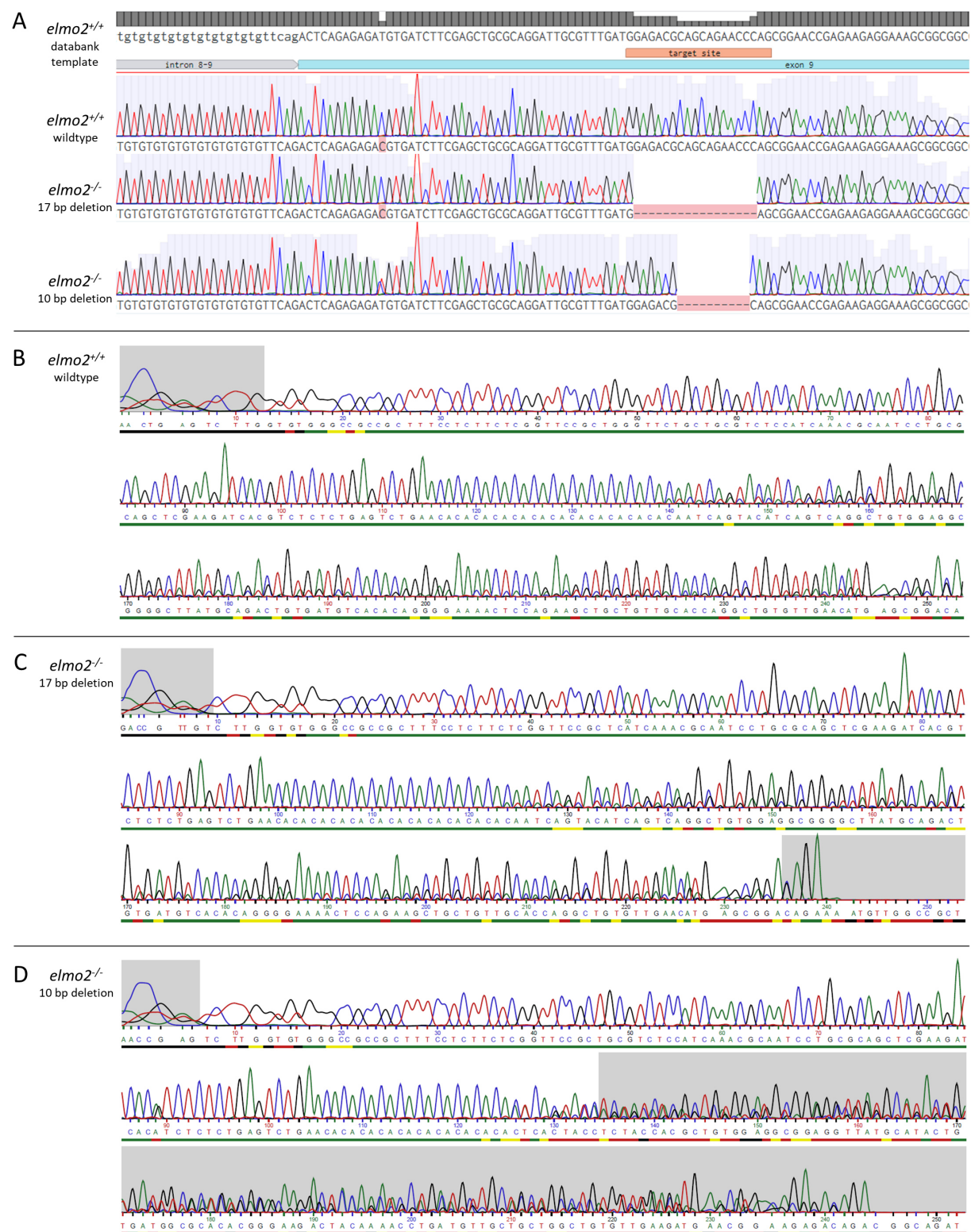
Supplementary Table List

Supplementary Table 1. The loss of Elmo1 led to an increase of amino acids in zebrafish larvae.	91
Supplementary Table 2. The loss of Elmo2 led to an increase of fatty acids in zebrafish larvae.	91
Supplementary Table 3. The loss of Elmo1 and Elmo3 respectively led to decreased ADP and ATP levels in zebrafish larvae.	92



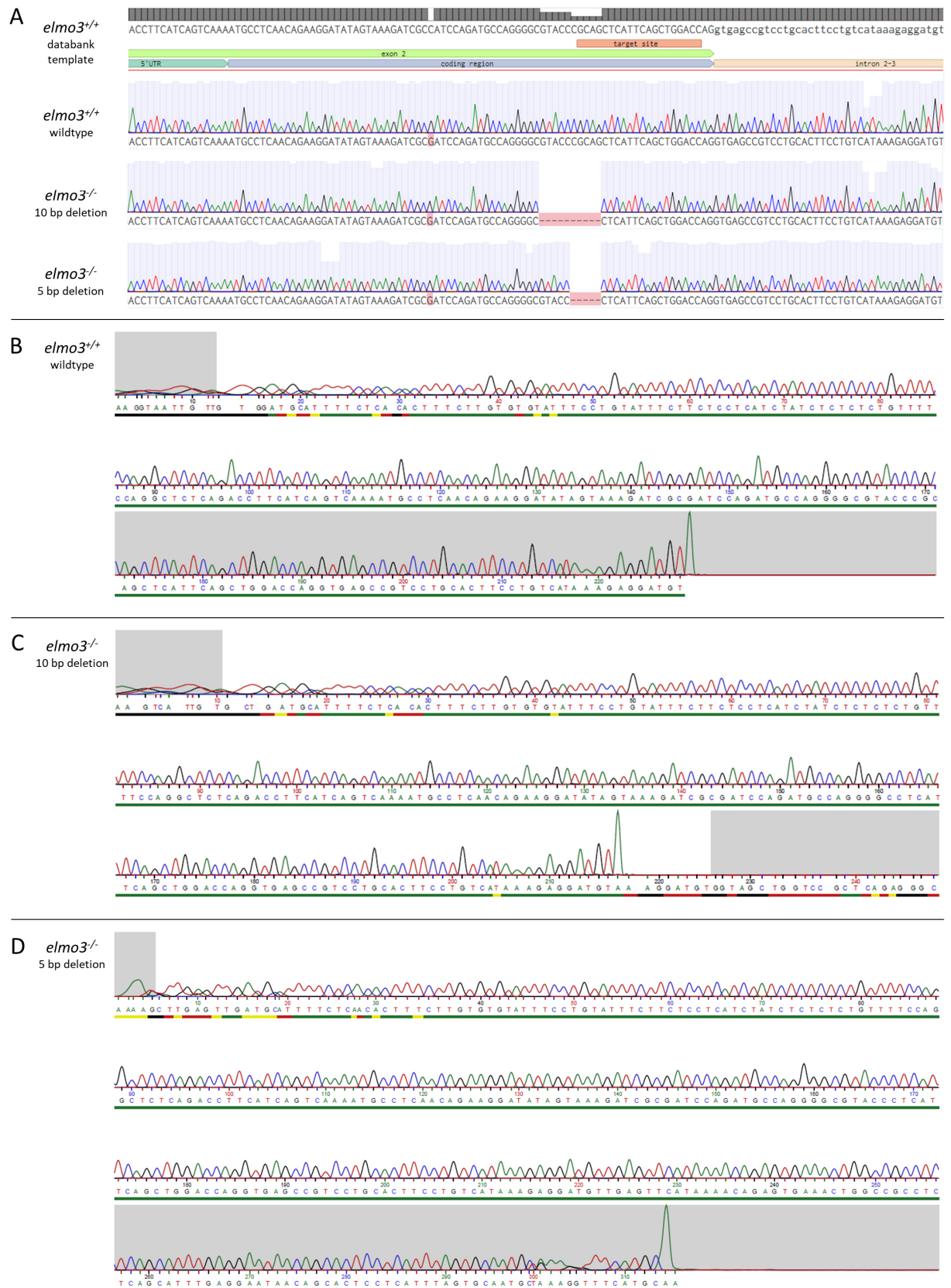
Supplementary Figure 2. Visualization and sequencing results of the target site area of wildtype zebrafish *elmo1* and the two generated *elmo1*^{-/-} mutant lines. (A) Visualization of the used target site area of the genomic DNA of zebrafish *elmo1* (ensembl transcript ID: ENSDART00000172618.2). Exemplary sequencing results of the target site area of wildtype *elmo1* and the homozygous *elmo1*^{-/-} mutant working line (10 bp insertion) and the homozygous *elmo1*^{-/-} mutant backup line (19 bp deletion). (B) Full genotyping sequencing result of the target site area of wildtype *elmo1*. (C) Full genotyping sequencing result of the target site area of homozygous *elmo1*^{-/-} mutant working line with the 10 bp

insertion. **(D)** Full genotyping sequencing result of the target site area of homozygous *elmo1*^{-/-} mutant backup line with the 19 bp deletion. UTR, untranslated region; bp, base pair. Sanger sequencing of genomic DNA was performed by Eurofins Genomics (www.eurofinsgenomics.eu; Ebersberg).



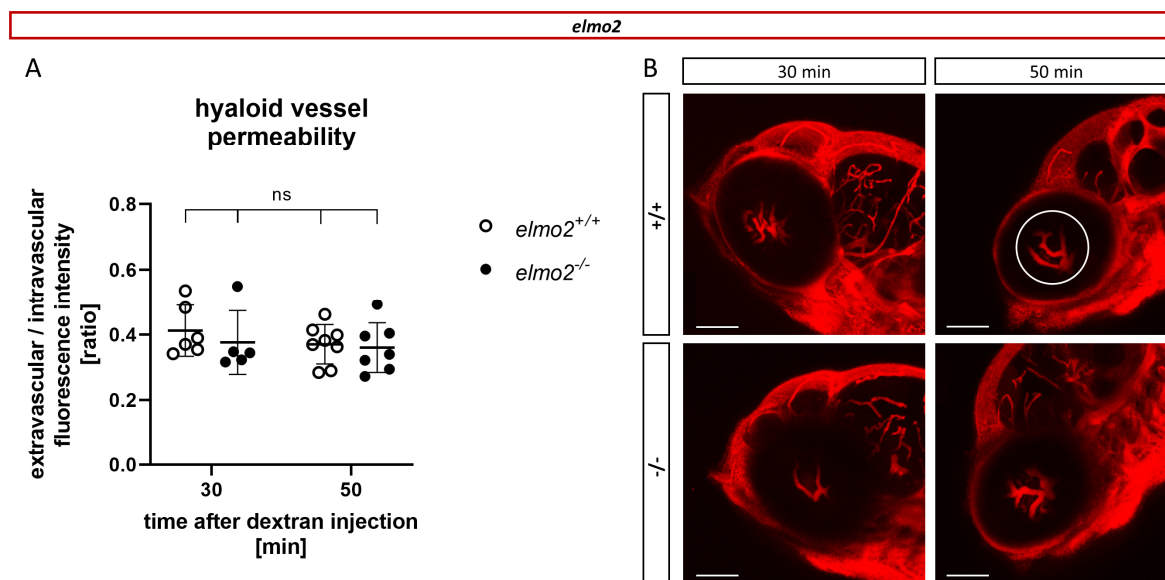
Supplementary Figure 3. Visualization and sequencing results of the target site area of wildtype zebrafish *elmo2* and the two generated *elmo2*^{-/-} mutant lines. (A) Visualization of the used target

site area of the genomic DNA of zebrafish *elmo2* (ensembl transcript ID: ENSDART00000162982.2). Exemplary sequencing results of the target site area of wildtype *elmo2* and the homozygous *elmo2*^{-/-} mutant working line (17 bp deletion) and the homozygous *elmo2*^{-/-} mutant backup line (10 bp deletion). **(B)** Full genotyping sequencing result of the target site area of wildtype *elmo2*. **(C)** Full genotyping sequencing result of the target site area of homozygous *elmo2*^{-/-} mutant working line with the 17 bp deletion. **(D)** Full genotyping sequencing result of the target site area of homozygous *elmo2*^{-/-} mutant backup line with the 10 bp deletion. UTR, untranslated region; bp, base pair. Sanger sequencing of genomic DNA was performed by Eurofins Genomics (www.eurofinsgenomics.eu; Ebersberg).

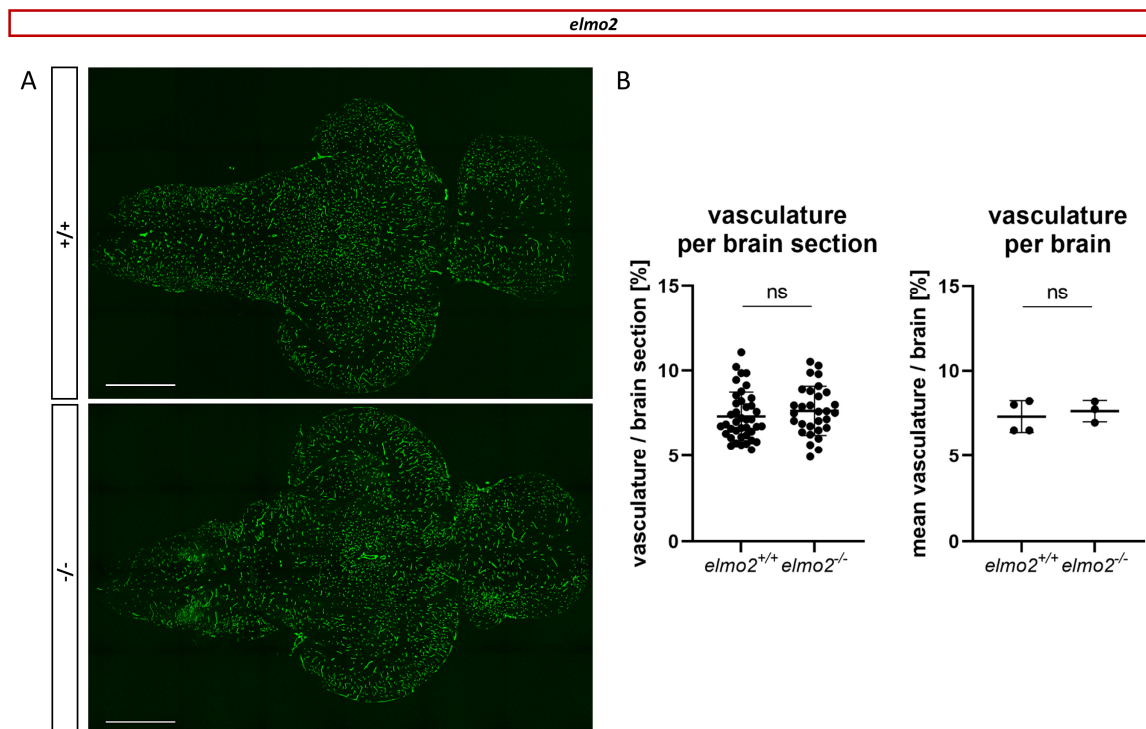


Supplementary Figure 4. Visualization and sequencing results of the target site area of wildtype zebrafish *elmo3* and the two generated *elmo3*^{-/-} mutant lines. (A) Visualization of the used target site area of the genomic DNA of zebrafish *elmo3* (ensembl transcript ID: ENSDART00000061738.7). Exemplary sequencing results of the target site area of wildtype *elmo3* and the homozygous *elmo3*^{-/-} mutant working line (10 bp deletion) and the homozygous *elmo3*^{-/-} mutant backup line (5 bp deletion).

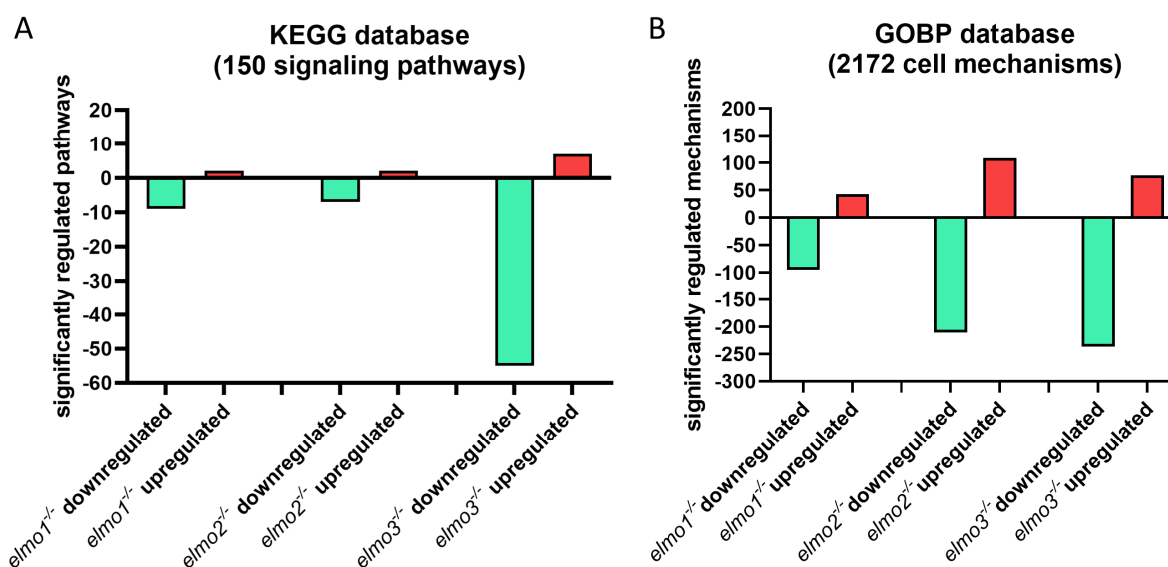
vessel. Quantification and imaging were performed by Katrin Bennewitz, David Wohlfart and Johannes Gschwind.



Supplementary Figure 6. Unaltered hyaloid vessel permeability of *elmo2*^{-/-} zebrafish larvae at 120 hpf. (A) Quantification of the ratio of extravascular to intravascular fluorescence signal of the hyaloid vessels of *elmo2*^{-/-} showed no alterations in vessel permeability, 30 and 50 min after Antonia Red Dextran injection in sinus venosus, compared to *elmo2*^{+/+} zebrafish larvae at 120 hpf. **(B)** Representative confocal microscopy images of the hyaloid vasculature of *elmo2*^{+/+} and *elmo2*^{-/-} zebrafish larvae at 120 hpf, 30 and 50 min after Antonia Red Dextran injection in sinus venosus. Analyzed hyaloid vessel area is indicated with a white circle. Scale bar is 100 μ m. Statistical analysis was done with two-way ANOVA. hpf, hours post fertilization; min, minutes.



Supplementary Figure 7. Unaltered vascular density in adult brains of *elmo2*^{-/-} zebrafish. (A) Representative confocal microscopy images of the vasculature of a brain section of adult *elmo2*^{+/+} and *elmo2*^{-/-} zebrafish. Scale bar is 600 μ m. **(B)** Quantification of the amount of vasculature (GFP signal) per total area of brain section showed no changes in the vascular density in the brain of adult *elmo2*^{-/-} compared to *elmo2*^{+/+} zebrafish. Analyzed brains were obtained from animals of 9 mpf. Statistical analysis was done with Mann-Whitney test. ns, not significant; mpf, months post fertilization.



Supplementary Figure 8. The loss of Elmo1, Elmo2 and Elmo3 led to different intensities of changes in the regulation of the transcriptome of zebrafish larvae. Comparison of the regulation of signaling pathways (A) and cell mechanisms (B) in the transcriptomes of *elmo1*^{-/-}, *elmo2*^{-/-} and *elmo3*^{-/-}

zebrafish larvae respectively compared to *elmo1*^{+/+}, *elmo2*^{+/+} and *elmo3*^{+/+} showed that the number of pathways and mechanisms which were significantly regulated, were mostly diverse between the three knock out lines. Shown are the numbers of pathways and mechanisms which are significantly regulated. 150 signaling pathways were analyzed with Kyoto Encyclopedia of Genes and Genomes (KEGG) based analysis and 2172 cell mechanisms were analyzed with Gene Ontology Biological Process (GOBP) based analysis in total. Analyses were done using RNA-sequencing data from zebrafish larvae at 120 hpf. n = 6 samples per genotype, each containing 30 larvae. Library preparation and RNA-sequencing were performed by BGI (www.bgi.com; Shenzhen, China) and statistical analysis was done by Carsten Sticht from the Next-Generation Sequencing (NGS) Core Facility of the Medical Faculty Mannheim.

Supplementary Table 1. The loss of Elmo1 led to an increase of amino acids in zebrafish larvae.

Data to Figure 18. Quantification of amino acids of *elmo1*^{+/+}, *elmo1*^{-/-}, *elmo2*^{+/+}, *elmo2*^{-/-}, *elmo3*^{+/+} and *elmo3*^{-/-} larvae. n = 5-6 samples per genotype, each containing 40 larvae at 96 hpf. Mean and standard deviation are given in pmol / larva. Statistical analysis was done with t-test and Mann-Whitney test. * p < 0.05, ** p < 0.01. Ala, alanine; Arg, arginine; Asp, aspartic acid; Gln, glutamine; Glu, glutamic acid; Gly, glycine; His, histidine; Ile, isoleucine; Leu, leucine; Lys, lysine; Met, methionine; Orn, ornithine; Phe, phenylalanine; Pro, proline; Ser, serine; Thr, threonine; Tyr, tyrosine; Val, valine; SD, standard deviation; sig., level of significance. Measurements were performed by the Metabolomics Core Technology Platform of the Centre of Organismal Studies Heidelberg.

compound	<i>elmo1</i> ^{+/+}		<i>elmo1</i> ^{-/-}		sig.	<i>elmo2</i> ^{+/+}		<i>elmo2</i> ^{-/-}		sig.	<i>elmo3</i> ^{+/+}		<i>elmo3</i> ^{-/-}		sig.
	mean	SD	mean	SD		mean	SD	mean	SD		mean	SD	mean	SD	
Asp	112,60	13,93	141,16	15,03	*	115,03	20,26	130,05	13,40	ns	163,82	5,19	154,64	44,20	ns
Glu	457,46	17,84	527,88	59,00	*	481,83	54,25	534,73	22,52	ns	553,46	42,01	561,80	83,89	ns
Asn	95,41	10,37	115,27	11,22	*	101,22	9,13	100,11	10,40	ns	109,94	8,72	105,04	18,24	ns
Ser	209,14	11,26	210,36	35,50	ns	191,46	34,94	178,61	13,56	ns	215,08	8,24	193,62	38,78	ns
Gln	815,07	73,89	841,89	115,40	ns	740,50	195,95	682,90	144,69	ns	1037,70	175,72	1011,58	121,42	ns
Gly	440,69	43,47	469,49	41,24	ns	465,18	29,00	429,08	52,87	ns	435,14	64,31	389,74	79,23	ns
His	274,75	19,64	297,85	34,58	ns	286,72	26,53	302,26	22,42	ns	276,28	29,74	286,30	34,02	ns
Arg	64,41	5,97	70,45	6,12	ns	51,85	7,67	52,28	10,84	ns	71,92	3,78	78,34	9,67	ns
Taurin	314,51	19,32	308,10	40,93	ns	268,50	21,19	288,17	34,22	ns	221,00	15,39	237,18	45,85	ns
Thr	100,56	4,68	108,14	5,28	*	86,92	9,92	91,70	18,03	ns	107,70	7,83	107,90	17,67	ns
Ala	134,08	7,84	159,55	11,07	**	150,93	18,64	192,17	13,17	*	132,24	29,47	141,22	15,87	ns
Pro	115,02	11,54	139,35	17,17	*	94,57	13,09	110,87	15,22	ns	121,50	12,28	111,86	14,33	ns
Tyr	267,53	33,77	317,75	51,55	ns	352,13	67,07	324,55	28,73	ns	321,60	32,72	302,94	76,52	ns
Val	175,62	6,07	199,01	10,77	**	169,35	16,84	183,52	20,22	ns	225,74	16,09	216,26	21,76	ns
Met	163,98	18,95	177,38	13,15	ns	153,96	27,98	166,72	24,07	ns	152,70	14,32	151,22	9,52	ns
Orn	99,42	7,63	95,89	11,82	ns	87,77	11,16	81,16	19,14	ns	103,62	26,29	120,50	11,82	ns
Ile	133,34	9,65	158,57	10,34	**	133,74	14,07	147,52	17,09	ns	185,56	13,13	172,94	16,52	ns
Leu	207,11	16,12	242,11	21,13	*	202,82	21,03	226,96	27,14	ns	278,18	15,85	266,28	30,27	ns
Lys	172,82	16,36	171,88	17,90	ns	133,32	14,72	132,52	30,77	ns	186,62	28,35	208,54	13,94	ns
Phe	174,85	30,54	193,45	19,17	ns	182,39	24,87	167,27	10,09	ns	240,08	35,60	234,86	85,56	ns

Supplementary Table 2. The loss of Elmo2 led to an increase of fatty acids in zebrafish larvae.

Data to Figure 19. Quantification of fatty acids of *elmo1*^{+/+}, *elmo1*^{-/-}, *elmo2*^{+/+}, *elmo2*^{-/-}, *elmo3*^{+/+} and *elmo3*^{-/-} larvae. n = 5-7 samples per genotype, each containing 40 larvae at 96 hpf. Mean and standard deviation are given as normalized relative abundance. Statistical analysis was done with t-test and Mann-Whitney test. * p < 0.05, ** p < 0.01, *** p < 0.001. SD, standard deviation; sig., level of

significance. Measurements were performed by the Metabolomics Core Technology Platform of the Centre of Organismal Studies Heidelberg.

compound	<i>elmo1</i> ^{+/+}			<i>elmo1</i> ^{-/-}			<i>elmo2</i> ^{+/+}			<i>elmo2</i> ^{-/-}			<i>elmo3</i> ^{+/+}			<i>elmo3</i> ^{-/-}		
	mean	SD	sig.															
C12:0	1,00	0,52	ns	0,90	0,16	ns	1,00	1,16	ns	0,43	0,14	ns	1,00	0,11	ns	1,24	0,06	ns
C14:0	1,00	0,12	*	1,39	0,18	*	1,00	0,27	ns	0,96	0,14	ns	1,00	0,31	ns	1,11	0,25	ns
C15:0	1,00	0,05	ns	1,11	0,10	ns	1,00	0,11	ns	0,99	0,07	ns	1,00	0,17	ns	0,97	0,11	ns
C16:1	1,00	0,06	ns	1,05	0,13	ns	1,00	0,14	ns	1,08	0,07	ns	1,00	0,18	ns	1,16	0,15	ns
C16:0	1,00	0,06	ns	1,08	0,11	ns	1,00	0,08	*	1,10	0,02	*	1,00	0,07	ns	1,03	0,07	ns
C17:1	1,00	0,14	ns	1,03	0,16	ns	1,00	0,11	ns	0,92	0,08	ns	1,00	0,17	ns	1,20	0,21	ns
C18:2n6	1,00	0,08	ns	1,00	0,15	ns	1,00	0,16	ns	1,14	0,11	ns	1,00	0,17	ns	1,03	0,18	ns
C18:1n9c	1,00	0,08	ns	1,02	0,15	ns	1,00	0,10	ns	1,08	0,04	ns	1,00	0,15	ns	1,08	0,19	ns
C18:1n9t	1,00	0,13	ns	0,98	0,14	ns	1,00	0,08	ns	1,06	0,05	ns	1,00	0,12	ns	1,14	0,21	ns
C18:0	1,00	0,04	ns	1,12	0,15	ns	1,00	0,06	ns	1,02	0,05	ns	1,00	0,09	ns	1,04	0,09	ns
C20:4n6	1,00	0,09	ns	1,09	0,09	ns	1,00	0,12	*	1,17	0,08	*	1,00	0,10	ns	1,02	0,11	ns
C20:5n3	1,00	0,13	ns	1,04	0,12	ns	1,00	0,12	ns	1,35	0,12	***	1,00	0,11	ns	1,26	0,13	ns
C20:3n6	1,00	0,14	ns	1,29	0,45	ns	1,00	0,11	ns	0,97	0,05	ns	1,00	0,10	ns	0,99	0,15	ns
C20:2	1,00	0,13	ns	1,02	0,15	ns	1,00	0,11	**	1,27	0,12	**	1,00	0,19	ns	1,28	0,32	ns
C20:1n9	1,00	0,08	ns	0,86	0,09	ns	1,00	0,12	**	1,29	0,14	**	1,00	0,12	ns	0,93	0,13	ns
C20:3n3	1,00	0,16	ns	0,97	0,10	ns	1,00	0,09	ns	0,96	0,08	ns	1,00	0,56	ns	0,92	0,48	ns
C20:0	1,00	0,10	ns	1,06	0,14	ns	1,00	0,15	ns	0,98	0,12	ns	1,00	0,12	ns	0,85	0,16	ns
C22:6n3	1,00	0,11	ns	1,12	0,15	ns	1,00	0,06	**	1,23	0,09	**						
C22:1n9	1,00	0,08	ns	0,77	0,20	ns	1,00	0,17	*	1,27	0,16	*						
C22:0	1,00	0,13	ns	1,10	0,19	ns	1,00	0,22	ns	0,91	0,17	ns	1,00	0,27	ns	1,01	0,22	ns
C24:1n9	1,00	0,23	ns	1,07	0,26	ns	1,00	0,10	*	1,27	0,17	*						
C24:0	1,00	0,45	ns	1,17	0,32	ns	1,00	0,40	ns	0,71	0,29	ns	1,00	0,13	ns	1,05	0,10	ns

Supplementary Table 3. The loss of Elmo1 and Elmo3 respectively led to decreased ADP and ATP levels in zebrafish larvae. Data to Figure 20. Quantification of adenosines of *elmo1*^{+/+}, *elmo1*^{-/-}, *elmo2*^{+/+}, *elmo2*^{-/-}, *elmo3*^{+/+} and *elmo3*^{-/-} larvae. n = 5-6 samples per genotype, each containing 40 larvae at 96 hpf. Mean and standard deviation are given in pmol / mg. Statistical analysis was done with t-test and Mann-Whitney test. * p < 0.05, ** p < 0.01. ADP, adenosine diphosphate; AMP, adenosine monophosphate; ATP, adenosine triphosphate; MTA, methylthioadenosine; NAD/NADH, nicotinamide adenine dinucleotide; NADPH, nicotinamide adenine dinucleotide phosphate; SAHC/SHC, S-adenosylhomocystein; SAM, S-adenosyl-methionine; SD, standard deviation; sig., level of significance. Measurements were performed by the Metabolomics Core Technology Platform from the Centre of Organismal Studies Heidelberg.

compound	<i>elmo1</i> ^{+/+}			<i>elmo1</i> ^{-/-}			<i>elmo2</i> ^{+/+}			<i>elmo2</i> ^{-/-}			<i>elmo3</i> ^{+/+}			<i>elmo3</i> ^{-/-}		
	mean	SD	sig.															
adenosine	313,96	24,78	ns	321,00	34,40	ns	308,85	26,98	ns	272,67	30,12	ns	260,22	35,35	ns	272,89	35,11	ns
AMP	3576,00	160,08	ns	3581,76	304,73	ns	3367,06	234,63	ns	3105,62	224,73	ns	2741,51	189,37	ns	3122,77	459,28	ns
ADP	448,15	82,63	*	326,89	39,97	*	269,14	18,63	ns	247,44	33,22	ns	507,66	69,00	ns	373,17	42,05	**
ATP	442,32	99,04	*	313,89	63,95	*	275,98	18,76	ns	255,47	79,01	ns	689,85	167,40	ns	443,07	109,85	*
SAM	19,27	1,50	ns	18,49	0,74	ns	13,00	1,47	ns	12,23	1,39	ns	8,10	0,57	ns	7,12	0,57	*
SAHC	5,47	0,45	*	6,88	1,06	*	7,17	1,03	ns	7,29	0,82	ns	7,25	0,70	ns	7,50	1,07	ns
MTA	4,11	0,30	ns	4,07	0,21	ns	3,62	0,75	ns	3,37	1,53	ns	4,56	0,75	ns	3,62	0,74	ns
NAD	63,54	2,32	ns	66,12	3,80	ns	67,46	2,65	ns	62,38	6,57	ns	45,64	5,32	ns	45,67	10,55	ns
NADH	15,70	0,45	ns	16,97	1,37	ns	18,04	2,15	ns	19,29	1,62	ns	21,79	3,56	ns	19,61	4,53	ns
NADPH	7,64	1,05	ns	6,76	1,12	ns	4,42	0,63	ns	4,44	1,16	ns	4,33	0,30	ns	3,86	1,59	ns

Abbreviations

Abbreviation	Written-out
%	percent
°C	degree Celsius
α	anti / significance level
μ L	microliter
μ m	micrometer
μ M	micromolar
A	adenine
ad	adjust to
ADP	adenosine diphosphate
AGE	advanced glycation end product
Ala	alanine
Amp	ampicillin
AMP	adenosine monophosphate
Arf	adenosine diphosphate-ribosylation factors
Arg	arginine
arnt2	aryl hydrocarbon receptor nuclear translocator 2
Asp	aspartic acid
ATP	adenosine triphosphate
AXL	AXL receptor tyrosine kinase
BAI1	brain-specific angiogenesis inhibitor 1
bp	base pair
BSA	bovine serum albumin
C	cytosine
CDC42	cell division cycle 42
cDNA	complementary DNA
CED-12	cell death abnormality protein 12
Cas9	CRISPR-associated protein-9 nuclease
cm	centimeter
CRISPR	clustered regularly interspaced short palindromic repeats
Cys	cysteine
dL	deciliter

DLAV	dorsal longitudinal anastomotic vessel
DMSO	dimethylsulfoxid
DN	diabetic nephropathy
DNA	desoxyribonucleic acid
DOCK	dedicator of cytokinesis
dpf	days post fertilization
E. coli	Escherichia coli
ECM	extracellular matrix
EDTA	ethylenediaminetetraacetic acid
EGFP	enhanced green fluorescent protein
ELMO/Elmo/elmo	engulfment and cell motility
ELMOD	ELMO domain containing
ERM	egg water with methylene blue
et al.	and others
FDR	false discovery rate
fli1	friend leukemia integration1
g	gram
G	guanine
g6pc1a.1	glucose-6-phosphatase catalytic subunit 1a, tandem duplicate 1
GAP	GTPase-activating proteins
GBM	glomerular basement membrane
GC-MS	gas chromatography-mass spectrometry
gck	glucokinase
GDI	Rho guanine dissociation inhibitors
GDP	guanosine diphosphate
GEF	guanine nucleotide exchange factor
GEO	Gene Expression Omnibus
GFP	green fluorescent protein
Gln	glutamine
Glu	glutamic acid
Glut	glucose transporter
Gly	Glycine
GOBP	Gene Ontology Biological Process

gRNA	guide ribonucleic acid
GSEA	gene set enrichment analysis
GSH	glutathione
GSSG	glutathione disulfide
GTP	guanosine triphosphate
h	hour(s)
His	histidine
hk	hexokinase
hpf	hours post fertilization
HRP	horse radish peroxidase
Hz	hertz
Ile	isoleucine
ins	preproinsulin
insra	insulin receptor a
insrb	insulin receptor b
ISV	intersegmental vessel
kDa	kilodalton
KEGG	Kyoto Encyclopedia of Genes and Genomes
L	liter
LB	lysogeny broth
Leu	leucine
log	logarithm
Leu	leucine
Lys	lysine
M	molar
max	maximum
Met	methionine
mg	milligram
min	minute
mL	milliliter
mm	millimeter
mM	millimolar
mpf	month post fertilization
mRNA	messenger ribonucleic acid

MTA	methylthioadenosine
n	number of samples
NAD/NADH	nicotinamide adenine dinucleotide
NADPH	nicotinamide adenine dinucleotide phosphate
NCBI	National Center for Biotechnology Information
NES	normalized enrichment score
ng	nanogram
NGS	next-generation sequencing
nL	nanoliter
nm	nanometer
NO	nitric oxide
NOX	NADPH oxidase
ns	not significant
Orn	ornithine
p	probability-value
PAM	protospacer adjacent motif
PAS	periodic acid-Schiff
PBS	phosphate buffered saline
PBST	phosphate buffered saline with 0.05 % Tween 20
pck	phosphoenolpyruvate carboxykinase
PCR	polymerase chain reaction
PFA	paraformaldehyde
pfkl	phosphofructokinase, liver
pH	potential of hydrogen
PH	pleckstrin homology
Phe	phenylalanine
pklr	pyruvate kinase liver
pmol	picomole
Pro	proline
PTU	1-phenyl-2-thiourea
RAC1/Rac1	Rac family small GTPase 1
Rho	Ras homologue
RhoA	Ras homolog family member A
RhoG	Ras homolog family member G

RNA	ribonucleic acid
RNA-seq	RNA-sequencing
ROS	reactive oxygen species
RT	room temperature
RT-PCR	reverse transcription polymerase chain reaction
RT-qPCR	real-time quantitative polymerase chain reaction
rpm	rounds per minute
SAHC/SHC	S-adenosylhomocystein
SAM	S-adenosyl-methionine
sec	second
Ser	serine
sig.	level of significance
SD	standard deviation
SDS	sodium dodecyl sulfate
SDS-PAGE	sodium dodecyl sulfate polyacrylamide gel electrophoresis
SNP	single nucleotide polymorphism
T	thymine
T1D	type one diabetes
T2D	type two diabetes
TAE	Tris base, acetic acid and EDTA
TALEN	transcription activator-like effector nuclease
tg	transgenic
Thr	threonine
Tris	Tris-aminomethan
Tyr	tyrosine
UPLC-FLR	ultra-performance liquid chromatography with fluorescence detection
UTR	untranslated region
V	volt
Val	valine
VEGF	vascular endothelial growth factor
vs.	versus
WT	wild type
x/X	times

References

1. Møller LLV, Klip A, Sylow L (2019) Rho GTPases—Emerging Regulators of Glucose Homeostasis and Metabolic Health. *Cells* 8. <https://doi.org/10.3390/cells8050434>
2. Yang Z (2002) Small GTPases: Versatile Signaling Switches in Plants. *Plant Cell* 14:s375-88. <https://doi.org/10.1105/tpc.001065>
3. Bos JL, Rehmann H, Wittinghofer A (2007) GEFs and GAPs: critical elements in the control of small G proteins. *Cell* 129:865–877. <https://doi.org/10.1016/j.cell.2007.05.018>
4. Rossman KL, Der CJ, Sondek J (2005) GEF means go: turning on RHO GTPases with guanine nucleotide-exchange factors. *Nat Rev Mol Cell Biol* 6:167–180. <https://doi.org/10.1038/nrm1587>
5. Cherfils J, Zeghouf M (2013) Regulation of small GTPases by GEFs, GAPs, and GDIs. *Physiological reviews* 93:269–309. <https://doi.org/10.1152/physrev.00003.2012>
6. Pleines I, Dütting S, Cherpokova D et al. (2013) Defective tubulin organization and proplatelet formation in murine megakaryocytes lacking Rac1 and Cdc42. *Blood* 122:3178–3187. <https://doi.org/10.1182/blood-2013-03-487942>
7. Nie F, Zhao S-Y, Song F-X et al. (2014) Changes of cytoskeleton and cell cycle in Lovo cells via deletion of Rac1. *Cancer Biomark* 14:335–342. <https://doi.org/10.3233/CBM-140408>
8. Navarro-Lérida I, Sánchez-Perales S, Calvo M et al. (2012) A palmitoylation switch mechanism regulates Rac1 function and membrane organization. *EMBO J* 31:534–551. <https://doi.org/10.1038/emboj.2011.446>
9. Sylow L, Jensen TE, Kleinert M et al. (2013) Rac1 is a novel regulator of contraction-stimulated glucose uptake in skeletal muscle. *Diabetes* 62:1139–1151. <https://doi.org/10.2337/db12-0491>
10. Hall A, Nobes CD (2000) Rho GTPases: molecular switches that control the organization and dynamics of the actin cytoskeleton. *Philos Trans R Soc Lond B Biol Sci* 355:965–970
11. Jaffe AB, Hall A (2005) Rho GTPases: biochemistry and biology. *Annu Rev Cell Dev Biol* 21:247–269. <https://doi.org/10.1146/annurev.cellbio.21.020604.150721>
12. Sun CX, Downey GP, Zhu F et al. (2004) Rac1 is the small GTPase responsible for regulating the neutrophil chemotaxis compass. *Blood* 104:3758–3765. <https://doi.org/10.1182/blood-2004-03-0781>
13. Shen G, Zhou E, Alspaugh JA et al. (2012) Wsp1 is downstream of Cin1 and regulates vesicle transport and actin cytoskeleton as an effector of Cdc42 and Rac1 in *Cryptococcus neoformans*. *Eukaryot Cell* 11:471–481. <https://doi.org/10.1128/EC.00011-12>
14. Dun Y, Yan J, Wang M et al. (2020) Rac1-dependent endocytosis and Rab5-dependent intracellular trafficking are required by Enterovirus A71 and Coxsackievirus A10 to establish infections. *Biochem Biophys Res Commun* 529:97–103. <https://doi.org/10.1016/j.bbrc.2020.05.058>
15. Murga C, Zohar M, Teramoto H et al. (2002) Rac1 and RhoG promote cell survival by the activation of PI3K and Akt, independently of their ability to stimulate JNK and NF-kappaB. *Oncogene* 21:207–216. <https://doi.org/10.1038/sj.onc.1205036>
16. Zhao J, Jie Q, Li G et al. (2018) Rac1 promotes the survival of H9c2 cells during serum deficiency targeting JNK/c-JUN/Cyclin-D1 and AKT2/MCL1 pathways. *Int J Med Sci* 15:1062–1071. <https://doi.org/10.7150/ijms.25527>

17. Moore KA, Sethi R, Doanes AM et al. (1997) Rac1 is required for cell proliferation and G2/M progression. *Biochem J* 326 (Pt 1):17–20. <https://doi.org/10.1042/bj3260017>
18. Haga RB, Ridley AJ (2016) Rho GTPases: Regulation and roles in cancer cell biology. *Small GTPases* 7:207–221. <https://doi.org/10.1080/21541248.2016.1232583>
19. Vader P, van der Meel R, Symons MH et al. (2011) Examining the role of Rac1 in tumor angiogenesis and growth: a clinically relevant RNAi-mediated approach. *Angiogenesis* 14:457–466. <https://doi.org/10.1007/s10456-011-9229-x>
20. Baugher PJ, Krishnamoorthy L, Price JE et al. (2005) Rac1 and Rac3 isoform activation is involved in the invasive and metastatic phenotype of human breast cancer cells. *Breast Cancer Res* 7:R965-74. <https://doi.org/10.1186/bcr1329>
21. Wang X, Liu D, Wei F et al. (2020) Stress-Sensitive Protein Rac1 and Its Involvement in Neurodevelopmental Disorders. *Neural Plast* 2020. <https://doi.org/10.1155/2020/8894372>
22. Schiattarella GG, Carrizzo A, Iardi F et al. (2018) Rac1 Modulates Endothelial Function and Platelet Aggregation in Diabetes Mellitus. *J Am Heart Assoc* 7. <https://doi.org/10.1161/JAHA.117.007322>
23. Acevedo A, González-Billault C (2018) Crosstalk between Rac1-mediated actin regulation and ROS production. *Free radical biology & medicine* 116:101–113. <https://doi.org/10.1016/j.freeradbiomed.2018.01.008>
24. Cheng G, Diebold BA, Hughes Y et al. (2006) Nox1-dependent reactive oxygen generation is regulated by Rac1. *J Biol Chem* 281:17718–17726. <https://doi.org/10.1074/jbc.M512751200>
25. Hordijk PL (2006) Regulation of NADPH oxidases: the role of Rac proteins. *Circ Res* 98:453–462. <https://doi.org/10.1161/01.RES.0000204727.46710.5e>
26. Jha JC, Banal C, Chow BSM et al. (2016) Diabetes and Kidney Disease: Role of Oxidative Stress. *Antioxid Redox Signal* 25:657–684. <https://doi.org/10.1089/ars.2016.6664>
27. Mohammad G, Duraisamy AJ, Kowluru A et al. (2019) Functional Regulation of an Oxidative Stress Mediator, Rac1, in Diabetic Retinopathy. *Mol Neurobiol* 56:8643–8655. <https://doi.org/10.1007/s12035-019-01696-5>
28. Zimmer S, Goody PR, Oelze M et al. (2021) Inhibition of Rac1 GTPase Decreases Vascular Oxidative Stress, Improves Endothelial Function, and Attenuates Atherosclerosis Development in Mice. *Front Cardiovasc Med* 8:680775. <https://doi.org/10.3389/fcvm.2021.680775>
29. Stevenson C, La Rosa G de, Anderson CS et al. (2014) Essential role of Elmo1 in Dock2-dependent lymphocyte migration. *J Immunol* 192:6062–6070. <https://doi.org/10.4049/jimmunol.1303348>
30. Gumienny TL, Brugnera E, Tosello-Tramont AC et al. (2001) CED-12/ELMO, a novel member of the CrkII/Dock180/Rac pathway, is required for phagocytosis and cell migration. *Cell* 107:27–41. [https://doi.org/10.1016/s0092-8674\(01\)00520-7](https://doi.org/10.1016/s0092-8674(01)00520-7)
31. Geisbrecht ER, Haralalka S, Swanson SK et al. (2008) Drosophila ELMO/CED-12 interacts with Myoblast city to direct myoblast fusion and ommatidial organization. *Dev Biol* 314:137–149. <https://doi.org/10.1016/j.ydbio.2007.11.022>
32. Akakura S, Kar B, Singh S et al. (2005) C-terminal SH3 domain of CrkII regulates the assembly and function of the DOCK180/ELMO Rac-GEF. *J Cell Physiol* 204:344–351. <https://doi.org/10.1002/jcp.20288>

33. Katoh H, Negishi M (2003) RhoG activates Rac1 by direct interaction with the Dock180-binding protein Elmo. *Nature* 424:461–464. <https://doi.org/10.1038/nature01817>
34. Lu M, Kinchen JM, Rossman KL et al. (2004) PH domain of ELMO functions in trans to regulate Rac activation via Dock180. *Nat Struct Mol Biol* 11:756–762. <https://doi.org/10.1038/nsmb800>
35. Cetinkaya A, Xiong JR, Vargel İ et al. (2016) Loss-of-Function Mutations in ELMO2 Cause Intraosseous Vascular Malformation by Impeding RAC1 Signaling. *Am J Hum Genet* 99:299–317. <https://doi.org/10.1016/j.ajhg.2016.06.008>
36. Tran V, Goyette M-A, Martínez-García M et al. (2021) Biallelic ELMO3 mutations and loss of function for DOCK-mediated RAC1 activation result in intellectual disability. *Small GTPases*:1–8. <https://doi.org/10.1080/21541248.2021.1888557>
37. Brugnera E, Haney L, Grimsley C et al. (2002) Unconventional Rac-GEF activity is mediated through the Dock180-ELMO complex. *Nat Cell Biol* 4:574–582. <https://doi.org/10.1038/ncb824>
38. Gumienny TL, Brugnera E, Tosello-Trampont AC et al. (2001) CED-12/ELMO, a novel member of the CrkII/Dock180/Rac pathway, is required for phagocytosis and cell migration. *Cell* 107:27–41
39. Komander D, Patel M, Laurin M et al. (2008) An alpha-helical extension of the ELMO1 pleckstrin homology domain mediates direct interaction to DOCK180 and is critical in Rac signaling. *Mol Biol Cell* 19:4837–4851. <https://doi.org/10.1091/mbc.e08-04-0345>
40. Lu M, Kinchen JM, Rossman KL et al. (2005) A Steric-inhibition model for regulation of nucleotide exchange via the Dock180 family of GEFs. *Curr Biol* 15:371–377. <https://doi.org/10.1016/j.cub.2005.01.050>
41. Zhou Z, Caron E, Hartwig E et al. (2001) The *C. elegans* PH domain protein CED-12 regulates cytoskeletal reorganization via a Rho/Rac GTPase signaling pathway. *Dev Cell* 1:477–489
42. Bowzard JB, Cheng D, Peng J et al. (2007) ELMOD2 is an Arl2 GTPase-activating protein that also acts on Arfs. *J Biol Chem* 282:17568–17580. <https://doi.org/10.1074/jbc.M701347200>
43. East MP, Bowzard JB, Dacks JB et al. (2012) ELMO domains, evolutionary and functional characterization of a novel GTPase-activating protein (GAP) domain for Arf protein family GTPases. *J Biol Chem* 287:39538–39553. <https://doi.org/10.1074/jbc.M112.417477>
44. Park D, Tosello-Trampont A-C, Elliott MR et al. (2007) BAI1 is an engulfment receptor for apoptotic cells upstream of the ELMO/Dock180/Rac module. *Nature* 450:430–434. <https://doi.org/10.1038/nature06329>
45. Weng Z, Situ C, Lin L et al. (2019) Structure of BAI1/ELMO2 complex reveals an action mechanism of adhesion GPCRs via ELMO family scaffolds. *Nat Commun* 10. <https://doi.org/10.1038/s41467-018-07938-9>
46. Epting D, Wendik B, Bennewitz K et al. (2010) The Rac1 regulator ELMO1 controls vascular morphogenesis in zebrafish. *Circ Res* 107:45–55. <https://doi.org/10.1161/CIRCRESAHA.109.213983>
47. Abu-Thuraia A, Gauthier R, Chidiac R et al. (2015) Axl phosphorylates Elmo scaffold proteins to promote Rac activation and cell invasion. *Mol Cell Biol* 35:76–87. <https://doi.org/10.1128/MCB.00764-14>

48. Grimsley CM, Kinchen JM, Tosello-Trampont A-C et al. (2004) Dock180 and ELMO1 proteins cooperate to promote evolutionarily conserved Rac-dependent cell migration. *J Biol Chem* 279:6087–6097. <https://doi.org/10.1074/jbc.M307087200>
49. Wu YC, Tsai MC, Cheng LC et al. (2001) *C. elegans* CED-12 acts in the conserved crkII/DOCK180/Rac pathway to control cell migration and cell corpse engulfment. *Dev Cell* 1:491–502
50. Peotter JL, Phillips J, Tong T et al. (2016) Involvement of Tiam1, RhoG and ELMO2/ILK in Rac1-mediated phagocytosis in human trabecular meshwork cells. *Exp Cell Res* 347:301–311. <https://doi.org/10.1016/j.yexcr.2016.08.009>
51. Hamoud N, Tran V, Croteau L-P et al. (2014) G-protein coupled receptor BAI3 promotes myoblast fusion in vertebrates. *Proc Natl Acad Sci U S A* 111:3745–3750. <https://doi.org/10.1073/pnas.1313886111>
52. Sun Y, Ren W, Côté J-F et al. (2015) ClipR-59 interacts with Elmo2 and modulates myoblast fusion. *J Biol Chem* 290:6130–6140. <https://doi.org/10.1074/jbc.M114.616680>
53. Elliott MR, Zheng S, Park D et al. (2010) Unexpected requirement for ELMO1 in clearance of apoptotic germ cells in vivo. *Nature* 467:333–337. <https://doi.org/10.1038/nature09356>
54. Franke K, Otto W, Johannes S et al. (2012) miR-124-regulated RhoG reduces neuronal process complexity via ELMO/Dock180/Rac1 and Cdc42 signalling. *EMBO J* 31:2908–2921. <https://doi.org/10.1038/emboj.2012.130>
55. Biersmith B, Liu ZC, Bauman K et al. (2011) The DOCK protein sponge binds to ELMO and functions in *Drosophila* embryonic CNS development. *PLoS ONE* 6:e16120. <https://doi.org/10.1371/journal.pone.0016120>
56. Namekata K, Watanabe H, Guo X et al. (2012) Dock3 regulates BDNF-TrkB signaling for neurite outgrowth by forming a ternary complex with Elmo and RhoG. *Genes Cells* 17:688–697. <https://doi.org/10.1111/j.1365-2443.2012.01616.x>
57. Mehawej C, Hoischen A, Farah RA et al. (2018) Homozygous mutation in ELMO2 may cause Ramon syndrome. *Clin Genet* 93:703–706. <https://doi.org/10.1111/cge.13166>
58. Lanoue V, Usardi A, Sigoillot SM et al. (2013) The adhesion-GPCR BAI3, a gene linked to psychiatric disorders, regulates dendrite morphogenesis in neurons. *Molecular Psychiatry* 18:943–950. <https://doi.org/10.1038/mp.2013.46>
59. Makihara S, Morin S, Ferent J et al. (2018) Polarized Dock Activity Drives Shh-Mediated Axon Guidance. *Dev Cell* 46:410–425.e7. <https://doi.org/10.1016/j.devcel.2018.07.007>
60. Mikdache A, Fontenas L, Albadri S et al. (2019) Elmo1 function, linked to Rac1 activity, regulates peripheral neuronal numbers and myelination in zebrafish. *Cell Mol Life Sci*. <https://doi.org/10.1007/s00018-019-03167-5>
61. Hathaway CK, Chang AS, Grant R et al. (2016) High Elmo1 expression aggravates and low Elmo1 expression prevents diabetic nephropathy. *Proc Natl Acad Sci U S A* 113:2218–2222. <https://doi.org/10.1073/pnas.1600511113>
62. Shimazaki A, Kawamura Y, Kanazawa A et al. (2005) Genetic variations in the gene encoding ELMO1 are associated with susceptibility to diabetic nephropathy. *Diabetes* 54:1171–1178. <https://doi.org/10.2337/diabetes.54.4.1171>
63. Arandjelovic S, Perry JSA, Zhou M et al. (2021) ELMO1 signaling is a promoter of osteoclast function and bone loss. *Nat Commun* 12:4974. <https://doi.org/10.1038/s41467-021-25239-6>

64. Sayed IM, Suarez K, Lim E et al. (2020) Host engulfment pathway controls inflammation in inflammatory bowel disease. *FEBS J* 287:3967–3988. <https://doi.org/10.1111/febs.15236>
65. Hu Y, Yu Q, Zhong Y et al. (2018) Silencing ELMO3 Inhibits the Growth, Invasion, and Metastasis of Gastric Cancer. *Biomed Res Int* 2018:3764032. <https://doi.org/10.1155/2018/3764032>
66. Pan C, Zhang Y, Meng Q et al. (2019) Down Regulation of the Expression of ELMO3 by COX2 Inhibitor Suppresses Tumor Growth and Metastasis in Non-Small-Cell Lung Cancer. *Front Oncol* 9:363. <https://doi.org/10.3389/fonc.2019.00363>
67. Peng H-Y, Yu Q-F, Shen W et al. (2016) Knockdown of ELMO3 Suppresses Growth, Invasion and Metastasis of Colorectal Cancer. *Int J Mol Sci* 17. <https://doi.org/10.3390/ijms17122119>
68. Kadletz L, Heiduschka G, Wiebringhaus R et al. (2017) ELMO3 expression indicates a poor prognosis in head and neck squamous cell carcinoma - a short report. *Cell Oncol (Dordr)* 40:193–198. <https://doi.org/10.1007/s13402-016-0310-8>
69. Fan W, Yang H, Xue H et al. (2015) ELMO3 is a novel biomarker for diagnosis and prognosis of non-small cell lung cancer. *Int J Clin Exp Pathol* 8:5503–5508
70. Haymerle G, Kadletz L, Wiebringhaus R et al. (2017) ELMO3 predicts poor outcome in T1 laryngeal cancer. *Clin Otolaryngol* 42:1181–1186. <https://doi.org/10.1111/coa.12845>
71. Schäker K, Bartsch S, Patry C et al. (2015) The bipartite rac1 Guanine nucleotide exchange factor engulfment and cell motility 1/dedicator of cytokinesis 180 (elmo1/dock180) protects endothelial cells from apoptosis in blood vessel development. *J Biol Chem* 290:6408–6418. <https://doi.org/10.1074/jbc.M114.633701>
72. Alberto Ramirez-Garcia S, Charles-Niño C, Mazariegos-Rubí M et al. (2015) Asociación del gen ELMO1 (snp rs1345365) con el desarrollo de diabetes mellitus tipo 2 en población mestiza Mexicana (Association of the ELMO1 gene (snp rs1345365) with development of type 2 diabetes mellitus in the Mexican mestizo population). *Invest Clin* 56:341–355
73. Hanson RL, Millis MP, Young NJ et al. (2010) ELMO1 variants and susceptibility to diabetic nephropathy in American Indians. *Mol Genet Metab* 101:383–390. <https://doi.org/10.1016/j.ymgme.2010.08.014>
74. Leak TS, Perlegas PS, Smith SG et al. (2009) Variants in intron 13 of the ELMO1 gene are associated with diabetic nephropathy in African Americans. *Ann Hum Genet* 73:152–159. <https://doi.org/10.1111/j.1469-1809.2008.00498.x>
75. Turki A, Mzoughi S, Mtitaoui N et al. (2018) Gender differences in the association of ELMO1 genetic variants with type 2 diabetes in Tunisian Arabs. *J Endocrinol Invest* 41:285–291. <https://doi.org/10.1007/s40618-017-0734-7>
76. Wu HY, Wu YH, Wang Y et al. (2013) Association of ELMO1 gene polymorphisms with diabetic nephropathy in Chinese population. *J Endocrinol Invest* 36:298–302. <https://doi.org/10.3275/8525>
77. Bento JL, Palmer ND, Zhong M et al. (2008) Heterogeneity in Gene Loci Associated with Type 2 Diabetes on Human Chromosome 20q13.1. *Genomics* 92:226–234. <https://doi.org/10.1016/j.ygeno.2008.06.004>
78. Liu R, Lee K, He JC (2015) Genetics and Epigenetics of Diabetic Nephropathy. *Kidney Dis (Basel)* 1:42–51. <https://doi.org/10.1159/000381796>

79. Sun Y, Côté J-F, Du K (2016) Elmo2 Is a Regulator of Insulin-dependent Glut4 Membrane Translocation. *J Biol Chem* 291:16150–16161. <https://doi.org/10.1074/jbc.M116.731521>
80. Pittman RN (2011) Oxygen gradients in the microcirculation. *Acta Physiol (Oxf)* 202:311–322. <https://doi.org/10.1111/j.1748-1716.2010.02232.x>
81. Evans HM (1909) On the development of the aortae, cardinal and umbilical veins, and the other blood vessels of vertebrate embryos from capillaries. *Anat Rec* 3:498–518. <https://doi.org/10.1002/ar.1090030903>
82. Krüger-Genge A, Blocki A, Franke R-P et al. (2019) Vascular Endothelial Cell Biology: An Update. *Int J Mol Sci* 20. <https://doi.org/10.3390/ijms20184411>
83. Marziano C, Genet G, Hirschi KK (2021) Vascular endothelial cell specification in health and disease. *Angiogenesis* 24:213–236. <https://doi.org/10.1007/s10456-021-09785-7>
84. Kolte D, McClung JA, Aronow WS (2016) Chapter 6 - Vasculogenesis and Angiogenesis. In: McClung JA, Aronow WS (eds) *Translational research in coronary artery disease: Pathophysiology to treatment*. Academic Press an imprint of Elsevier, London, pp 49–65
85. Risau W, Flamme I (1995) Vasculogenesis. *Annu Rev Cell Dev Biol* 11:73–91. <https://doi.org/10.1146/annurev.cb.11.110195.000445>
86. Risau W, Sariola H, Zerwes HG et al. (1988) Vasculogenesis and angiogenesis in embryonic-stem-cell-derived embryoid bodies. *Development* 102:471–478. <https://doi.org/10.1242/dev.102.3.471>
87. Haar JL, Ackerman GA (1971) A phase and electron microscopic study of vasculogenesis and erythropoiesis in the yolk sac of the mouse. *Anat Rec* 170:199–223. <https://doi.org/10.1002/ar.1091700206>
88. Potente M, Gerhardt H, Carmeliet P (2011) Basic and therapeutic aspects of angiogenesis. *Cell* 146:873–887. <https://doi.org/10.1016/j.cell.2011.08.039>
89. Carmeliet P (2003) Angiogenesis in health and disease. *Nat Med* 9:653–660. <https://doi.org/10.1038/nm0603-653>
90. Adams RH, Alitalo K (2007) Molecular regulation of angiogenesis and lymphangiogenesis. *Nat Rev Mol Cell Biol* 8:464–478. <https://doi.org/10.1038/nrm2183>
91. Carmeliet P, Jain RK (2000) Angiogenesis in cancer and other diseases. *Nature* 407:249–257. <https://doi.org/10.1038/35025220>
92. Sellke FW, Simons M (1999) Angiogenesis in cardiovascular disease: current status and therapeutic potential. *Drugs* 58:391–396. <https://doi.org/10.2165/00003495-199958030-00001>
93. van Groningen JP, Wenink AC, Testers LH (1991) Myocardial capillaries: increase in number by splitting of existing vessels. *Anat Embryol (Berl)* 184:65–70. <https://doi.org/10.1007/BF01744262>
94. Djonov V, Schmid M, Tschanz SA et al. (2000) Intussusceptive angiogenesis: its role in embryonic vascular network formation. *Circ Res* 86. <https://doi.org/10.1161/01.res.86.3.286>
95. Burri PH, Hlushchuk R, Djonov V (2004) Intussusceptive angiogenesis: its emergence, its characteristics, and its significance. *Dev Dyn* 231:474–488. <https://doi.org/10.1002/dvdy.20184>
96. Webb RC (2003) Smooth muscle contraction and relaxation. *Adv Physiol Educ* 27:201–206. <https://doi.org/10.1152/advan.00025.2003>

97. Jackson WF (2018) KV channels and the regulation of vascular smooth muscle tone. *Microcirculation* 25. <https://doi.org/10.1111/micc.12421>
98. Kather JN, Kroll J (2013) Rho guanine exchange factors in blood vessels: fine-tuners of angiogenesis and vascular function. *Exp Cell Res* 319:1289–1297. <https://doi.org/10.1016/j.yexcr.2012.12.015>
99. Sawada N, Salomone S, Kim H-H et al. (2008) Regulation of endothelial nitric oxide synthase and postnatal angiogenesis by Rac1. *Circ Res* 103:360–368. <https://doi.org/10.1161/CIRCRESAHA.108.178897>
100. Bryan BA, D'Amore PA (2007) What tangled webs they weave: Rho-GTPase control of angiogenesis. *Cell Mol Life Sci* 64:2053–2065. <https://doi.org/10.1007/s00018-007-7008-z>
101. Liu Y, Petreaca M, Martins-Green M (2008) Cell and molecular mechanisms of insulin-induced angiogenesis. *J Cell Mol Med* 13:4492–4504. <https://doi.org/10.1111/j.1582-4934.2008.00555.x>
102. Tan W, Palmby TR, Gavard J et al. (2008) An essential role for Rac1 in endothelial cell function and vascular development. *FASEB J* 22:1829–1838. <https://doi.org/10.1096/fj.07-096438>
103. Shirai H, Autieri M, Eguchi S (2007) Small GTP-binding proteins and mitogen-activated protein kinases as promising therapeutic targets of vascular remodeling. *Curr Opin Nephrol Hypertens* 16:111–115. <https://doi.org/10.1097/MNH.0b013e3280148e4f>
104. Sauzeau V, Sevilla MA, Montero MJ et al. (2010) The Rho/Rac exchange factor Vav2 controls nitric oxide-dependent responses in mouse vascular smooth muscle cells. *J Clin Invest* 120:315–330. <https://doi.org/10.1172/JCI38356>
105. Loirand G, Pacaud P (2014) Involvement of Rho GTPases and their regulators in the pathogenesis of hypertension. *Small GTPases* 5. <https://doi.org/10.4161/sgtp.28846>
106. Radi ZA (2019) Kidney Pathophysiology, Toxicology, and Drug-Induced Injury in Drug Development. *Int J Toxicol* 38:215–227. <https://doi.org/10.1177/1091581819831701>
107. Preuss HG (1993) Basics of renal anatomy and physiology. *Clin Lab Med* 13:1–11
108. Costantini F, Kopan R (2010) Patterning a complex organ: branching morphogenesis and nephron segmentation in kidney development. *Dev Cell* 18:698–712. <https://doi.org/10.1016/j.devcel.2010.04.008>
109. Lindström NO, McMahon JA, Guo J et al. (2018) Conserved and Divergent Features of Human and Mouse Kidney Organogenesis. *J Am Soc Nephrol* 29:785–805. <https://doi.org/10.1681/ASN.2017080887>
110. McMahon AP (2016) Development of the Mammalian Kidney. *Curr Top Dev Biol* 117:31–64. <https://doi.org/10.1016/bs.ctdb.2015.10.010>
111. Larsson L, Aperia A, Elinder G (1983) Structural and functional development of the nephron. *Acta Paediatr Scand Suppl* 305:56–60. <https://doi.org/10.1111/j.1651-2227.1983.tb09860.x>
112. Song R, Yosypiv IV (2012) Development of the kidney medulla. *Organogenesis* 8:10–17. <https://doi.org/10.4161/org.19308>
113. Tisher CC (1978) Functional anatomy of the kidney. *Hosp Pract* 13:UNKNOWN. <https://doi.org/10.1080/21548331.1978.11707333>

-
114. Miner JH (2012) The glomerular basement membrane. *Exp Cell Res* 318:973–978. <https://doi.org/10.1016/j.yexcr.2012.02.031>
115. Byron A, Randles MJ, Humphries JD et al. (2014) Glomerular cell cross-talk influences composition and assembly of extracellular matrix. *J Am Soc Nephrol* 25:953–966. <https://doi.org/10.1681/ASN.2013070795>
116. Haraldsson B, Nyström J, Deen WM (2008) Properties of the glomerular barrier and mechanisms of proteinuria. *Physiological reviews* 88:451–487. <https://doi.org/10.1152/physrev.00055.2006>
117. Pollak, Quaggin SE, Hoenig MP et al. (2014) The glomerulus: the sphere of influence. *Clinical journal of the American Society of Nephrology : CJASN* 9. <https://doi.org/10.2215/CJN.09400913>
118. Guasch A, Deen WM, Myers BD (1993) Charge selectivity of the glomerular filtration barrier in healthy and nephrotic humans. *J Clin Invest* 92:2274–2282. <https://doi.org/10.1172/JCI116831>
119. Hinchliffe SA, Sargent PH, Howard CV et al. (1991) Human intrauterine renal growth expressed in absolute number of glomeruli assessed by the disector method and Cavalieri principle. *Lab Invest* 64:777–784
120. Puddu M, Fanos V, Podda F et al. (2009) The kidney from prenatal to adult life: perinatal programming and reduction of number of nephrons during development. *Am J Nephrol* 30:162–170. <https://doi.org/10.1159/000211324>
121. Sulemanji M, Vakili K (2013) Neonatal renal physiology. *Semin Pediatr Surg* 22:195–198. <https://doi.org/10.1053/j.sempedsurg.2013.10.008>
122. Drummond I (2003) Making a zebrafish kidney: a tale of two tubes. *Trends Cell Biol* 13:357–365. [https://doi.org/10.1016/s0962-8924\(03\)00124-7](https://doi.org/10.1016/s0962-8924(03)00124-7)
123. Drummond IA, Davidson AJ (2010) Chapter 9 - Zebrafish Kidney Development. In: Detrich HW, Westerfield M, Zon LI (eds) *Methods in Cell Biology : The Zebrafish: Cellular and Developmental Biology, Part A, vol 100*. Academic Press, pp 233–260
124. Ichimura K, Bubenshchikova E, Powell R et al. (2012) A comparative analysis of glomerulus development in the pronephros of medaka and zebrafish. *PLoS ONE* 7:e45286. <https://doi.org/10.1371/journal.pone.0045286>
125. Outtandy P, Russell C, Kleta R et al. (2019) Zebrafish as a model for kidney function and disease. *Pediatr Nephrol* 34:751–762. <https://doi.org/10.1007/s00467-018-3921-7>
126. Swanhart LM, Cosentino CC, Diep CQ et al. (2011) Zebrafish Kidney Development: Basic Science to Translational Research. *Birth Defects Res C Embryo Today* 93:141–156. <https://doi.org/10.1002/bdrc.20209>
127. Jerman S, Sun Z (2017) Using Zebrafish to Study Kidney Development and Disease. *Curr Top Dev Biol* 124:41–79. <https://doi.org/10.1016/bs.ctdb.2016.11.008>
128. Attias O, Jiang R, Aoudjit L et al. (2010) Rac1 contributes to actin organization in glomerular podocytes. *Nephron Exp Nephrol* 114:e93-e106. <https://doi.org/10.1159/000262317>
129. Mouawad F, Tsui H, Takano T (2013) Role of Rho-GTPases and their regulatory proteins in glomerular podocyte function. *Can J Physiol Pharmacol* 91:773–782. <https://doi.org/10.1139/cjpp-2013-0135>

-
130. Li S-Y, Chu P-H, Huang P-H et al. (2019) FHL2 mediates podocyte Rac1 activation and foot process effacement in hypertensive nephropathy. *Sci Rep* 9. <https://doi.org/10.1038/s41598-019-42328-1>
131. Robins R, Baldwin C, Aoudjit L et al. (2017) Rac1 activation in podocytes induces the spectrum of nephrotic syndrome. *Kidney Int* 92. <https://doi.org/10.1016/j.kint.2017.03.010>
132. Shibata S, Nagase M, Yoshida S et al. (2008) Modification of mineralocorticoid receptor function by Rac1 GTPase: implication in proteinuric kidney disease. *Nat Med* 14:1370–1376. <https://doi.org/10.1038/nm.1879>
133. Asao R, Seki T, Takagi M et al. (2018) Rac1 in podocytes promotes glomerular repair and limits the formation of sclerosis. *Sci Rep* 8:5061. <https://doi.org/10.1038/s41598-018-23278-6>
134. Blattner SM, Hodgins JB, Nishio M et al. (2013) Divergent functions of the Rho GTPases Rac1 and Cdc42 in podocyte injury. *Kidney Int* 84:920–930. <https://doi.org/10.1038/ki.2013.175>
135. Zhang Q, Conley SM, Li G et al. (2019) Rac1 GTPase Inhibition Blocked Podocyte Injury and Glomerular Sclerosis during Hyperhomocysteinemia via Suppression of Nucleotide-Binding Oligomerization Domain-Like Receptor Containing Pyrin Domain 3 Inflammasome Activation. *Kidney Blood Press Res* 44:513–532. <https://doi.org/10.1159/000500457>
136. Shimazaki A, Tanaka Y, Shinosaki T et al. (2006) ELMO1 increases expression of extracellular matrix proteins and inhibits cell adhesion to ECMs. *Kidney Int* 70:1769–1776. <https://doi.org/10.1038/sj.ki.5001939>
137. (2009) Diagnosis and Classification of Diabetes Mellitus. *Diabetes Care* 32:S62-7. <https://doi.org/10.2337/dc09-S062>
138. Campbell JE, Newgard CB (2021) Mechanisms controlling pancreatic islet cell function in insulin secretion. *Nat Rev Mol Cell Biol* 22:142–158. <https://doi.org/10.1038/s41580-020-00317-7>
139. Sano H, Kane S, Sano E et al. (2003) Insulin-stimulated phosphorylation of a Rab GTPase-activating protein regulates GLUT4 translocation. *J Biol Chem* 278:14599–14602. <https://doi.org/10.1074/jbc.C300063200>
140. Boucher J, Kleinridders A, Kahn CR (2014) Insulin Receptor Signaling in Normal and Insulin-Resistant States. *Cold Spring Harb Perspect Biol* 6. <https://doi.org/10.1101/cshperspect.a009191>
141. Saeedi P, Petersohn I, Salpea P et al. (2019) Global and regional diabetes prevalence estimates for 2019 and projections for 2030 and 2045: Results from the International Diabetes Federation Diabetes Atlas, 9th edition. *Diabetes Res Clin Pract* 157:107843. <https://doi.org/10.1016/j.diabres.2019.107843>
142. Bluestone JA, Herold K, Eisenbarth G (2010) Genetics, pathogenesis and clinical interventions in type 1 diabetes. *Nature* 464:1293–1300. <https://doi.org/10.1038/nature08933>
143. Anderson MS, Bluestone JA (2005) The NOD mouse: a model of immune dysregulation. *Annu Rev Immunol* 23:447–485. <https://doi.org/10.1146/annurev.immunol.23.021704.115643>
144. Negre-Salvayre A, Salvayre R, Augé N et al. (2009) Hyperglycemia and glycation in diabetic complications. *Antioxid Redox Signal* 11:3071–3109. <https://doi.org/10.1089/ars.2009.2484>

-
145. Reddy VP, Obrenovich ME, Atwood CS et al. (2002) Involvement of Maillard reactions in Alzheimer disease. *Neurotoxicity research* 4. <https://doi.org/10.1080/1029840290007321>
 146. Orasanu G, Plutzky J (2009) The pathologic continuum of diabetic vascular disease. *J Am Coll Cardiol* 53:S35-42. <https://doi.org/10.1016/j.jacc.2008.09.055>
 147. Flyvbjerg A, Goldstein BJ, Cockram CS et al. (eds) (2016) *Textbook of diabetes*, Fifth edition. Wiley-Blackwell, Chichester, West Sussex, UK, Hoboken, NJ
 148. Giacco F, Brownlee M (2010) Oxidative stress and diabetic complications. *Circ Res* 107:1058–1070. <https://doi.org/10.1161/CIRCRESAHA.110.223545>
 149. Rask-Madsen C, King GL (2013) Vascular complications of diabetes: mechanisms of injury and protective factors. *Cell Metab* 17:20–33. <https://doi.org/10.1016/j.cmet.2012.11.012>
 150. Yagihashi S, Mizukami H, Sugimoto K (2011) Mechanism of diabetic neuropathy: Where are we now and where to go? *J Diabetes Investig* 2:18–32. <https://doi.org/10.1111/j.2040-1124.2010.00070.x>
 151. Kriz W, Löwen J, Federico G et al. (2017) Accumulation of worn-out GBM material substantially contributes to mesangial matrix expansion in diabetic nephropathy. *Am J Physiol Renal Physiol* 312:F1101-F1111. <https://doi.org/10.1152/ajprenal.00020.2017>
 152. Chen S, Khoury C, Ziyadeh FN (2012) Pathophysiology and Pathogenesis of Diabetic Nephropathy. In: Alpern RJ, Seldin DW (eds) *Seldin and Giebisch's The kidney: Physiology and pathophysiology*, 5th ed. Elsevier, Acad. Press, Amsterdam, pp 2605–2632
 153. Kowluru A (2011) Friendly, and not so friendly, roles of Rac1 in islet β -cell function: Lessons learnt from pharmacological and molecular biological approaches. *Biochem Pharmacol* 81:965–975. <https://doi.org/10.1016/j.bcp.2011.01.013>
 154. Sylow L, Kleinert M, Pehmøller C et al. (2014) Akt and Rac1 signaling are jointly required for insulin-stimulated glucose uptake in skeletal muscle and downregulated in insulin resistance. *Cell Signal* 26:323–331. <https://doi.org/10.1016/j.cellsig.2013.11.007>
 155. Sahajpal N, Kowluru A, Kowluru RA (2019) The Regulatory Role of Rac1, a Small Molecular Weight GTPase, in the Development of Diabetic Retinopathy. *J Clin Med* 8. <https://doi.org/10.3390/jcm8070965>
 156. Lee SR, An EJ, Kim J et al. (2020) Function of NADPH Oxidases in Diabetic Nephropathy and Development of Nox Inhibitors. *Biomol Ther (Seoul)* 28:25–33. <https://doi.org/10.4062/biomolther.2019.188>
 157. Hamilton F (1822) *An account of the fishes found in the river Ganges and its branches / by Francis Hamilton, (formerly Buchanan,) ...; With a volume of plates in royal quarto. Printed for A. Constable and company; [etc., etc.]*, Edinburgh
 158. Lieschke GJ, Currie PD (2007) Animal models of human disease: zebrafish swim into view. *Nat Rev Genet* 8:353–367. <https://doi.org/10.1038/nrg2091>
 159. Yuxiao Yao, Shaoyang Sun, Fei Fei et al. (2017) Screening in larval zebrafish reveals tissue-specific distribution of fifteen fluorescent compounds. *Dis Model Mech* 10:1155. <https://doi.org/10.1242/dmm.028811>
 160. Kimmel CB, Ballard WW, Kimmel SR et al. (1995) Stages of embryonic development of the zebrafish. *Dev Dyn* 203:253–310. <https://doi.org/10.1002/aja.1002030302>

-
161. Menke AL, Spitsbergen JM, Wolterbeek APM et al. (2011) Normal anatomy and histology of the adult zebrafish. *Toxicol Pathol* 39:759–775. <https://doi.org/10.1177/0192623311409597>
162. Howe K, Clark MD, Torroja CF et al. (2013) The zebrafish reference genome sequence and its relationship to the human genome. *Nature* 496:498–503. <https://doi.org/10.1038/nature12111>
163. Nasevicius A, Ekker SC (2000) Effective targeted gene 'knockdown' in zebrafish. *Nat Genet* 26:216–220. <https://doi.org/10.1038/79951>
164. Sander JD, Cade L, Khayter C et al. (2011) Targeted gene disruption in somatic zebrafish cells using engineered TALENs. *Nat Biotechnol* 29:697–698. <https://doi.org/10.1038/nbt.1934>
165. Hwang WY, Fu Y, Reyon D et al. (2013) Efficient genome editing in zebrafish using a CRISPR-Cas system. *Nat Biotechnol* 31:227–229. <https://doi.org/10.1038/nbt.2501>
166. Jao L-E, Wente SR, Chen W (2013) Efficient multiplex biallelic zebrafish genome editing using a CRISPR nuclease system. *Proc Natl Acad Sci U S A* 110:13904–13909. <https://doi.org/10.1073/pnas.1308335110>
167. Seth A, Stemple DL, Barroso I (2013) The emerging use of zebrafish to model metabolic disease. *Dis Model Mech* 6:1080–1088. <https://doi.org/10.1242/dmm.011346>
168. Argenton F, Zecchin E, Bortolussi M (1999) Early appearance of pancreatic hormone-expressing cells in the zebrafish embryo. *Mech Dev* 87:217–221. [https://doi.org/10.1016/S0925-4773\(99\)00151-3](https://doi.org/10.1016/S0925-4773(99)00151-3)
169. Pozios KC, Ding J, Degger B et al. (2001) IGFs stimulate zebrafish cell proliferation by activating MAP kinase and PI3-kinase-signaling pathways. *Am J Physiol Regul Integr Comp Physiol* 280:R1230-9. <https://doi.org/10.1152/ajpregu.2001.280.4.R1230>
170. Toyoshima Y, Monson C, Duan C et al. (2008) The role of insulin receptor signaling in zebrafish embryogenesis. *Endocrinology* 149:5996–6005. <https://doi.org/10.1210/en.2008-0329>
171. Capiotti KM, Antonioli R, Kist LW et al. (2014) Persistent impaired glucose metabolism in a zebrafish hyperglycemia model. *Comp Biochem Physiol B Biochem Mol Biol* 171:58–65. <https://doi.org/10.1016/j.cbpb.2014.03.005>
172. Gleeson M, Connaughton V, Arneson LS (2007) Induction of hyperglycaemia in zebrafish (*Danio rerio*) leads to morphological changes in the retina. *Acta Diabetol* 44:157–163. <https://doi.org/10.1007/s00592-007-0257-3>
173. Wiggenhauser LM, Qi H, Stoll SJ et al. (2020) Activation of Retinal Angiogenesis in Hyperglycemic *pdx1*^{-/-} Zebrafish Mutants. *Diabetes* 69:1020–1031. <https://doi.org/10.2337/db19-0873>
174. Wiggenhauser LM, Metzger L, Bennewitz K et al. (2022) *pdx1* Knockout Leads to a Diabetic Nephropathy-Like Phenotype in Zebrafish and Identifies Phosphatidylethanolamine as Metabolite Promoting Early Diabetic Kidney Damage. *Diabetes*. <https://doi.org/10.2337/db21-0645>
175. Olsen AS, Sarras MP, Intine RV (2010) Limb regeneration is impaired in an adult zebrafish model of diabetes mellitus. *Wound Repair Regen* 18:532–542. <https://doi.org/10.1111/j.1524-475X.2010.00613.x>

176. Dorsemans A-C, Soulé S, Weger M et al. (2017) Impaired constitutive and regenerative neurogenesis in adult hyperglycemic zebrafish. *J Comp Neurol* 525:442–458. <https://doi.org/10.1002/cne.24065>
177. El-Brolosy MA, Stainier DYR (2017) Genetic compensation: A phenomenon in search of mechanisms. *PLoS Genet* 13:e1006780. <https://doi.org/10.1371/journal.pgen.1006780>
178. El-Brolosy MA, Kontarakis Z, Rossi A et al. (2019) Genetic compensation triggered by mutant mRNA degradation. *Nature* 568:193–197. <https://doi.org/10.1038/s41586-019-1064-z>
179. Sztal TE, Stainier DYR (2020) Transcriptional adaptation: a mechanism underlying genetic robustness. *Development* 147. <https://doi.org/10.1242/dev.186452>
180. Denecke J, Kranz C, Kemming D et al. (2004) An activated 5' cryptic splice site in the human ALG3 gene generates a premature termination codon insensitive to nonsense-mediated mRNA decay in a new case of congenital disorder of glycosylation type Id (CDG-Id). *Hum Mutat* 23:477–486. <https://doi.org/10.1002/humu.20026>
181. Inácio A, Silva AL, Pinto J et al. (2004) Nonsense mutations in close proximity to the initiation codon fail to trigger full nonsense-mediated mRNA decay. *J Biol Chem* 279:32170–32180. <https://doi.org/10.1074/jbc.M405024200>
182. Dabrowska M, Juzwa W, Krzyzosiak WJ et al. (2018) Precise Excision of the CAG Tract from the Huntingtin Gene by Cas9 Nickases. *Front Neurosci* 12:75. <https://doi.org/10.3389/fnins.2018.00075>
183. Lawson ND, Weinstein BM (2002) In vivo imaging of embryonic vascular development using transgenic zebrafish. *Dev Biol* 248:307–318. <https://doi.org/10.1006/dbio.2002.0711>
184. Saint-Geniez M, D'Amore PA (2004) Development and pathology of the hyaloid, choroidal and retinal vasculature. *Int J Dev Biol* 48:1045–1058. <https://doi.org/10.1387/ijdb.041895ms>
185. Sylow L, Jensen TE, Kleinert M et al. (2013) Rac1 Signaling Is Required for Insulin-Stimulated Glucose Uptake and Is Dysregulated in Insulin-Resistant Murine and Human Skeletal Muscle. *Diabetes* 62:1865–1875. <https://doi.org/10.2337/db12-1148>
186. Raun SH, Ali M, Kjøbsted R et al. (2018) Rac1 muscle knockout exacerbates the detrimental effect of high-fat diet on insulin-stimulated muscle glucose uptake independently of Akt. *J Physiol (Lond)* 596:2283–2299. <https://doi.org/10.1113/JP275602>
187. Hobeika L, Barati MT, Caster DJ et al. (2017) Characterization of glomerular extracellular matrix by proteomic analysis of laser-captured microdissected glomeruli. *Kidney Int* 91:501–511. <https://doi.org/10.1016/j.kint.2016.09.044>
188. Zitka O, Skalickova S, Gumulec J et al. (2012) Redox status expressed as GSH:GSSG ratio as a marker for oxidative stress in paediatric tumour patients. *Oncol Lett* 4:1247–1253. <https://doi.org/10.3892/ol.2012.931>
189. Costa F, Biaggioni I (1998) Role of Nitric Oxide in Adenosine-Induced Vasodilation in Humans. *Hypertension* 31:1061–1064. <https://doi.org/10.1161/01.HYP.31.5.1061>
190. Meza CA, La Favor JD, Kim D-H et al. (2019) Endothelial Dysfunction: Is There a Hyperglycemia-Induced Imbalance of NOX and NOS? *Int J Mol Sci* 20. <https://doi.org/10.3390/ijms20153775>
191. Daff S (2010) NO synthase: structures and mechanisms. *Nitric Oxide* 23:1–11. <https://doi.org/10.1016/j.niox.2010.03.001>

192. Kok FO, Shin M, Ni C-W et al. (2015) Reverse genetic screening reveals poor correlation between morpholino-induced and mutant phenotypes in zebrafish. *Dev Cell* 32:97–108. <https://doi.org/10.1016/j.devcel.2014.11.018>
193. Maulik N, Das DK (2002) Redox signaling in vascular angiogenesis^{1,2} 1Guest Editor: Toshikazu Yoshikawa 2This article is part of a series of reviews on “Vascular Dysfunction and Free Radicals.” The full list of papers may be found on the homepage of the journal. *Free Radical Biology and Medicine* 33:1047–1060. [https://doi.org/10.1016/S0891-5849\(02\)01005-5](https://doi.org/10.1016/S0891-5849(02)01005-5)
194. Peng Z, Shu B, Zhang Y et al. (2019) Endothelial Response to Pathophysiological Stress. *Arterioscler Thromb Vasc Biol* 39:e233-e243. <https://doi.org/10.1161/ATVBAHA.119.312580>
195. Kim Y-W, Byzova TV (2014) Oxidative stress in angiogenesis and vascular disease. *Blood* 123:625–631. <https://doi.org/10.1182/blood-2013-09-512749>
196. Xian D, Song J, Yang L et al. (2019) Emerging Roles of Redox-Mediated Angiogenesis and Oxidative Stress in Dermatoses. *Oxid Med Cell Longev* 2019:2304018. <https://doi.org/10.1155/2019/2304018>
197. Wolf G, Ziyadeh FN (1999) Molecular mechanisms of diabetic renal hypertrophy. *Kidney Int* 56:393–405. <https://doi.org/10.1046/j.1523-1755.1999.00590.x>
198. Habib SL (2018) Kidney atrophy vs hypertrophy in diabetes: which cells are involved? *Cell Cycle* 17:1683–1687. <https://doi.org/10.1080/15384101.2018.1496744>
199. Fogo A, Hawkins EP, Berry PL et al. (1990) Glomerular hypertrophy in minimal change disease predicts subsequent progression to focal glomerular sclerosis. *Kidney Int* 38. <https://doi.org/10.1038/ki.1990.175>
200. Marshall CB (2016) Rethinking glomerular basement membrane thickening in diabetic nephropathy: adaptive or pathogenic? *Am J Physiol Renal Physiol* 311:F831-F843. <https://doi.org/10.1152/ajprenal.00313.2016>
201. Catania JM, Chen G, Parrish AR (2007) Role of matrix metalloproteinases in renal pathophysiology. *Am J Physiol Renal Physiol* 292. <https://doi.org/10.1152/ajprenal.00421.2006>
202. Abrass CK (1995) Diabetic nephropathy. Mechanisms of mesangial matrix expansion. *West J Med* 162:318–321
203. Thomson SE, McLennan SV, Kirwan PD et al. (2008) Renal connective tissue growth factor correlates with glomerular basement membrane thickness and prospective albuminuria in a non-human primate model of diabetes: possible predictive marker for incipient diabetic nephropathy. *J Diabetes Complications* 22:284–294. <https://doi.org/10.1016/j.jdiacomp.2007.07.001>
204. Zhao F-Q, Keating AF (2007) Functional properties and genomics of glucose transporters. *Curr Genomics* 8:113–128. <https://doi.org/10.2174/138920207780368187>
205. Marshall BA, Ren JM, Johnson DW et al. (1993) Germline manipulation of glucose homeostasis via alteration of glucose transporter levels in skeletal muscle. *J Biol Chem* 268:18442–18445
206. Thorens B (1996) Glucose transporters in the regulation of intestinal, renal, and liver glucose fluxes. *Am J Physiol* 270:G541-53. <https://doi.org/10.1152/ajpgi.1996.270.4.G541>

-
207. Burant CF, Takeda J, Brot-Laroche E et al. (1992) Fructose transporter in human spermatozoa and small intestine is GLUT5. *J Biol Chem* 267:14523–14526
208. Kane S, Seatter MJ, Gould GW (1997) Functional studies of human GLUT5: effect of pH on substrate selection and an analysis of substrate interactions. *Biochem Biophys Res Commun* 238. <https://doi.org/10.1006/bbrc.1997.7204>
209. Douard V, Ferraris RP (2008) Regulation of the fructose transporter GLUT5 in health and disease. *Am J Physiol Endocrinol Metab* 295:E227-37. <https://doi.org/10.1152/ajpendo.90245.2008>
210. Stuart CA, Howell MEA, Yin D (2007) Overexpression of GLUT5 in diabetic muscle is reversed by pioglitazone. *Diabetes Care* 30:925–931. <https://doi.org/10.2337/dc06-1788>
211. Hajduch E, Darakhshan F, Hundal HS (1998) Fructose uptake in rat adipocytes: GLUT5 expression and the effects of streptozotocin-induced diabetes. *Diabetologia* 41:821–828. <https://doi.org/10.1007/s001250050993>
212. Miyamoto K, Hase K, Takagi T et al. (1993) Differential responses of intestinal glucose transporter mRNA transcripts to levels of dietary sugars. *Biochem J* 295 (Pt 1):211–215. <https://doi.org/10.1042/bj2950211>
213. Printz RL, Koch S, Potter LR et al. (1993) Hexokinase II mRNA and gene structure, regulation by insulin, and evolution. *J Biol Chem* 268:5209–5219
214. Osawa H, Sutherland C, Robey RB et al. (1996) Analysis of the signaling pathway involved in the regulation of hexokinase II gene transcription by insulin. *J Biol Chem* 271:16690–16694. <https://doi.org/10.1074/jbc.271.28.16690>
215. Esteves JV, Yonamine CY, Pinto-Junior DC et al. (2018) Diabetes Modulates MicroRNAs 29b-3p, 29c-3p, 199a-5p and 532-3p Expression in Muscle: Possible Role in GLUT4 and HK2 Repression. *Front Endocrinol (Lausanne)* 9:536. <https://doi.org/10.3389/fendo.2018.00536>
216. Cryer PE, Axelrod L, Grossman AB et al. (2009) Evaluation and management of adult hypoglycemic disorders: an Endocrine Society Clinical Practice Guideline. *J Clin Endocrinol Metab* 94:709–728. <https://doi.org/10.1210/jc.2008-1410>
217. Khunti K, Alsifri S, Aronson R et al. (2016) Rates and predictors of hypoglycaemia in 27 585 people from 24 countries with insulin-treated type 1 and type 2 diabetes: the global HAT study. *Diabetes Obes Metab* 18:907–915. <https://doi.org/10.1111/dom.12689>
218. Heinrich M, Maison N, Achenbach P et al. (2018) Fasting hypoglycemia is associated with disease progression in presymptomatic early stage type 1 diabetes. *Pediatr Diabetes* 19:1238–1242. <https://doi.org/10.1111/pedi.12739>
219. Vlachos D, Malisova S, Lindberg FA et al. (2020) Glycemic Index (GI) or Glycemic Load (GL) and Dietary Interventions for Optimizing Postprandial Hyperglycemia in Patients with T2 Diabetes: A Review. *Nutrients* 12. <https://doi.org/10.3390/nu12061561>
220. Yari Z, Behrouz V, Zand H et al. (2020) New Insight into Diabetes Management: From Glycemic Index to Dietary Insulin Index. *Curr Diabetes Rev* 16:293–300. <https://doi.org/10.2174/1573399815666190614122626>
221. Nathan DM, Genuth S, Lachin J et al. (1993) The effect of intensive treatment of diabetes on the development and progression of long-term complications in insulin-dependent diabetes mellitus. *N Engl J Med* 329:977–986. <https://doi.org/10.1056/NEJM199309303291401>

222. Im Stratton, Kohner EM, Aldington SJ et al. (2001) UKPDS 50: risk factors for incidence and progression of retinopathy in Type II diabetes over 6 years from diagnosis. *Diabetologia* 44. <https://doi.org/10.1007/s001250051594>
223. Chen S, Akter S, Kuwahara K et al. (2019) Serum amino acid profiles and risk of type 2 diabetes among Japanese adults in the Hitachi Health Study. *Sci Rep* 9:7010. <https://doi.org/10.1038/s41598-019-43431-z>
224. Lu Y, Wang Y, Liang X et al. (2019) Serum Amino Acids in Association with Prevalent and Incident Type 2 Diabetes in A Chinese Population. *Metabolites* 9. <https://doi.org/10.3390/metabo9010014>
225. Vangipurapu J, Stancáková A, Smith U et al. (2019) Nine Amino Acids Are Associated With Decreased Insulin Secretion and Elevated Glucose Levels in a 7.4-Year Follow-up Study of 5,181 Finnish Men. *Diabetes* 68:1353–1358. <https://doi.org/10.2337/db18-1076>
226. Szendroedi J, Schmid AI, Chmelik M et al. (2007) Muscle Mitochondrial ATP Synthesis and Glucose Transport/Phosphorylation in Type 2 Diabetes. *PLoS Med* 4. <https://doi.org/10.1371/journal.pmed.0040154>
227. Kim J-A, Wei Y, Sowers JR (2008) Role of mitochondrial dysfunction in insulin resistance. *Circ Res* 102:401–414. <https://doi.org/10.1161/CIRCRESAHA.107.165472>
228. Rucker B, Abreu-Vieira G, Bischoff LB et al. (2010) The nucleotide hydrolysis is altered in blood serum of streptozotocin-induced diabetic rats. *Arch Physiol Biochem* 116:79–87. <https://doi.org/10.3109/13813451003777067>
229. Katoh H, Fujimoto S, Ishida C et al. (2006) Differential distribution of ELMO1 and ELMO2 mRNAs in the developing mouse brain. *Brain Res* 1073-1074:103–108. <https://doi.org/10.1016/j.brainres.2005.12.085>
230. Sato Y, Sato A, Mizuno S et al. (2019) Comparative gene expression analysis of the engulfment and cell motility (ELMO) protein family in the mouse brain. *Gene Expr Patterns* 34:119070. <https://doi.org/10.1016/j.gep.2019.119070>
231. Zang L, Shimada Y, Nishimura Y et al. (2015) Repeated Blood Collection for Blood Tests in Adult Zebrafish. *J Vis Exp*:e53272. <https://doi.org/10.3791/53272>
232. Wiggerhauser LM, Kohl K, Dietrich N et al. (2017) Studying Diabetes Through the Eyes of a Fish: Microdissection, Visualization, and Analysis of the Adult tg(fli:EGFP) Zebrafish Retinal Vasculature. *J Vis Exp*. <https://doi.org/10.3791/56674>
233. H BTW, Girke T (2016) systemPipeR: NGS workflow and report generation environment. *BMC bioinformatics* 17. <https://doi.org/10.1186/s12859-016-1241-0>
234. Bray NL, Pimentel H, Melsted P et al. (2016) Near-optimal probabilistic RNA-seq quantification. *Nat Biotechnol* 34:525–527. <https://doi.org/10.1038/nbt.3519>
235. Ritchie ME, Phipson B, Di Wu et al. (2015) limma powers differential expression analyses for RNA-sequencing and microarray studies. *Nucleic Acids Res* 43:e47. <https://doi.org/10.1093/nar/gkv007>
236. Walter W, Sánchez-Cabo F, Ricote M (2015) GOplot: an R package for visually combining expression data with functional analysis. *Bioinformatics* 31:2912–2914. <https://doi.org/10.1093/bioinformatics/btv300>
237. Gu Z, Eils R, Schlesner M (2016) Complex heatmaps reveal patterns and correlations in multidimensional genomic data. *Bioinformatics* 32:2847–2849. <https://doi.org/10.1093/bioinformatics/btw313>

238. Lodd E, Wigenhauser LM, Morgenstern J et al. (2019) The combination of loss of glyoxalase1 and obesity results in hyperglycemia. *JCI Insight* 4. <https://doi.org/10.1172/jci.insight.126154>
239. Hill JT, Demarest BL, Bisgrove BW et al. (2014) Poly peak parser: Method and software for identification of unknown indels using sanger sequencing of polymerase chain reaction products. *Dev Dyn* 243:1632–1636. <https://doi.org/10.1002/dvdy.24183>